REPUBLIC OF TURKEY
YILDIZ TECHNICAL UNIVERSITY
GRADUATE SCHOOL OF NATURAL AND APPLIED SCIENCES

FABRICATION AND CHARACTERIZATION OF POLYVINYLIDENE FLUORIDE BASED HOLLOW FIBER ULTRAFILTRATION MEMBRANES BLENDED WITH NANOPARTICLES

YAPRAK SUBAŞI

MSc. THESIS
DEPARTMENT OF MATERIALS SCIENCE AND ENGINEERING
PROGRAM OF METALLURGICAL AND MATERIALS ENGINEERING

ADVISER
ASST. PROF. DR. BUĞRA ÇİÇEK

İSTANBUL, 2018

REPUBLIC OF TURKEY

YILDIZ TECHNICAL UNIVERSITY

GRADUATE SCHOOL OF NATURAL AND APPLIED SCIENCES

FABRICATION AND CHARACTERIZATION OF POLYVINYLIDENE FLUORIDE BASED HOLLOW FIBER ULTRAFILTRATION MEMBRANES BLENDED WITH NANOPARTICLES

A thesis submitted by Yaprak SUBAŞI in partial fulfillment of the requirements for the degree of **MASTER OF SCIENCE** is approved by the committee on 21.03.2018 in Department of Materials Science and Engineering, Program of Metallurgical and Materials Engineering.

Thesis Adviser

Asst. Prof. Dr. Buğra ÇİÇEK

Yıldız Technical University

Approved By the Examining Committee

Asst. Prof. Dr. Buğra ÇİÇEK

Yıldız Technical University

Prof. Dr. Ahmet KARAASLAN, Member

Yıldız Technical University

Prof. Dr. Mehmet SOMER, Member

Koç University

ACKNOWLEDGEMENTS

First of all, I would like to express the deepest appreciation to my supervisor Asst. Prof. Dr. Buğra ÇİÇEK who supported me through my master studies and enable me to perform my thesis studies at Ak-Kim Kimya Sanayi ve Ticaret A.Ş. and Koç University, Boron Based Materials and High Technology Chemicals Research and Application Center (KABAM). Without his guidance and persistent help this thesis would not have been possible.

I would like to thank Dr. Alp SARIOĞLU and Dr. Semih DURMUŞ for their suggestions and kind support. I am also grateful for the assistance given by all workers of Ak-Kim, Directorate of Water Solutions and Research and Development Center.

Finally, my deepest gratitude is definitely for my parents for their love, continuous encouragement, understanding and support through my whole life. This accomplishment would not have been possible without them.

March, 2018

Yaprak SUBAŞI

TABLE OF CONTENTS

Page

LIST OF SYMBOLS viii

LIST OF ABBREVIATIONS xi

LIST OF FIGURES xiv

LIST OF TABLES xiiivii

ABSTRACT xviii

ÖZET xx

CHAPTER 1

INTRODUCTION .....

1.1 Literature Review 1
1.2 Objective of the Thesis 3
1.3 Hypothesis 3

CHAPTER 2

MEMBRANE SEPARATION 5

2.1 Membrane Classification 5
2.2 Some Basic Membrane Terms for Hollow Fiber Ultrafiltration Membranes 10

CHAPTER 3

MEMBRANE FABRICATION METHODS 12

3.1 Phase Inversion 13
3.2 Hollow Fiber Membrane Fabrication 16
3.3 Phase Inversion Fabrication Methods for Hollow Fiber Membranes 18
3.4 Spinning Parameters 19
3.4.1 Type of Polymer 19
3.4.2 Type of Solvents 20
3.4.3 Type of Additives 21
3.4.4 Air Gap 22

3.4.5 Viscosity of the Polymer Solution....23
3.4.6 Bore Fluid....24
3.4.7 Coagulation Bath....24
3.4.8 Take-up Speed....26
3.5 Effect of Post Treatment of Hollow Fiber Membranes....28

CHAPTER 4

MEMBRANE FOULING....31

4.1 Membrane Foulants and Fouling Mechanisms....32
4.1.1 Organic Fouling....32
4.1.2 Biofouling....33
4.1.3 Inorganic Fouling....34
4.2 Mitigation of Membrane Fouling....35
4.2.1 Surface Modification of PVDF Membranes....36
4.2.2 Blending Modification of PVDF Membranes....39
4.2.2.1 Dispersion of Nanoparticles in Polymers....42
4.2.2.2 Inorganic Nanoparticles....43
4.2.2.3 Carbon Nanotubes....44
4.2.2.4 Halloysite Nanotubes....47
4.2.2.5 Boron Nitride....54

CHAPTER 5

EXPERIMENTAL METHOD....56

5.1 Materials....56
5.2 Surface Modification of HNTs with Silane Coupling Agent....57
5.3 Surface Modification of h-BN with Silane Coupling Agent....60
5.4 Preparation of Polymer (Dope) Solution....62
5.5 Viscosity Measurement of Dope Solutions....67
5.6 Spinning of Hollow Fiber Membranes....68
5.7 Post Treatment of Hollow Fiber Membranes....70
5.8 Preparation of Hollow Fiber Test Modules....71

CHAPTER 6

CHARACTERIZATION....73

6.1 Characterization of Nanoparticles....73
6.1.1 Fourier-transform Infrared Spectroscopy (FT-IR)....73
6.1.2 Thermogravimetric Analysis (TGA)....74
6.1.3 X-ray Diffraction Analysis (XRD)....74
6.2 Membrane Characterization Techniques....74
6.2.1 Light Microscopy....74
6.2.2 Calculation of Pure Water Permeability Value....75
6.2.3 Determination of the Molecular Weight Cut-off (MWCO) Values....77
6.2.4 Tensile Test....79
6.2.5 Bubble Point Pressure Measurements....80
6.2.6 Contact Angle Measurements....82

6.2.7 Scanning Electron Microscopy (SEM) 83

CHAPTER 7

RESULTS AND DISCUSSION 86

7.1 Characterization of Nanoparticles 86
7.1.1 FT-IR Spectra Results 86
7.1.2 TGA Results 88
7.1.3 X-ray Diffraction Analysis (XRD) 91
7.2 Membrane Characterization Results 92
7.2.1 Viscosity of Dope Solutions 92
7.2.2 Light Microscopy 94
7.2.3 Pure Water Permeability and MWCO Values of Hollow Fiber Membranes 96
7.2.4 Mechanical Properties and Bubble Point Pressure of Hollow Fiber Membranes 98
7.2.5 Dynamic Contact Angle 100
7.2.6 Morphologies of Hollow Fiber Membranes 102

CHAPTER 8

CONCLUSIONS AND RECOMMENDATIONS 108

REFERENCES 111

CURRICULUM VITAE 134

LIST OF SYMBOLS

η	Dynamic viscosity
%	Percentage
°	Degree
°C	Degree Celsius
°K	Degree kelvin
A	Area of the hollow fiber membrane, m^2
A_o	Cross sectional area of the membrane before elongation, mm^2
Å	Angstrom, 10^{-10} m
Ag	Silver
AlOH	Aluminol
Al_2O_3	Alumina
atm	Atmosphere
Au	Gold
B	Boron
Bar	Pressure unit
BN	Boron nitride
B_2O_3	Boron trioxide
C	Carbon
C_P	Permeate concentration
COOH	Carboxylic
C_f	Feed concentration
cP	Centipoise, mPa.s
cm	Centimeter
cm^{-1}	1/centimeter
CO_2	Carbon dioxide
Cu	Copper
Da	Dalton
F	Force, N
F	Correction factor of pure water temperature, $(1.03^{(T-25°C)})$
G	Gram
GPa	Gigapascal
h	Hour
H	Hydrogen
H_3BO_3	Boric acid
HNO_3	Nitric acid
H_2O	Hydrogen oxide
H_2SO_4	Sulfuric acid
J	Permeability, $L/m^2.h.bar$

KCN	Potassium cyanide
kV	Kilovolts
K	Kelvin
Kg	Kilogram
KDa	Kilodalton
L	Liter
L	Length, m
Lo	Initial length of the membrane (mm)
LiCl	Lithium chloride
$LiClO_4$	Lithium perchloride
λ	Wavelength
m	Meter
m^2	Square meter
µm	Micrometer
nm	Nanometer
mA	Milliamper
min	Minute
mg	Milligram
mL	Milliliter
mm	Millimeter
MPa	Megapascal
M_w	Molecular weight, g/mol
N	Number
N_2	Nitrogen gas
NaOCl	Sodium hypochlorite
NH_2	Amine
O_2	Oxygen
OH	Hydroxide
ΔL	Displacement at maximum load, mm
ΔP	Transmembrane pressure, bar
Pa	Pascal
pH	Potential of hydrogen
ppm	Parts per million
psig	Pound-force per square inch
Q	Volume of the permeated pure water, L
r	Radius, m
r_p	Radius of a given capillary-shaped pore
rpm	Revolution per minute
R	Retention
S	Effective surface area, m^2
SiO_2	Silica
SiOH	Silanol
θ	Contact angle
t	Time
T	Temperature
TiO_2	Titanium oxide
TPa	Terapascal
W	Watt
V	Volume
wt.%	Weight percent

γ	Surface tension at the liquid/air interface, 71.96 x 10^{-3} $N.m^{-1}$
ZnO	Zinc oxide
ZrO_2	Zirconia

LIST OF ABBREVIATIONS

AA	Acrylic Acid
AEAPS	3-(2-Aminoethylamino)propyltrimethoxysilane
AFM	Atomic Force Microscopy
A-BN	APTES Modified Boron Nitride
A-HNT	APTES Modified Halloysite Nanotube
A-MWCNTs	APTES Modified MWCNTs
APS	3-Aminopropyltrimethoxysilane
APTES	3-Aminopropyltriethoxysilane
ATRP	Atom Transfer Radical Polymerization
BNNPs	Boron Nitride Nanoparticles
BNNSs	Boron Nitride Nanosheets
BNNTs	Boron Nitride Nanotubes
BSA	Bovine Serum Albumin
CA	Cellulose Acetate
CA	Contact Angle
c-BN	Cubic Boron Nitride
CNT	Carbon Nanotube
DIW	Deionized Water
DMAc	Dimethylacetamide
DMF	N,N-Dimethylformamide
DMSO	Dimethylsulfoxide
E.coli	Escherichia Coli
EDA	Ethylene Diamine
FSMs	Flat Sheet Membrane
FESEM	Field Emission Scanning Electron Microcopy
FTIR	Fourier Transform Infrared Spectroscopy

GO	Graphene Oxide
GPC	Gel Permeation Chromatography
GPTS	3-Glycidoxypropyltrimethoxysilane
h-BN	Hexagonal Boron Nitride
HEMA	2-hydroxyethylmethacrylate
HF	Hollow Fiber
HFM	Hollow Fiber Membrane
HMPA	Hexamethylphosphoramide
HNTs	Halloysite Nanotubes
HPAE	Hyperbranched Polyamine Ester
ID	Inner Diameter
IPA	Isopropyl Alcohol
MAPTMS	3-Methacryloyloxypropyl Trimethoxysilane
MD	Membrane Distillation
MF	Microfiltration
MWCNTs	Multi Walled Carbon Nanotubes
MWCO	Molecular Weight Cut-off
NF	Nanofiltration
NMP	N-methyl-2-pyrrolidone
NOM	Natural Organic Matter
NPs	Nanoparticles
OD	Outer Diameter
OMWCNTs	Oxidized Multi Walled Carbon Nanotubes
PAN	Polyacryonitrile
PDA	2,4-phenylenediamine
Pdop	Polydopamine
PEBAX	Polyetherblockamide
PEG	Poleytehyleneglycol
PEGMA	Polyethylene Glycol Methacrylate
PEI	Polyetherimide
PES	Polyethersulfone
PI	Phase Inversion
PMAA	Polymethacrylic Acid
PMMA	Polymethyl Methacrylate
POEM	Polyoxyethylene Methacrylate

PS	Polysulfone
PTFE	Polytetrafluoroethylene
PVA	Polyvinylalcohol
PVDF	Polyvinylidenefluoride
PVDF-HFP	Polyvinylidene fluoride-co-hexafluropropylene
PVP	Polyvinylpyrolidone
PWF	Pure Water Flux
PWP	Pure Water Permeability
RAFT	Reversible Addition Fragmentation Chain Transfer
RGO	Reduced Graphene Oxide
RO	Reverse Osmosis
SEM	Scanning Electron Microscopy
SL	Silver Lactate
SWCNTs	Single Walled Carbon Nanotubes
TEP	Triethylphosphate
TEOS	Tetraethoxysilane
TFC	Thin Film Composite
TFN	Thin Film Nanocomposite
TGA	Thermogravimetric Analysis
TMU	Tetramethylurea
UF	Ultrafiltration
UFM	Ultrafiltration Membrane
UV	Ultra Violet
VTMS	Vinyltrimethoxysilane
w-BN	Wurtzite Boron Nitride
XRD	X-ray Diffraction Analysis

LIST OF FIGURES

Page

Figure 2.1 Schematic illustration of various classes of membranes 7
Figure 2.2 Schematic representation of membrane configurations..... 8
Figure 2.3 Schematic illustration of membrane filtration spectrum 9
Figure 3.1 Schematic representation of three DIPS processes: A) precipitation with non-solvent vapor, B) evaporation of solvent, C) immersion precipitation 14
Figure 3.2 Schematic diagram of ternary phase diagram of a polymer/solvent/non-solvent system with various compositions..... 14
Figure 3.3 Comparison of polymers (a) oxidation resistance, (b) chlorine resistance of polymers..... 16
Figure 3.4 Comparison of strength and elongation percent of polymers 16
Figure 3.5 Schematic of the principal types of hollow fiber membranes..... 17
Figure 3.6 Schematic diagram of area nearby the spinneret and the formation of nascent hollow fiber membrane 18
Figure 3.7 Schematic illustration of the spinning set up 19
Figure 3.8 SEM pictures of the cross sections of membranes cast from polymer dope containing 15% PVDF and different solvents: (A) TEP, (B) NMP, (C) DMF, and (D) DMAc 21
Figure 3.9 Cross-sectional SEM pictures of the PVDF hollow fiber membranes. (a) air gap distance: 5cm (b) air gap distance: 80 cm 22
Figure 3.10 Schematic temperature profile for the fabricated membrane with difference coagulation bath temperatures: (A): 10 °C; (B): 23 °C and (C): 40 °C..... 24
Figure 3.11 SEM micrographs of the PVDF membranes prepared by immersion in (a) 15 °C, (b) 25 °C, and (c) 60 °C deionized water, left: top surface, right: cross section 26
Figure 3.12 Effects of elongational draw ratio on the morphology of dry-jet wet-spin PES single-layer hollow fiber membranes..... 27
Figure 3.13 SEM cross-section images of P84 polyimide membranes with various take-up speeds 27
Figure 3.14 Chain scission of PVP via radical reactions: (a) disproportionation and (b) oxidative reaction 28
Figure 3.15 Reaction mechanism of PVP with NaOCl solution..... 29
Figure 3.16 Pure water flux and retention for a 1 g/L BSA solution of PES/PVP ultrafiltration membranes treated with a 4000 ppm hypochlorite solution for different times 29
Figure 3.17 Typical SEM images of virgin membrane (a) and membranes exposed to different exposure doses and concentrations of sodium hypochlorite (b, c and d) 30

Figure 4.1 Schematic representation of organic fouling mechanism 33
Figure 4.2 Schematic representation of biofilm formation on solid surface 34
Figure 4.3 Schematic illustrations of bulk and surface crystallization from inorganic fouling 35
Figure 4.4 Schematic representation of inorganic scaling mechanism 35
Figure 4.5 Illustration of contact angles formed by sessile liquid drops on a smooth homogeneous solid surface 36
Figure 4.6 Schematic of surface modification of PVDF membrane 37
Figure 4.7 Typical types of nanocomposite membranes 40
Figure 4.8 Fabrication of conventional nanocomposite membranes through the PI process and the main effects of nanofillers on final products 41
Figure 4.9 Flow chart of oxidization and silanization process 46
Figure 4.10 Schematic diagram of (a) crystalline structure of Halloysite-(10 Å), (b) structure of halloysite particle 48
Figure 4.11 Schematic representation (a) of the proposed mechanism of the formation of cross-linked network, and (b) of the grafting between bidentate bonded Si and AlOH groups 51
Figure 4.12 Preparation process of PVDF/A-HNTs nanofiltration membranes 51
Figure 4.13 The schematic illustration of the preparation of TiO2-HNTs/PVDF 53
Figure 5.1 The molecular structure of (a) PVP and (b) PVDF polymers 57
Figure 5.2 Hydrolysis reaction of APTES 58
Figure 5.3 Reflux system of silanization reaction 59
Figure 5.4 (a) Centrifugation of the solution, (b) Precipitate A-HNTs after centrifugation 59
Figure 5.5 NÜVE NF 800R Centrifuge bench 60
Figure 5.6 Schematic representation of A-HNTs synthesis 60
Figure 5.7 Mixing of h-BN with ethanol 61
Figure 5.8 Reflux system of silanization reaction 61
Figure 5.9 (a) Centrifugation of the solution, (b) Precipitate A-BN after centrifugation 62
Figure 5.10 Sonication of nanoparticles by ultrasonic bath 62
Figure 5.11 Preparation of dope solutions 64
Figure 5.12 Preparation of bore liquid consisted of solvent/deionized water/non-solvent 65
Figure 5.13 (a) Solvent, non-solvent, nanoparticle mixture, (b) Polymer mixture 66
Figure 5.14 Pilot scale dope tanks with rotator 67
Figure 5.15 Viscosity measurement 68
Figure 5.16 Flow of dope solution 69
Figure 5.17 (a) Spinning line, (b) Take-up of hollow fiber fabrication 69
Figure 5.18 Schematic illustration of the pilot scale spinning set up 70
Figure 5.19 NaOCl post treatment of hollow fiber membranes 71
Figure 5.20 Schematic illustration of HF test modules 71
Figure 5.21 (a) Preparation of HF test modules, (b) Glued and plugged HF test modules 72
Figure 6.1 THERMO SCIENTIFIC NICOLET iS10 FT-IR Spectrometer 73
Figure 6.2 PERKIN ELMER TGA 4000 74
Figure 6.3 NIKON ECLIPSE LV100ND Motorized Microscope 75
Figure 6.4 Installed hollow fibers for light microscopy 75
Figure 6.5 Pure water permeation set up 77
Figure 6.6 Schematic diagram for ultrafiltration experimental equipment 77

Figure 6.7 MWCO experimental set up....78
Figure 6.8 MALVERN GPC device....79
Figure 6.9 SHIMADZU AGS-X Tensile Tester....80
Figure 6.10 Test modules for bubble point pressure measurement....81
Figure 6.11 Bubble point measurement set up....82
Figure 6.12 (a) Contact angle measurement device, (b) prepared sample for the measurements....83
Figure 6.13 ZEISS FESEM....84
Figure 6.14 NUVE EV 018 vacuum oven....84
Figure 6.15 Prepared test samples....85
Figure 6.16 CRESSINGTON 108AUTO Sputter coater....85
Figure 7.1 FTIR spectra of (a) APTES and HNTs, (b) HNTs and HNTs-APTES....86
Figure 7.2 FTIR spectra of h-BN and hBN-APTES....88
Figure 7.3 TGA curve of (a) raw HNTs, (b) modified HNTs, (c) raw HNTs and modified HNTs....89
Figure 7.4 TGA results for the raw h-BN and modified h-BN....91
Figure 7.5 XRD patterns of HNTs and modified HNTs....92
Figure 7.6 Dope solution viscosities according to temperature....93
Figure 7.7 Dope solution viscosities....93
Figure 7.8 Cross section images of hollow fiber membranes (a) Pristine (1), (b) 0.2 HNT (1)....94
Figure 7.9 Cross sectional images of hollow fiber membranes (a) Pristine (2), (b) 0.2 HNT, (c) 0.4 HNT, (d) 0.6 HNT....95
Figure 7.10 Cross sectional images of h-BN blended hollow fiber membranes (a) 0.2 h-BN, (b) 0.4 h-BN, (c) 0.6 h-BN....96
Figure 7.11 Pure water permeability of hollow fiber membranes....96
Figure 7.12 MWCO results of hollow fiber membranes....97
Figure 7.13 Water contact angle values and images of HNTs blended PVDF hollow fiber membranes....101
Figure 7.14 Water contact angle values and images of hBN blended PVDF hollow fiber membranes....101
Figure 7.15 The cross-sectional images of the pristine hollow fiber membrane under different magnifications....102
Figure 7.16 The cross-sectional images of the 0.2 A-HNT hollow fiber membrane under different magnifications....103
Figure 7.17 The cross-sectional images of the 0.4 A-HNT hollow fiber membrane under different magnifications....103
Figure 7.18 The cross-sectional images of the 0.6 A-HNT hollow fiber membrane under different magnifications....104
Figure 7.19 The cross-sectional images of the 0.2 A-BN hollow fiber membrane under different magnifications....105
Figure 7.20 The cross-sectional images of the 0.4 A-BN hollow fiber membrane under different magnifications....106
Figure 7.21 The cross-sectional images of the 0.6 A-BN hollow fiber membrane under different magnifications....106

LIST OF TABLES

Page

Table 2.1 Membrane classification 6
Table 2.2 Comparison of types of membrane systems 10
Table 3.1 Preparation methods of polymeric membranes 13
Table 3.2 Main polymers used in membrane formation via immersion precipitation 15
Table 3.3 Composition and viscosity of PVDF solutions 23
Table 4.1 Examples of surface interaction between particles in liquid phase 42
Table 4.2 Comparison of the properties of HNTs and CNTs 48
Table 4.3 Chemical composition of silanes used for modification of HNTs 50
Table 4.4 Effects of nanoparticles on the performance of PVDF UF membranes 54
Table 4.5 Properties of low-dimensional and bulk h-BN materials 55
Table 5.1 Dope and bore liquid compositions of hollow fiber membranes 63
Table 5.2 Dope and bore liquid compositions of hollow fiber membranes 65
Table 7.1 TGA data for raw HNTs and modified HNTs 90
Table 7.2 Tensile test and bubble point test results of the hollow fiber membranes 98
Table 7.3 Bubble point measurement for different hollow fiber membranes to determine the largest pore size of the fiber 100
Table 7.4 Mean pore sizes and macrovoid lengths of the HNTs blended hollow fiber membranes 104
Table 7.5 Mean pore sizes and macrovoid lengths of h-BN blended hollow fiber membranes 107

ABSTRACT

FABRICATION AND CHARACTERIZATION OF POLYVINYLIDENE FLUORIDE BASED HOLLOW FIBER ULTRAFILTRATION MEMBRANES BLENDED WITH NANOPARTICLES

Yaprak SUBAŞI

Department of Metallurgical and Materials Engineering

MSc. Thesis

Adviser: Asst. Prof. Dr. Buğra ÇİÇEK

With the increasing importance of water treatment and wastewater recovery, the use of membrane processes to obtain drinking and tap water has been spreading rapidly in the world. Polyvinylidene fluoride (PVDF) membranes have been extensively used in ultrafiltration (UF) membranes because of its superior properties such as high mechanical strength, thermal stability, and chemical resistance. Nevertheless, PVDF membranes may susceptible to biofouling because of its strong hydrophobicity. Therefore, various hydrophilic modification techniques have been used to improve the antifouling property, permeability and separation performance as well as mechanical properties of the membranes. Blending with nanoparticles can be considered as a practical way in adaptation to large scale production of antifouling membranes.

In this study, halloysite nanotubes (HNTs) and hexagonal boron nitride nanoparticles (h-BNNPs) were functionalized by 3-Aminopropyltriethoxysilane (APTES) in order to increase the dispersion of nanofiller in PVDF matrix by reducing surface energy of nanoparticles. Pilot scale PVDF based hollow fiber UF membranes formed of different concentrations of nanofillers (0, 0.2, 0.4, 0.6 wt.%) were fabricated via the dry-wet spinning method to study influences of nanoparticles on the morphology and separation performance of PVDF membranes in terms of pore size, hydrophilicity, mechanical strength, pure water permeability (PWP) and molecular weight cut-off (MWCO) values. The Fourier-transform infrared (FT-IR) and thermogravimetric analysis (TGA) showed that APTES was successfully grafted on the surface of the nanoparticles. In addition,

Powder X-ray diffraction (XRD) measurements were performed to investigate the effect of silane coupling agents on the crystalline structure of HNTs.

The morphologies and pore size distributions of the developed HF membrane were characterized by scanning electron microscope (SEM). From the SEM images, the addition of HNTs and h-BN within the membrane structure suppressed macrovoids related to the increase of dope viscosities. The hydrophilicity of the PVDF hollow fiber membranes were improved significantly with the addition of A-HNTs and A-hBN, due to the change in membrane surface energy by silane treatment of nanoparticles. According to the filtration experiments, the PWP results gradually increased with the increase of nanoparticles depended on the hydrophilicity and porosity of the membrane. 0.6 A-HNT and 0.4 A-hBN achieved the maximum value at 639 and 674 $L/m^2.h.bar$, respectively which increased by 62% and 70% compared with the standard PVDF membrane. Additionally, the antifouling property was improved in accordance with the reduction of the contact angle and increase in the hydrophilicity of the PVDF membrane.

In this thesis study, h-BN was used for the first time in pressure-driven membrane processes. It was found that, with the addition HNTs and h-BNNPs, the CA of the modified membranes decreased, improving the hydrophilicity, permeability and antifouling property of the PVDF UF membrane. These results are in accordance with the previous studies revealing the effects of inorganic nanoparticles on the performance of membranes.

Keywords: Ultrafiltration, polyvinylidene fluoride, hollow fiber membranes, halloysite nanotubes, hexagonal boron nitride

ÖZET

NANOPARÇACIK KATKILI POLİVİNİLİDEN FLORÜR ESASLI DELİKLİ ELYAF ULTRAFİLTRASYON MEMBRANLARININ ÜRETİMİ VE KARAKTERİZASYONU

Yaprak SUBAŞI

Metalurji ve Malzeme Mühendisliği

Yüksek Lisans Tezi

Tez Danışmanı: Yrd. Doç. Dr. Buğra ÇİÇEK

Su arıtma ve atık su geri kazanımının artan önemi ile birlikte içme suyu ve musluk suyu elde edilmesinde membran proseslerinin kullanılması dünyaya hızla yayılmaktadır. Poliviniliden florür (PVDF) membranlar, yüksek mekanik dayanım, termal kararlılık ve kimyasal direnç gibi üstün özellikleri sayesinde ultrafiltrasyon (UF) membranlarında yaygın olarak kullanılmaktadırlar. Buna rağmen, PVDF membranlar hidrofobik özelliğinin yüksek olmasından dolayı biyolojik kirlenmeye karşı hassas olabilmektedirler. Bu nedenle, membranlara kirlenme karşıtı özellik (antifouling) kazandırmak, geçirgenlik, ayırma performansı ve mekanik özelliklerini iyileştirmek amacıyla çeşitli hidrofilik modifikasyon yöntemleri kullanılmaktadır. Nanoparçacıklar ile karıştırma tekniği, antifouling membranların büyük ölçekli üretime uyarlanmasında pratik bir yol olarak düşünülmektedir.

Bu çalışmada, nanoparçacıkların yüzey enerjisini azaltarak PVDF matriks içerisindeki dağılımını arttırmak amacıyla halloysit nanotüpler (HNT) ve hegzagonal bor nitrür (h-BN) nanoparçacıklar 3-Aminopropiltrietoksisilan (APTES) ile fonksiyonlandırılmıştır. Nanoparçacıkların membran morfolojisi ve performansı üzerindeki etkilerini incelemek amacıyla farklı konsantrasyonlarda nanokatkı (0, 0.2, 0.4, 0.6 wt.%) içeren pilot ölçekli PVDF esaslı delikli elyaf (hollow fiber) UF membranları kuru-ıslak çekme yöntemiyle üretilmiştir. Membranların gözenek boyutu, hidrofilik özelliği, mekanik dayanımı, saf su geçirgenliği ve molekül ağırlığı ayırma sınırı (MWCO) gibi özellikleri incelenmiştir. Fourier dönüşüm kızılötesi (FT-IR) ve termogravimetrik analiz (TGA) sonuçları,

nanoparçacıkların yüzeyine APTES'in başarıyla aşılandığını göstermiştir. Bununla birlikte, silan ajanlarının HNT'nin kristal yapısına etkisini incelemek amacıyla toz X-ışını kırınımı (XRD) ölçümleri yapılmıştır.

Geliştirilen delikli elyaf membranların morfolojileri ve gözenek boyut dağılımları taramalı elektron mikroskopu (SEM) ile karakterize edilmiştir. SEM görüntülerine göre, membran içerisine HNT ve h-BN ilavesi ile polimer çözeltilerinin viskozite artışına bağlı olarak makroboşluk oluşumu ortadan kaldırıldığı görülmüştür. PVDF hollow fiber membranların hidrofilikliği, nanoparçacıkların silan modifikasyonu ile membran yüzey enerjisindeki değişime bağlı olarak A-HNT ve A-hBN'in ilavesi ile önemli ölçüde geliştirilmiştir. Filtrasyon deneyleri sonucunda, nanoparçacıkların artışı ile saf su geçirgenlik değeri membranın hidrofilisitesi ve gözenekliğine bağlı olarak giderek artmıştır. 0.6 A-HNT ve 0.4 A-hBN, maksimum değerlerini sırasıyla 639 ve 674 $L/m^2.h.bar$ elde etmiş ve standart membrana kıyasla %62 ve %70 oranında artmıştır. Ayrıca, standart PVDF membranın temas açısı düşürülerek hidrofilikliğindeki artışa uygun olarak membrana antifouling özellik kazandırılmıştır.

Bu tez çalışmasında, basınç ile çalışan membran proseslerinde ilk defa h-BN kullanılmıştır. HNT ve h-BN ilavesi ile modifiye edilmiş membranların temas açısı düşürülerek hidrofilikliğin, geçirgenliğin ve kirlenme direncinin geliştirildiği sonucuna varılmıştır. Bu sonuçlar, inorganik nanoparçacıkların membran performansı üzerindeki etkilerini gösteren önceki çalışmalarla uyumludur.

Anahtar Kelimeler: Ultrafiltrasyon, poliviniliden florür, delikli elyaf membranlar, halloysit nanotüp, hegzagonal bor nitrür

CHAPTER 1

INTRODUCTION

1.1 Literature Review

According to the world population clock, the number of people on earth exceeded 7.6 billion in 2018 and is expected to reach 10 billion by 2050. Pure drinking water is set to be a major problem all around the world and is becoming even more serious especially for developing and undeveloped countries. Improving the efficiency and reducing the cost of water treatment are major challenges that need to be met in order to overcome the scarcity of portable water.

Microfiltration (MF), ultrafiltration (UF), nanofiltration (NF), reverse osmosis (RO) and membrane distillation (MD) are pressure driven membrane processes used for water treatment [1, 2]. Among these, UF has been used frequently for wastewater treatment because it is easy to control and maintain and compared with NF and RO it has a relatively low cost. On the other hand, the expense associated with operating membrane processes has been influenced by the cost of power, labor and materials, and membrane cleaning and replacement [3-5]. Membrane modules can be prepared as hollow fiber, flat sheet, spiral wound and tubular configurations. Of these, hollow fiber membranes (HFMs) have received notable attention due to their large surface area per volume and high packing density which result in faster mass transfer [6].

For pressure driven processes, the desired membrane material properties are thermal, chemical, and mechanical stability and hydrophilicity. Nevertheless, most commercial membranes are fabricated from hydrophobic polymers like poly(vinylidene fluoride) (PVDF), poly(ether sulfone) (PES), polypropylene (PP), poly(acrylonitrile) (PAN), and polysulfone (PS). Thus, these polymers are susceptible to adsorption of various solutes from the feed streams [7-9]. Membrane fouling represents the undesirable deposition of retained particles, colloids, and macromolecules on its surfaces, at its pore openings or

within its pores [10, 11]. Membrane fouling is considered an early warning for water production, as it reduces membrane flux, either temporarily or permanently. UF membranes can be prone to biofouling, which leads a reduction of permeability, membrane lifetime and also high operating expenses [12, 13].

PVDF has been extensively used in UF membranes on account of its superior characteristics like mechanical strength, thermal stability, and chemical resistance compared with other commercial polymers [14]. However, strong hydrophobic property of PVDF membranes causes membrane fouling and subsequently decreases water permeability [15]. Thus, the hydrophilicity of PVDF membranes have been developed using various surface modification methods to improve their filtration processes [14].

Surface coating, surface grafting and blending with hydrophilic agents, especially nanoparticles, like titanium oxide, silica, and alumina, carbon nanotubes and halloysite nanotubes have been extensively blended with polymeric membrane materials in order to increase the properties of membranes, such as antifouling property, mechanical properties as well as separation performances, all of which contribute to improving the surface hydrophilicity [6, 16].

Due to the simplicity of the process, blending with inorganic nanoparticles has been commonly utilized. Among the various nanoparticles, tubular aluminosilicate clay, also known as HNTs, with its abundance, high aspect ratio, biocompatibility, mechanical strength, loading efficiency and low cost, has attracted great interest in hydrophilic modifications of UF membranes [17-19]. Boron nitride nanoparticles (BNNPs) have similar structures and superior physiochemical properties such as mechanical properties, better dispersion in polymer matrix, thermal conductivity, electrical-insulating properties, resistance to oxidation and chemical inertness compared to carbon nanomaterials [20-22]. Due to these reasons, BN nanostructures have been widely used as reinforcing agent in polymer matrix composites.

It has been seen that the thermal conductivity, elastic modulus, mechanical strength enhanced, and electrical insulating was provided in polymer composites of BN [23-26]. Nevertheless, because of the hydrophilic property and surface energy of the nanoparticles, silane modification is performed to improve the dispersibility of nanofillers within polymeric matrix, which serves to increase the compatibility between nanoparticles and polymer [27, 28].

1.2 Objective of the Thesis

Many researchers have focused on PVDF owing to its superior properties like mechanical strength, thermal stability, chemical resistance than other polymers. However, hydrophobic PVDF membranes can be susceptible to fouling during the separation of feed streams which cause a reduction of permeability and also decrease the lifetime. Consequently, the development of PVDF membranes had become a hot topic by various researchers including surface modification techniques in order to increase hydrophilicity decreasing the contact angle values.

The main objective of this study is to investigate the fabrication of PVDF based hollow fiber UF membranes and the effects of HNTs and h-BNNPs on the morphology and performance of the membrane. In this study, HNTs and h-BNNPs were functionalized with a silane coupling agent to enhance the dispersion in the polymeric matrix by reducing surface energy of nanoparticles. By dispersing NPs into polymer matrix, it was aimed that PVDF membrane properties could be enhanced with a higher hydrophilicity, higher filtration performance, better morphology and mechanical stability. FTIR, TGA and XRD analyses were used to characterize nanoparticles. The performance of pristine and modified HFMs were determined through pure water permeability (PWP) measurements, molecular weight cut-off (MWCO) experiments, contact angle measurements, and tensile test.

1.3 Hypothesis

It is proposed that the blending of nanomaterials can cause an interfacial area between polymers and nanoparticles and subsequently improve the fundamental properties of the nanocomposite material depending on their large surface area. By dispersing inorganic nanoparticles into polymer matrix, it is expected that UF membrane properties can be enhanced with a higher surface hydrophilicity, permeability, fouling resistance, and also mechanical stability. The agglomeration of nanoparticles is considered as major problem whilst blending them into polymers. The instability of polymer solutions may lead non-homogeneous dispersion of particles in the membranes. The hydrophilic property and surface energy of nanomaterials can be decreased by using silane coupling agents in order to increase their interaction with polymer matrix and prevent the agglomeration phenomenon.

In this thesis study, HNTs and h-BNNPs were functionalized by 3-Aminopropyltriethoxysilane (APTES) as a silane coupling agent in order to increase the dispersion of particles in the polymeric base. It is assumed that the addition of HNTs and h-BNNPs within the membrane structure can improve the morphology, surface hydrophilicity, filtration performance and also mechanical properties of the pristine PVDF UF membrane.

CHAPTER 2

MEMBRANE SEPARATION

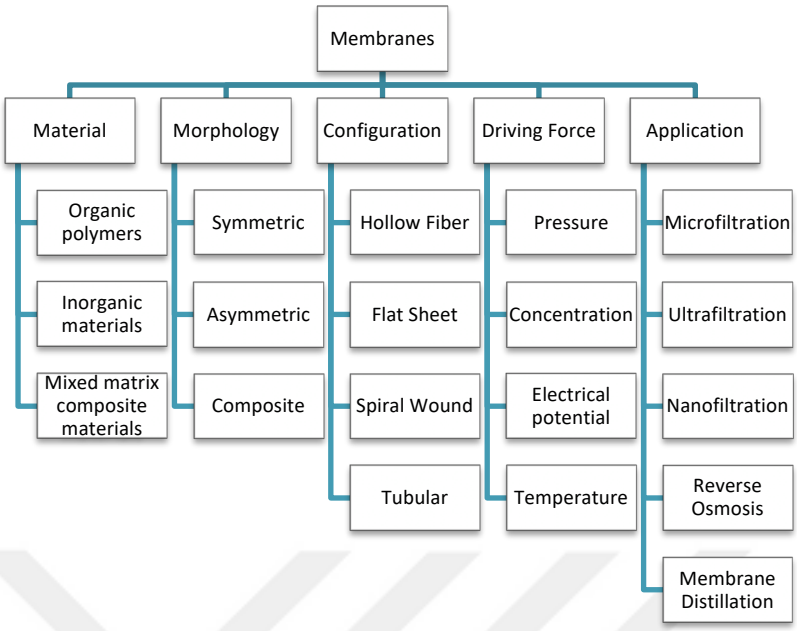
Membranes is described as a thin selective layer which separates molecules, ions according to their properties such as size, shape, chemical composition, electrical charge under a driving force like concentration, pressure, electrical potential or temperature difference [29]. Membrane technology can be considered as an emerging technology because it has been frequently used in most of the separation processes with a multidisciplinary character [30].

Membrane processes was first found in late of eighteenth century as a term of osmosis. Nowadays, membrane separation technology has been developed as an alternative technology of water and wastewater treatment. At the end of the World War II, membranes have been used to obtain drinking water. By 1960s, laboratory scale, slow and expensive membrane technology had been developed [31]. Loeb and Sourirajan fabricated asymmetric cellulose acetate (CA) RO membranes for sea water demineralization [32]. With the discovery of Loeb and Sourirajan, membranes found place in to industrial use due to its defect free, high flux property. Since 1980s, various membrane filtration techniques, such as MF, UF, NF, RO, MD have been employed for water treatment, in drinking, urban and industrial water supply as well as various industries such as pulp and paper, textile, pharmaceutical, food, beverage automotive, biotechnology and chemical industries [31].

2.1 Membrane Classification

Membranes can be categorized based on features such as material, morphology, configuration, driving force and application as shown in Table 2.1.

Table 2.1 Membrane classification [33].



Membrane materials can be divided into two categories such as organic and inorganic materials. Inorganic membranes have been fabricated from ceramics such as alumina, zirconia, titania and silica showing shows high mechanical, chemical and thermal resistance. However, polymeric based materials have been widely used because of their easy pore forming ability and lower cost than inorganic materials [34]. PVDF, PAN, PTFE, CA, PS, PES are widely used polymeric membrane materials [35].

There are three types of membranes according to their morphology; symmetric, asymmetric and composite membranes. Symmetric membranes can be also called isotropic porous or dense membranes with regard to their uniform compositions and morphologies. But then, asymmetric membranes have different pore sizes. Consequently, particles larger than the largest pores are completely rejected and particles smaller than the largest pores, but larger than the smaller pores are partially rejected by the membrane. There are two classes of membranes: isotropic and anistropic membranes as shown in Figure 2.1 [30].

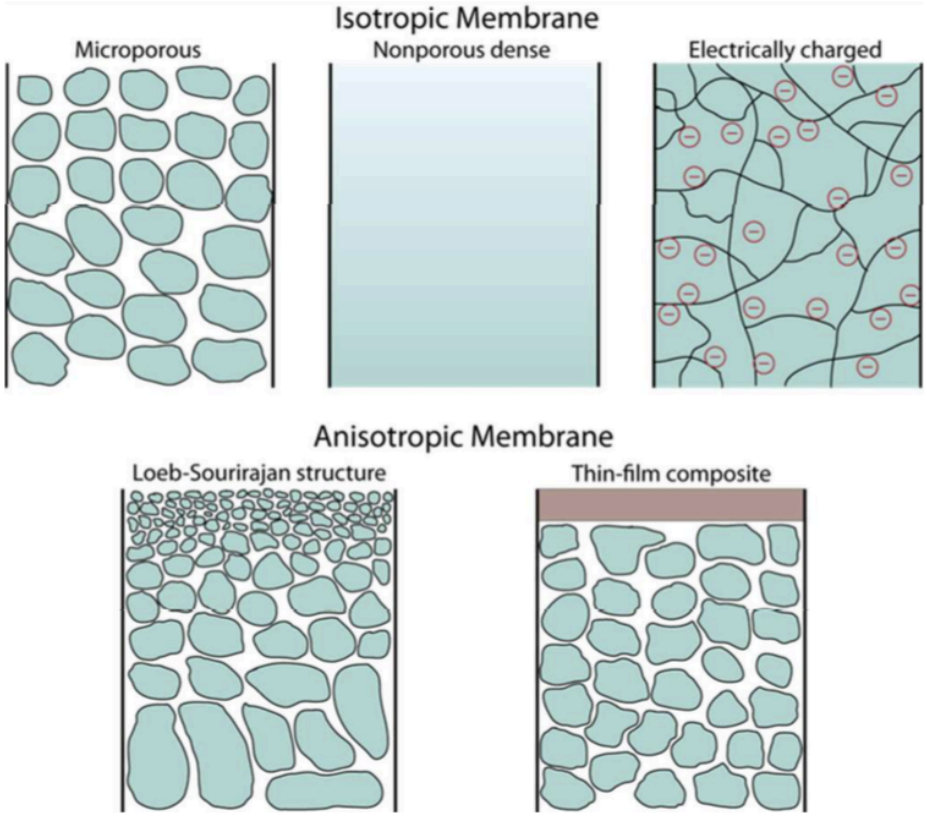


Figure 2.1 Schematic illustration of various classes of membranes [36].

Membrane modules can be prepared as hollow fiber, flat sheet, spiral wound and tubular configurations. Of these, hollow fiber membranes have received notable attention due to their large surface area per volume and high packing density which result in faster mass transfer [6, 37]. Membrane configurations are given in Figure 2.2.

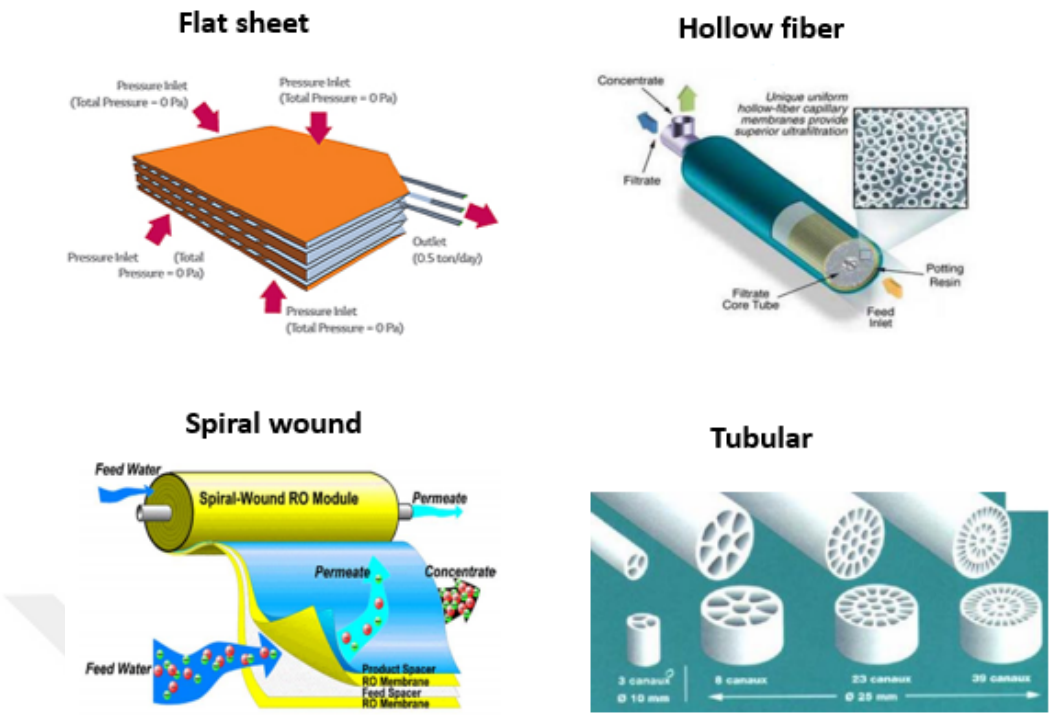


Figure 2.2 Schematic representation of membrane configurations.

Separation with hydrostatic pressure effect is common property of membrane filtration processes. MF process removes particles or biological entities in the 0,025 µm to 10,0 µm range. UF process separates smaller particles and dissolved molecules from fluids. On the other hand, NF and RO systems have been used to purify tap water to distilled water quality separating salts and small molecules from low molecular weight solutes [38]. Among these methods, UF is the most frequently used for wastewater treatment owing to its easy control and maintenance and relatively low cost than NF and RO systems [3-5]. Schematic illustration of membrane filtration spectrum is shown in Figure 2.3.

Comparison of types of membrane systems are given in Table 2.2 [2].

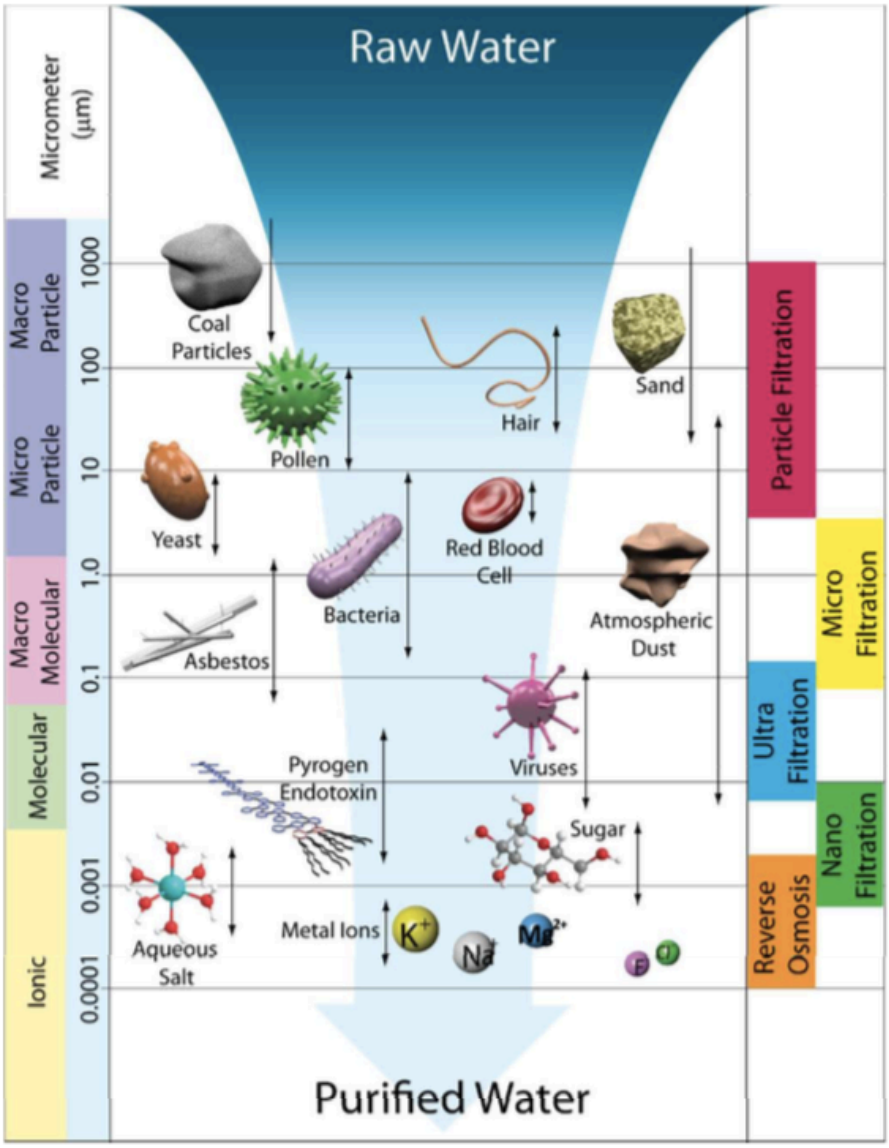


Figure 2.3 Schematic illustration of membrane filtration spectrum [36].

Table 2.2 Comparison of types of membrane systems [2].

Parameter	Microfiltration	Ultrafiltration	Nanofiltration	Reverse Osmosis
Pore size (µm)	0.01-1.0	0.001-0.01	0.0001-0.001	<0.0001
Molecular weight cut-off (Da)	>100,000	1,000-300,000	300-1,000	100-300
Operating pressure (bar)	<2	1-10	5-35	15-150
Materials	Ceramics PP, PS, PVDF	Ceramics PS, PVDF, CA Thin film composite	CA Thin film composite	CA, PS
Configuration	Tubular Hollow fiber	Tubular Hollow fiber Spiral wound Flat sheet	Tubular Spiral wound Flat sheet	Tubular Hollow fiber Spiral wound Flat sheet
Materials removed	clay, bacteria, viruses, suspended solids	proteins, starch, viruses, colloid silica, organics, dyes, fats, paint solids	starch, sugar, pesticides, herbicides, divalent anions, organics, BOD, COD, detergents	metal cations, acids, sugars, aqueous salts, amino acids, monovalent salts

2.2 Some Basic Terms for Hollow Fiber Ultrafiltration Membranes

- Dope Solution: Homogeneous thermodynamically stable polymer solution formed by polymer, additives (organic, inorganic particles, non-solvent) and solvent mixture [39].
- Bore Fluid: Kind of diluent that is used to prepare hollow fibers. Additionally, the inner surface of the hollow fiber membrane differs from the outer surface.
- Air gap: influences molecular chain orientation, solvent evaporation in the air, elongational stress, gravity and crystallization rate
- Coagulation bath: Coagulant chemistry and temperature determines the outer surface morphology of membranes. It can be either water, methanol or ethanol mixture [40].

- Cross-flow: Feed flow and filtration flow direction have a 90 degrees angle.
- Dead-end: the complete feed low is forced through membrane and the filtered matter is accumulated on the surface of the membrane. The flow of water is perpendicular to the membrane surface [38].
- Flux: Flow rate which is passing through membrane's specific surface area in a defined time ($L/m^2.h$)
- Hydraulic Permeability: Measure of the volume that can pass through membrane within a defined surface area, time and pressure ($L/m^2.h.bar$)
- Molecular weight cut-off: The minimum molecular weight of a solute to obtain a rejection of 90% in a membrane separation process. MWCO is expressed by daltons and determined by molecular weights of materials with different molecular weights e.g. albumin, dextrans [40].
- Contact angle: The contact angle formed between the liquid-gas tangent and membrane-liquid boundary determine hydrophilic-hydrophobic properties of the membrane [41].
- Bubble point pressure: The bubble point method determined the membrane pore size and pore size distribution indicating the pressure required to force an air bubble through a pore [42].
- Feed water: Flow contains dissolved or undissolved matters, suspended solids, colloidal matters, bacteria, virus that supplies modules. It can be wastewater, surface water, ground water.
- Permeate: Flow contains penetrants that leaves modules.
- Fouling: Membrane performances decrease because of the deposition of suspended or dissolved solids on external surfaces and pore openings or within its pore [43].

CHAPTER 3

MEMBRANE FABRICATION METHODS

There are various methods used in polymeric membrane fabrications. The selection of a fabrication technique majorly depends on the polymer type and required membrane morphology. Phase inversion, interfacial polymerization, stretching, sintering, track-etching, and electrospinning are the most important methods used for membrane production [1, 15]. Among these, the most frequently used method in all kind of morphologies of membranes is phase inversion process which involves a transformation of firstly homogenous polymer solution into a solid state in controlled manner. Table 3.1 summarizes preparation methods of polymeric membranes [15, 30].

Table 3.1 Preparation methods of polymeric membranes [15].

Preparation method	Mechanism
Phase inversion • Non-solvent induced phase separation (NIPS) • Thermally induced phase separation (TIPS) • Vapor induced phase separation (VIPS)	• Phase separation is induced by the exchange of the solvent in polymer solution with the non-solvent from the coagulation bath. • Phase separation is induced by the temperature change. • Phase separation is induced by the penetration of non-solvent vapor into the solution
Solution-casting	Polymer solution is cast and evaporated.
Casting-freezing	Polymer solution is cast and frozen at a temperature lower than solvent's freezing point.
Electro-spinning	Polymer solution is injected through the nozzle onto the electrode or collector to prepare nano-fibers.
Sintering	Polymer films are sintered.
Stretching	Polymer melts are subject to orientation.
Track etching	Dense polymer films are exposed to radiation to create holes for permeation.

3.1 Phase Inversion

There are several methods for the transformation of polymer solution to a solid state:

- Immersion precipitation (IP): The polymer solution is immersed in a non-solvent coagulation bath. Because of the exchange of solvent from polymer solution and non-solvent from coagulation bath, demixing and precipitation take place. The most frequently used method is IP.
- Thermally induced phase separation (TIPS): In this method when the temperature decreases, the solvent quality decreases. Polymer solution is prepared at an elevated temperature and then cooled down.
- Evaporation induced phase separation: The polymer solution is prepared in a solvent or in a mixture of a non-solvent. When the solvent evaporates, precipitation or demixing occurs.
- Vapor induced phase separation: The polymer solution is exposed to an atmosphere containing non-solvent (water) thus absorption of water causes precipitation [6, 44].

Schematic representation of three diffusion induced phase inversion processes are shown in Figure 3.1 [45].

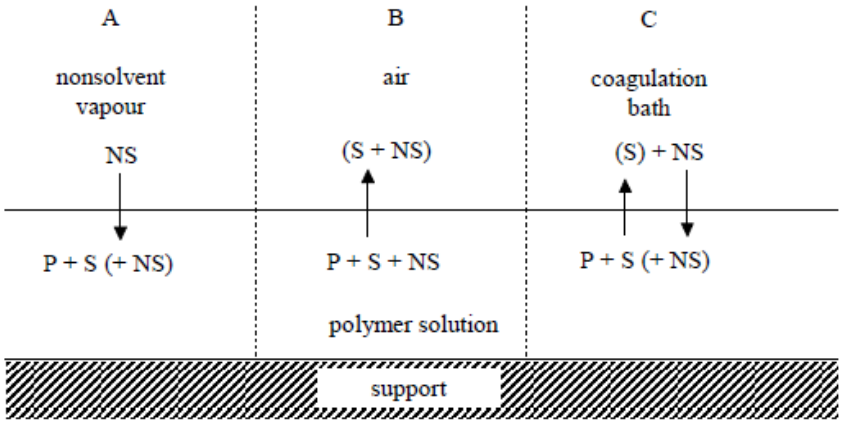


Figure 3.1 Schematic representation of three DIPS processes: A) precipitation with non-solvent vapor, B) evaporation of solvent, C) immersion precipitation (P: polymer, S: solvent, NS: non-solvent) [45].

A typical three component phase diagram for preparing membranes is shown in Figure 3.2 [46].

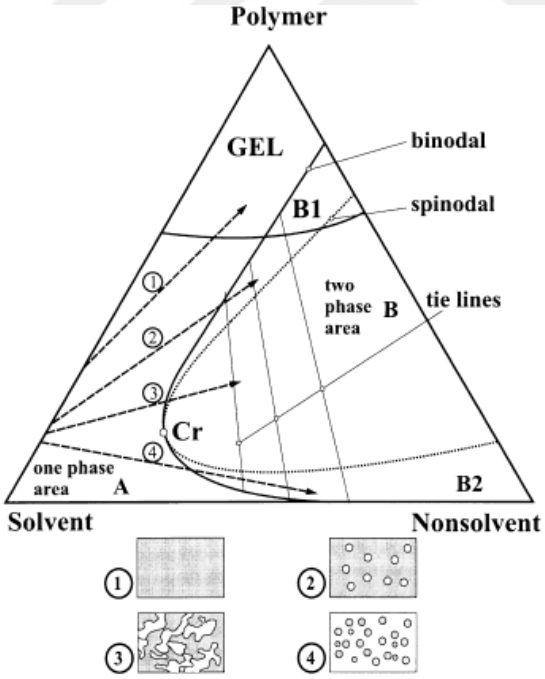


Figure 3.2 Schematic diagram of ternary phase diagram of a polymer/solvent/non-solvent system with various compositions [46].

Phase inversion method involves transition of two different phases. These are liquid-liquid phase separation and precipitation. At first homogenous polymer solvent mixture was thermodynamically stable. Demixing process takes place if the binodal is reached liquid-liquid. For the reason that non-solvent took place resulting instability of polymer solution [30].

Main polymers used in membrane formation via immersion precipitation and their advantages and disadvantages are given in Table 3.2 [1].

Table 3.2 Main polymers used in membrane formation via immersion precipitation [1].

Polymer	**Advantages**	**Disadvantages**
CA	• Hydrophilicity • Flexibility in fabrication • Low cost	• Low thermal resistance (<30 °C) • Low chemical resistance, pH range (2-8) • Poor resistance to chlorine
PS and PES	• High thermal resistance (up to 75 °C) • Wide pH tolerances (1-13) • Good chlorine resistance • Flexibility in membrane fabrication (wide range of pore size)	• Low operating pressure limits • Hydrophobicity
PVDF	• High mechanical characteristics • High mechanical strength and chemical resistance • High thermal stability (up to 75 °C)	• Hydrophobicity
PA	• Wide pH tolerance • High thermal stability • High mechanical properties	• Poor chlorine resistance

Figure 3.3 shows comparison of oxidation and chlorine resistance of different polymeric membrane materials. Mechanical properties of common membrane materials were given in Figure 3.4.

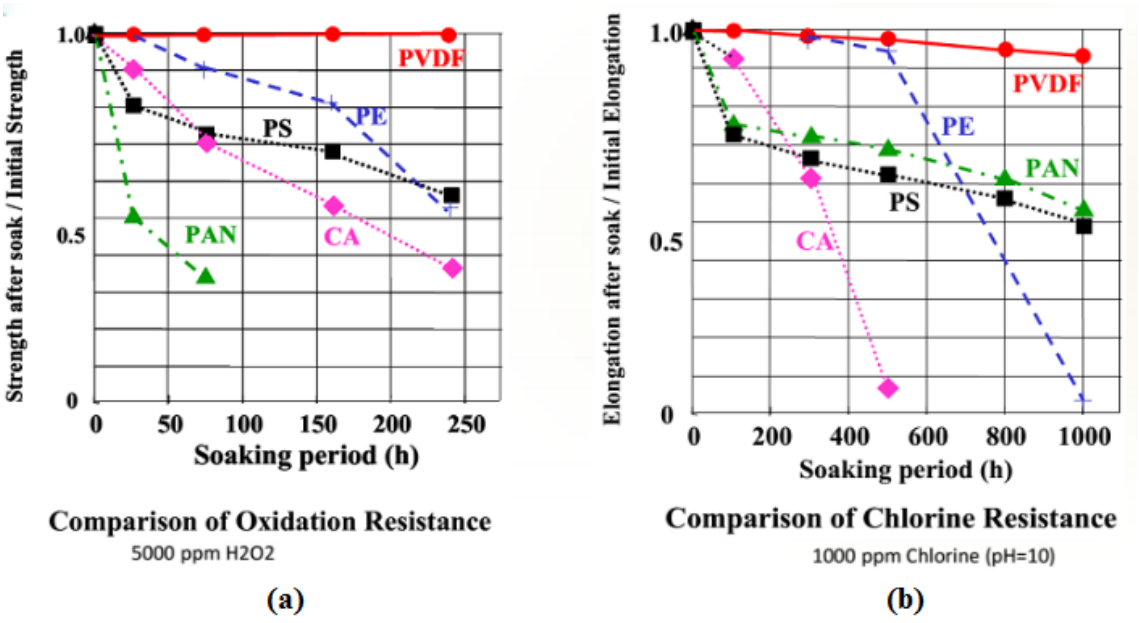


Figure 3.3 Comparison of polymers (a) oxidation resistance, (b) chlorine resistance.

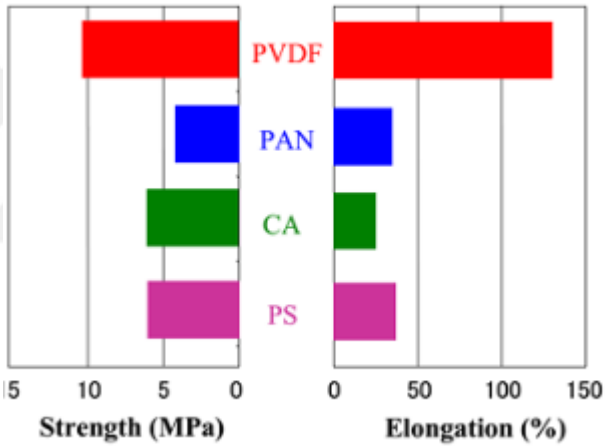


Figure 3.4 Comparison of strength and elongation percent of polymers.

3.2 Hollow Fiber Membrane Fabrication

In 1966, Mahon and the group Dow Chemical first developed hollow fiber membrane. [47]. And then Dow, Monsanto, Du Pont have been leading representatives of membrane technology [31]. Compared to flat sheet, tubular and spiral wound membranes, hollow fiber configuration is the superior of membrane since it has the following advantages: (i) the increased surface area per unit volume of membrane module, which renders enhanced efficiency; (ii) easy cleaning, handling, and preparation; (iii) consistent results; (iv) it does not need any mechanical support [48, 49].

The PI of hollow fiber membranes is more complicated compared with the flat sheet membranes. There are various factors controlling hollow fiber morphology such as dope formulation, internal and external coagulant, spinneret design, air-gap distance, moisture, elongational stresses. Differently from flat sheet dope formulation, for hollow fiber spinning, high polymer concentration is essential resulting much more complex PI process. Furthermore, hollow fiber production comprises internal and external coagulants. Inner skin structure is controlled by internal coagulant while the outer skin structure is controlled by external coagulant [50]. Figure 3.5 illustrates hollow fiber types [31].

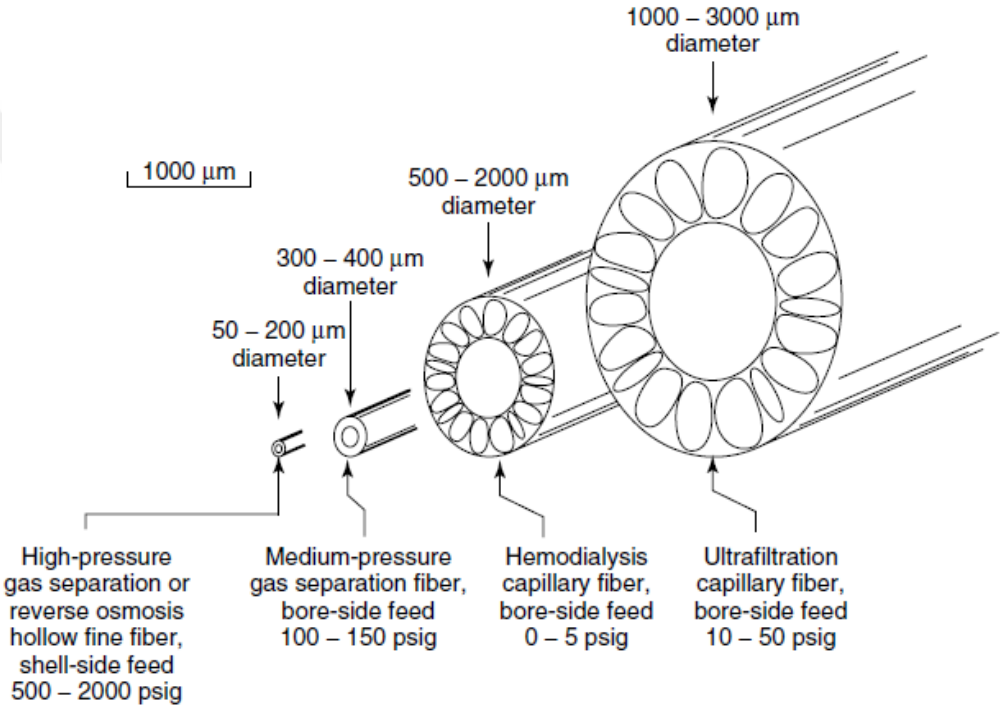


Figure 3.5 Schematic of the principal types of hollow fiber membranes [31].

The spinning process are commonly used to fabricate polymeric hollow fiber membranes using small air gap, high take up speed.

Schematic diagram of area nearby the spinneret and the formation of nascent hollow fiber during phase inversion is shown in Figure 3.6 [50].

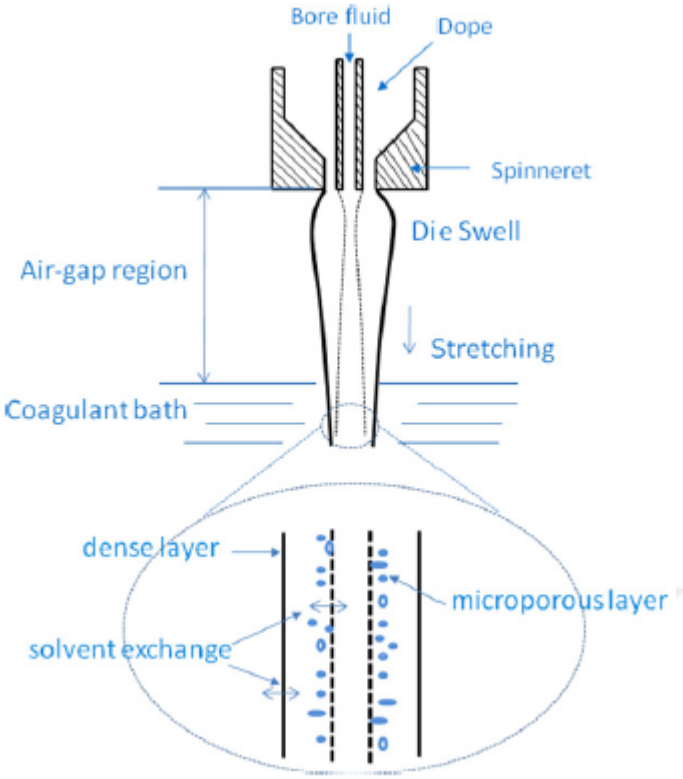


Figure 3.6 Schematic diagram of area nearby the spinneret and the formation of nascent hollow fiber membrane [50].

3.3 Phase Inversion Fabrication Methods for Hollow Fiber Membranes

Dry-wet spinning have been frequently used technique for hollow fiber membrane fabrication. Steps of the hollow fiber spinning process:

- Measurement of polymer solutions and bore liquids.
- The spinning solution is pumped through a spinneret.
- Inner side of the fiber is coagulated following the meeting of bore fluid with the dope.
- In the air gap area, the solvent is vaporized from the external surface of the fiber and moisture-induced phase separation occurs.
- The take-up unit initiate a stretching of fibers with gravity and elongational forces.
- The coagulation bath realizes phase inversion process and solidification of fiber wall.
- Post-treatments may be required for the purpose of eliminating solvents and control pore size, post-treatments may be required [50].

Wienk et al. revealed that vapor penetration of non-solvent at the outer surface in the air gap, immersion precipitation at the outer surface and immersion precipitation from the inside are three steps of phase inversion process. The most important parameter affecting outer surface pore structure of hollow fibers is air gap distance [51]. Qin et al. prepared various dope compositions with different viscosities and investigated the viscosity effect on the hollow fiber membrane performances [52]. Schematic drawing of the spinning machine is given in Figure 3.7.

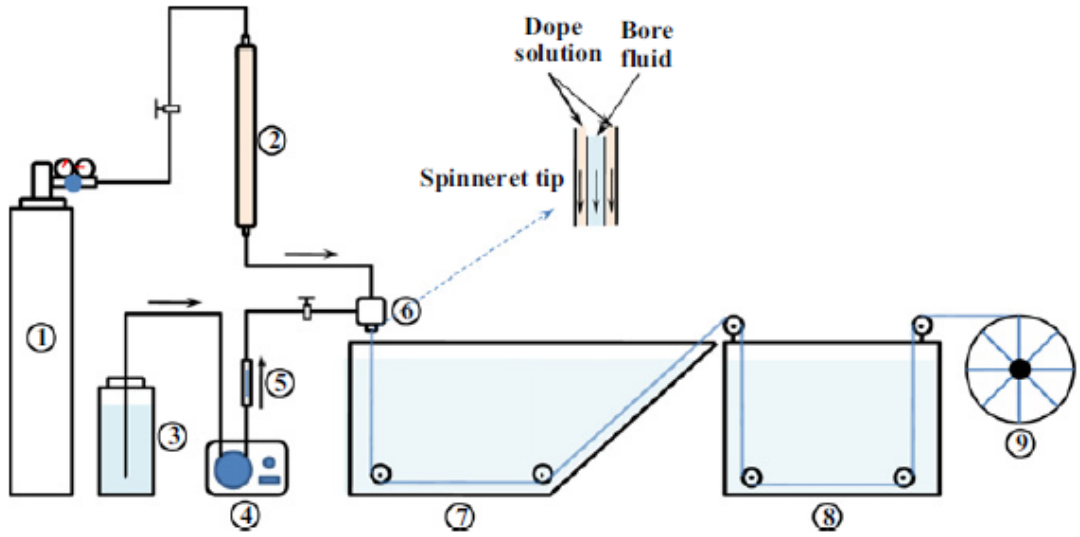


Figure 3.7 (a) Schematic illustration of the spinning machine. (1: N_2 gas cylinder, 2: dope tank, 3: bore liquid tank, 4: gear pump, 5: flow meter, 6: spinneret, 7: coagulation bath, 8: washing bath, 9: winder) [53].

3.4 Spinning Parameters

Hollow fiber membrane application is determined by chemical, mechanical and physicochemical properties of the membrane material, pore size distribution and morphology of the membrane [50]. There are various factors influencing membrane structure such as as type of polymer, solvents, additives, bore liquid, air gap, viscosity, dope extrusion rate, coagulation bath and take-up speed [54].

3.4.1 Type of Polymer

For pressure driven processes, desired membrane material properties are thermal, chemical, mechanical stability and hydrophilicity. PVDF, PES, PS, PAN and PTFE are the most used membrane materials owing to their superior properties like high thermal, chemical, mechanical stability. However, these materials can be susceptible to adsorption

of several dissolved materials from feed water due to their hydrophobic property [7-9]. Thus, high hydrophilic property is essential for membrane fouling resistance [55]. High polymer concentration can prevent the development of macrovoids in membranes. Therefore, the viscosity is considered as an important parameter on fiber morphology and porosity [50].

3.4.2 Type of Solvents

PVDF can be dissolved in some polar solvents with a high boiling point, such as N,N-Dimethylacetamide (DMAc), N-Methyl-2-Pyrrolidone (NMP), Dimethylsulfoxide (DMSO), and N,N-Dimethylformamide (DMF), due to the polar property derived from the alternative arrangement of $–CF_2–$ and $–CH_2–$ groups [56]. Bottino et al. studied the influences of solvents by using eight different solvents including DMAc, DMF, DMSO, NMP, hexamethylphosphoramide (HMPA), tetramethylurea (TMU) and triethylphosphate (TEP). It was found that the water flux, water content, membrane thickness and void volume per unit area was influenced by solvent type [57]. Yeow et al. also prepared PVDF flat sheet membranes by using different solvents such as DMAc, DMF, NMP and TEP and compared the effects of additives like ethanol, glycerol, lithium chloride (LiCl) and water using the PVDF/DMAc system. SEM pictures of the cross sections of membranes using different solvents are shown in Figure 3.8. In their previous study, DMAc was found the most effective solvent in fabrication PVDF membranes [58].

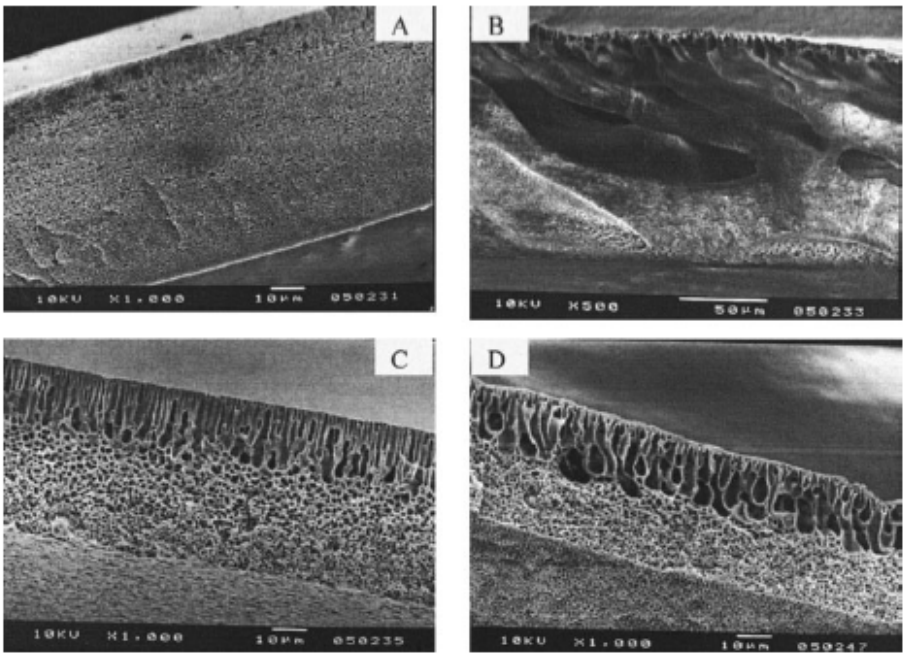


Figure 3.8 SEM pictures of the cross sections of membranes cast from polymer dope containing 15% PVDF and different solvents: (A) TEP, (B) NMP, (C) DMF, and (D) DMAc [58].

Wu et al. prepared PVDF/PES blend membrane and the results showed that using DMAc as solvent in polymer solution provided the maximum PWF and minimum retention to BSA [59].

3.4.3 Type of Additives

In order to control the morphology, there are various additives used in the fabrication of PVDF hollow fiber membranes like Polyvinylpyrrolidone (PVP) [59-61], Polyethylene glycol (PEG) [62-64], LiCl [56, 65, 66], lithium perchlorate ($LiClO_4$) [67] and glycerol as a non-solvent [58, 68]. Lang et al. investigated the precipitation kinetics, morphologies, permeability performances and crystallization behaviors of PVDF hollow fibers using four types of PVP with different molecular weight. The results showed that with the augmentation in molecular weight, pure water permeability (PWP) of the membranes increased at first and then decreased [61]. Wongshitphimon et al. studied the effects of PEG with different molecular weights and LiCl and also investigated the coagulation bath temperature on the fabrication of Polyvinylidene fluoride-co-hexafluropropylene (PVDF-HFP) hollow fiber membrane [64]. The addition of PVP and PEG as a pore forming additive favors macrovoid formation of PVDF membranes increasing the dope solution viscosity. Also, using LiCl as an additive can increase permeability performance but with

a failure in mechanical properties [58]. The addition of glycerol in the dope solution leads the initial composition of the solution closer to the binodal point of ternary phase diagram [58].

3.4.4 Air Gap

Air gap length have an important influence on hollow fiber structure and resultant performances [69, 70]. In order to increase the PWP of PVDF membranes and form a thinner skin layer, short air gap length is desired [71]. Khayet et al. investigated the effect of air gap on both interior and the exterior structure of PVDF membranes. The results showed that increasing air gap distance leads thinner and denser sponge-type cross section within membrane structure owing to a greater molecular orientation and chain package. Thus, PWP decreases and the solute rejection increases. SEM pictures of the PVDF hollow fiber membranes are shown in Figure 3.9 [69].

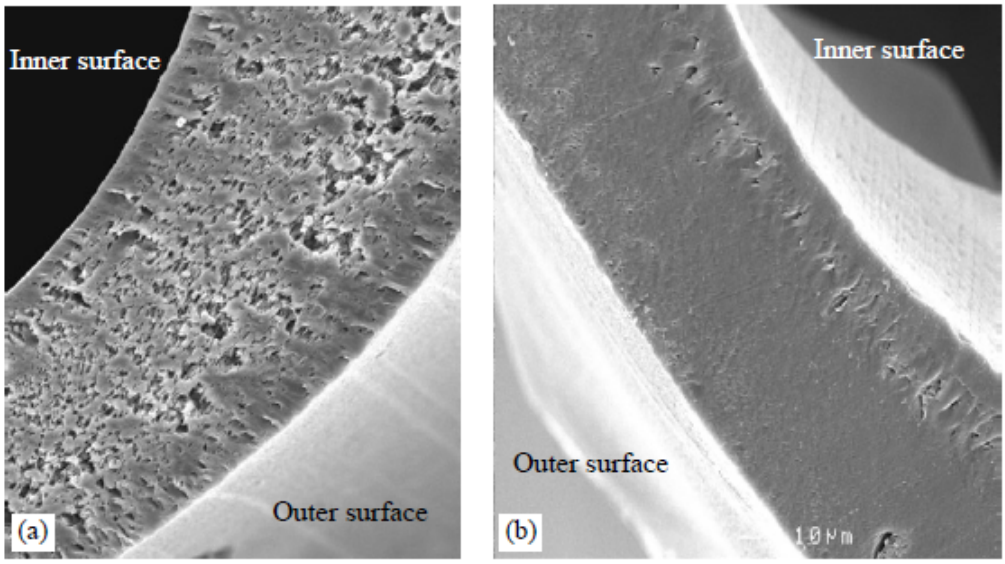


Figure 3.9 Cross-sectional SEM pictures of the PVDF hollow fiber membranes. (a) air gap distance: 5cm (b) air gap distance: 80 cm [69].

Besides with the increase of the air gap length (< 5 cm), the mean nodule sizes of the inner and the outer surfaces increase [69].

Peng et al. revealed that commercial hollow fiber membranes are fabricated from a hot spinneret with a short air gap length and a high take-up speed [50].

3.4.5 Viscosity of the Polymer Solution

Macrovoids formed in membranes are unaccepted because they can lead a reduction of mechanical properties of membranes deteriorating during separation processes [72]. In order to prevent macrovoid formation, solutions with high polymer concentrations and high viscosity components such as pore forming additives, non-solvent additives and inorganic nanoparticles can be used [50]. With regard to its hydrophilic nature, PVP has been added to dope solution to enhance the liquid-liquid demixing process during precipitation process. PVP promotes the non-solvent influx upon immersion in the coagulation bath and the formation of larger finger-like macrovoids in PVDF hollow fiber membranes [6]. Wang et al. studied the influences of polymer concentration, molecular weight of PVP on PVDF based hollow fiber performance and morphology. Composition and viscosity of PVDF solutions are given in Table 3.3 [71]. In addition to dope components, dope temperature also influences the viscosity value and shear rate of the dope solution system. The viscosity values are reduced with an increase in temperature. Yeow et al. revealed the effect of the polymer solution temperature on the PVDF membrane morphology using various additives such as glycerol, ethanol, LiCl, $LiClO_4$ and water. The results revealed that gelation was suppressed by using glycerol. With an increased dope temperature, dope and coagulant suppressed crystallization and liquid-liquid demixing could occur before gelation [58].

Table 3.3 Composition and viscosity of PVDF solutions [71].

Formulation	**PVDF (wt.%)**	**DMAc (wt.%)**	**PVP (wt.%)**	**η (cp) 25 °C**
1	20	73	2 (24K)	1620
2	22	70	8 (24K)	2500
3	20	73	7 (360K)	12000
4	20	73	7 (10K)	1130
5	25	73	2 (10K)	2000
6	25	70	5 (10K)	3190

3.4.6 Bore Fluid

The chemistry, compositions and flow rate of the bore fluid are considered as important parameters to control the internal skin morphology of hollow fiber membranes [73]. Kong et al. investigated the influences of the internal and external coagulants on the PVDF hollow fiber membranes by using ethanol, water and ethanol/water mixture as a bore fluid. The results showed that using the ethanol could eliminate the inner skin with a higher PWP performance of resulted membrane [74]. Wang et al. also compared water with ethanol as a bore liquid within PVDF hollow fiber membrane. It was found that using water made hollow fiber with circular lumen and higher PWP [75]. Khayet et al. revealed that a sponge-like membrane structure formed when a water/ethanol mixture (50% v/v) as bore fluid [76]. Wongchitphimon et al. used water, NMP and NMP/water mixture as a bore fluid. While a combination of NMP/water was utilized, coagulation bath temperature was varied from 10, 25 to 40 °C as shown in Figure 3.10 [64].

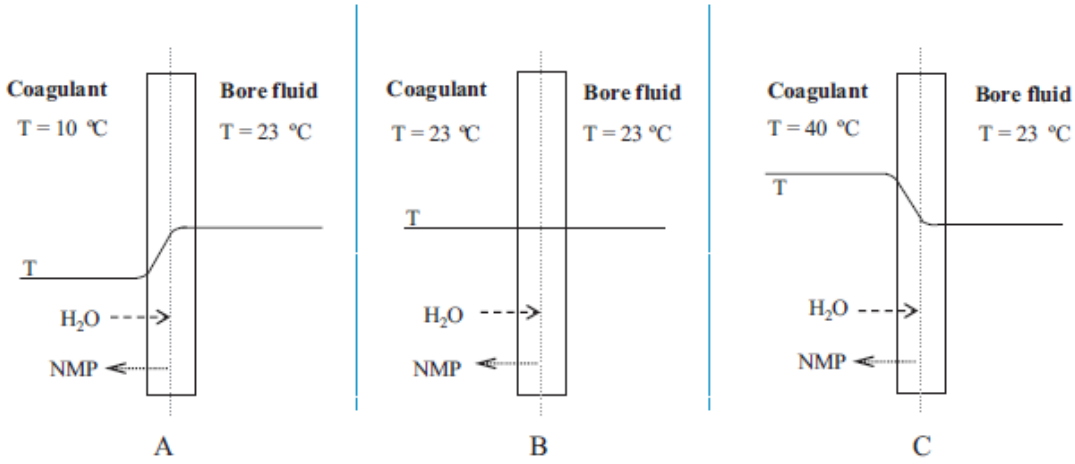


Figure 3.10 Schematic temperature profile for the fabricated membrane with difference coagulation bath temperatures: (A): 10 °C; (B): 23 °C and (C): 40 °C [64].

3.4.7 Coagulation Bath

Crystallization of the PVDF membrane fabricated by immersion precipitation is also influenced by composition and temperature of coagulation bath. Water as a coagulation bath causes quick liquid-liquid demixing process. Accordingly, the asymmetric membrane structure including finger-like macrovoids can be formed [6]. Bottino et al. investigated effects of coagulation medium on the morphology, performances of sulfonated PVDF membranes. Mixtures of water, methanol, ethanol, glycerol and solvent were used as external coagulants. Using water was generated larger voids compared to

using alcohol mixtures [77]. Deshmukh et al. also investigated the effects of coagulation bath composition on PVDF hollow fiber membrane structure increasing ethanol concentration from 0% to 50% in water bath [78]. Buonomenna et al. fabricated PVDF membranes and examined the effects of various parameters such as precipitation temperature, exposure time before immersion in the coagulation bath and coagulation bath medium in morphology, crystalline structure and properties of PVDF membranes [79].

The morphology and crystallinity of PVDF membrane is strongly influenced by precipitation temperature. At high coagulation bath temperatures, finger-like membrane structures can occur while at low temperatures, sponge-like structures can form [6]. Yeow et al. studied the effects of coagulation bath temperature on PVDF hollow fiber membrane performance using water as a coagulant. The results showed that high temperature leads to bigger pore size within membrane structure with higher PWP compared to that formed at lower temperature [80]. Cheng also studied the effect of coagulation bath temperature by varying from 25 °C to 85 °C. At high temperatures asymmetric structures were formed while at low temperatures uniform membrane structure was developed due to the liquid-liquid demixing process [81]. Wang et al. revealed that at low temperatures (15-25 °C), the liquid-liquid demixing induces by kinetics of the solvent out flux and water influx were slow and gelation governed membrane formation mechanism. On the other hand, at high temperature (60 °C) gelation could suppressed but demixing were the dominate mechanism. Figure 3.11 shows SEM pictures of the PVDF membranes prepared in various bath temperatures [82].

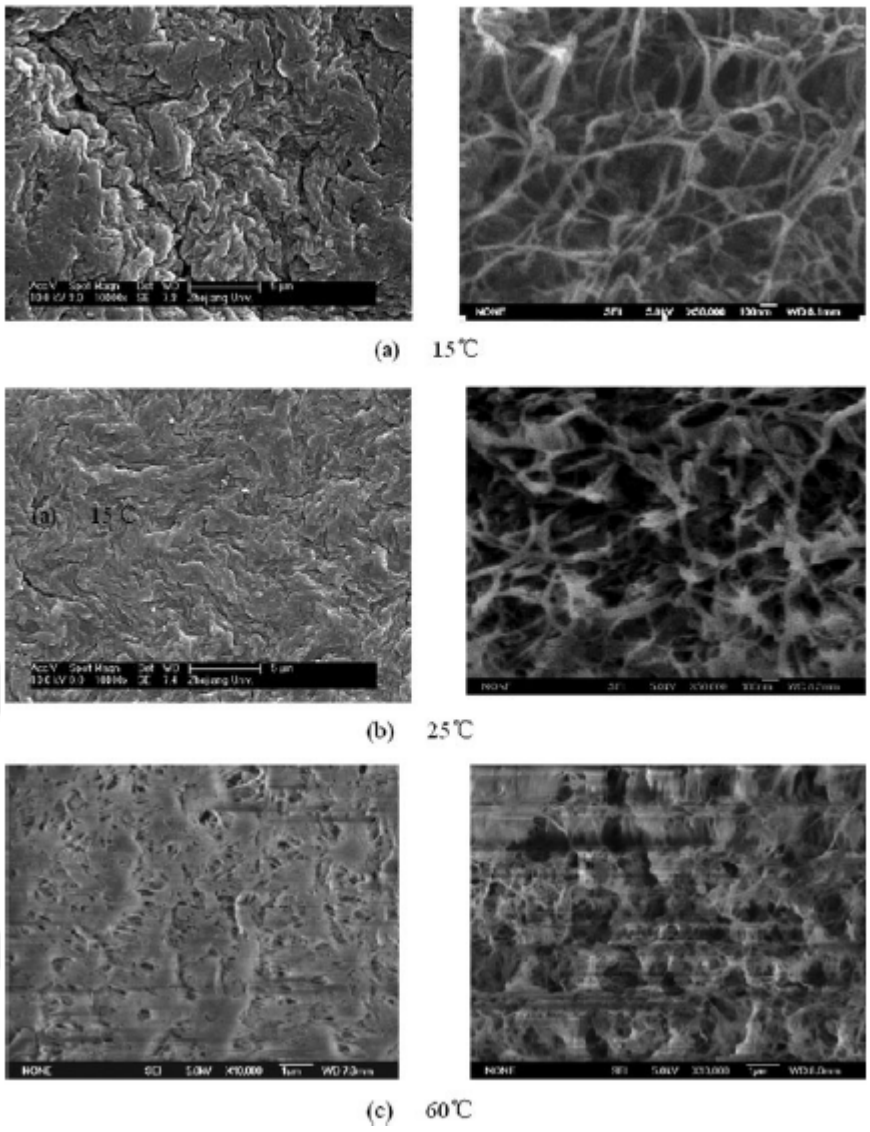


Figure 3.11 SEM micrographs of the PVDF membranes prepared by immersion in (a) 15 °C, (b) 25 °C, and (c) 60 °C deionized water, left: top surface, right: cross section [82].

3.4.8 Take-up Speed

The hollow fiber surface structure and cross-sections are also influenced by take-up speeds. With an increase in take-up speed, porosities within membrane structure may be reduced preventing macrovoid formation [54]. Wang et al. revealed that macrovoids within hollow fiber membranes can suppressed and even be removed at elevated elongational draws. As shown in Figure 3.12, if there is no elongational draw for hollow fiber membranes, a clear double-layer structure of macrovoids can be observed. The results showed that doubling the take-up speed caused reduction of finger-like macrovoids [83].

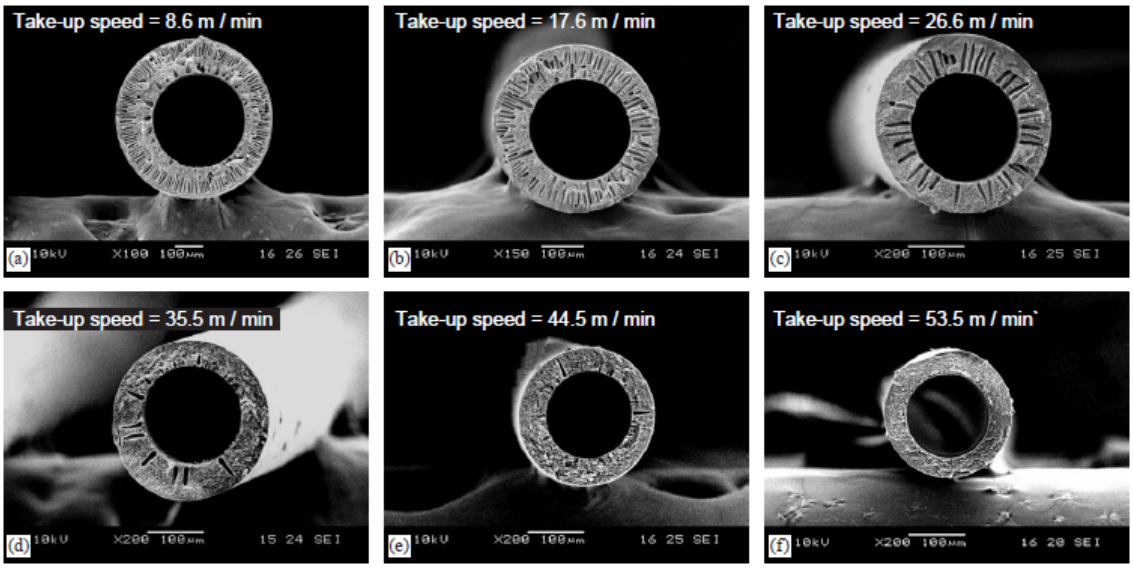


Figure 3.12 Effects of elongational draw ratio on the morphology of dry-jet wet-spin PES single-layer hollow fiber membranes [83].

In another study, their group examined the development of macrovoid-free hollow fiber membranes determining critical polymer concentration, critical take-up speed and critical air gap. As shown in Figure 3.13, the macrovoids could be prevented by increasing elongational stretch. In addition, when the take-up speed increased from 10 to 50 m/min, the inner structure of the membrane changed from close-cell structure to an open-cell structure [72].

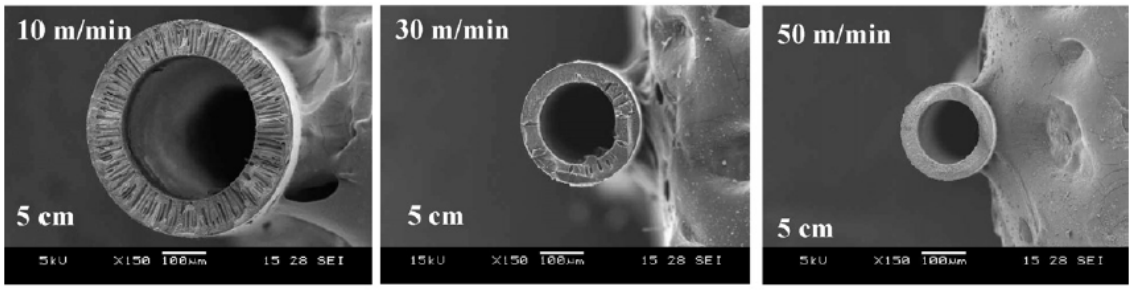


Figure 3.13 SEM cross-section images of P84 polyimide membranes with various take-up speeds [72].

Chou et al. investigated the effect of take-up speed on the mechanical properties, morphology, thermal properties, PWP, retention and surface characterization of CA ultrafiltration hollow fiber membranes. The results showed that retention decreased, PWP, tensile strength and breaking elongation increased [84].

3.5 Effect of Post Treatment of Hollow Fiber Membranes

PVP blend membranes were treated with sodium hypochlorite (NaOCl) solutions in order to enhance the membrane performances [85-89]. Roesink et al. found for the first time that sodium hypochlorite treatment of polyetherimide (PEI)/PVP microfiltration membranes leaded a higher PWP flux decreasing PVP content within the membrane [90]. Wienk et al. revealed the reaction mechanism of hypochlorite with PVP with two explanations:

1. The chain scission of the polymer occurs when PVP reacts with NaOCl as shown in Figure 3.14. PVP can be took off from the membrane matrix when the molecular weight of PVP decreased.
2. The ring opening of the pyrrolidone ring of the PVP occurs when PVP reacts with NaOCl with an oxidation of PVP in alkaline solution as shown in Figure 3.15 [91].

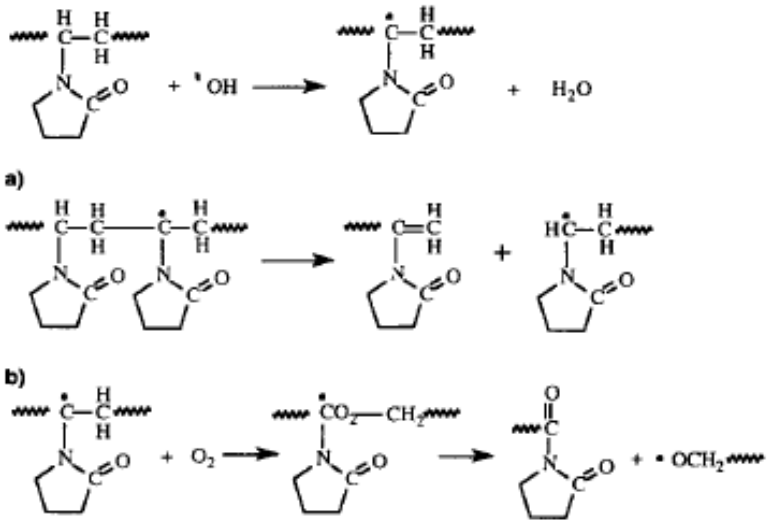


Figure 3.14 Chain scission of PVP via radical reactions: (a) disproportionation and (b) oxidative reaction [91].

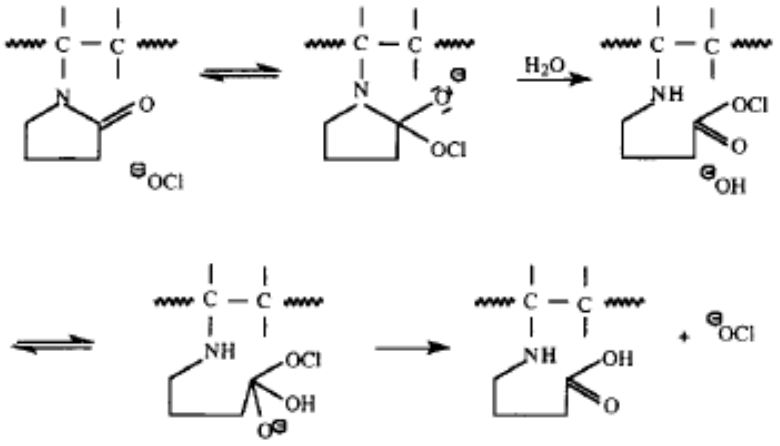


Figure 3.15 Reaction mechanism of PVP with NaOCl solution [91].

As a result of their study the sodium hypochlorite treatment of PES/PVP ultrafiltration membranes leaded increase in pure water flux with an increase in treatment time but BSA rejection remain constant as demonstrated in Figure 3.16 [91].

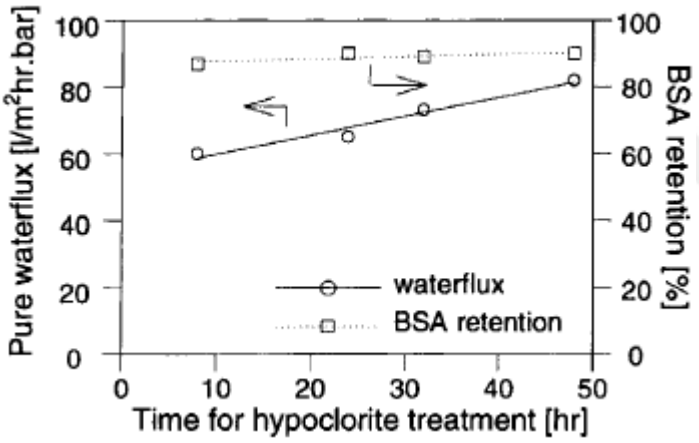


Figure 3.16 Pure water flux and retention for a 1 g/L BSA solution of PES/PVP ultrafiltration membranes treated with a 4000 ppm hypochlorite solution for different times [91].

Gao et al. investigated effects of NaOCl solutions at different times and concentrations on the morphology, separation performance as well as fouling characteristics of PVDF membranes [92]. Abdullah et al. also compared the effect of NaOCl exposure doses and concentrations on physical/chemical characteristics of PVDF/PVP hollow fiber membranes. SEM images revealed that due to the exposure of NaOCl, the porosity and pore size of the membrane increased with an increase in concentration of NaOCl as given in Figure 3.17 [93].

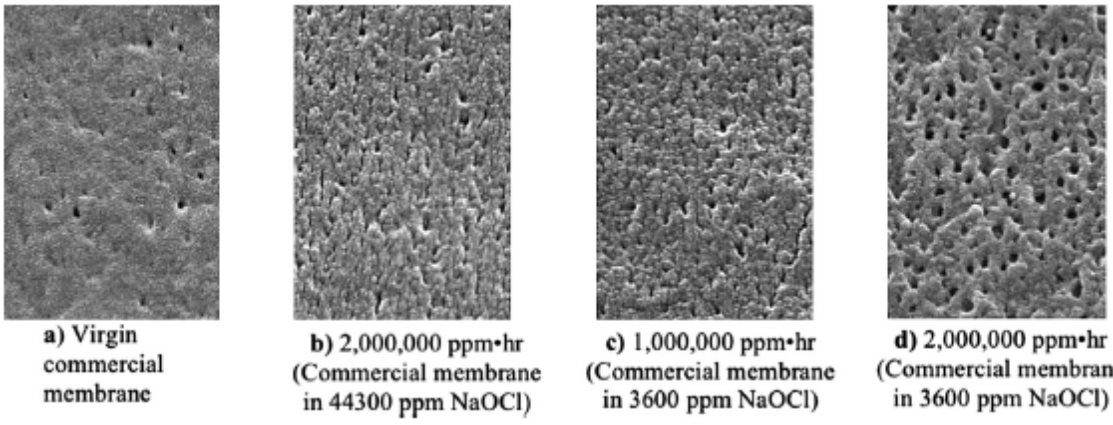


Figure 3.17 Typical SEM images of virgin membrane (a) and membranes exposed to different exposure doses and concentrations of sodium hypochlorite (b, c and d) [93].

Hollow fiber membranes can be post-treated in glycerol/water solutions as a non-solvent exchange and then they are dried at room temperatures to decrease fiber shrinkage pore collapse [51, 56, 94]. Wienk et al. placed hollow fiber membranes in a glycerol bath containing 10 wt.% glycerol in water after rinsing with water at 50 °C [44].

CHAPTER 4

MEMBRANE FOULING

Membrane fouling represents the undesirable accumulation of particles, colloids, macromolecules, salts on the membrane surface and in its pores. Various types of fouling can occur in membrane systems such as inorganic fouling or scaling, organic fouling and colloidal/biocolloidal fouling which depends on the membrane process and chemical nature of foulants [3, 10, 11]. The membrane fouling is considered as an early warning for drinking water production [95]. Membrane flux can be decreased either temporarily or permanently by fouling phenomenon. While the initial flux can be preserved by washing the membrane or by applying back pressures to the temporarily fouled membrane, it cannot restored for the permanently fouled membranes [55].

PVDF has been paid great attention by researchers and manufacturers because of its extraordinary characteristics including high mechanical properties, thermal stability, chemical resistance than other polymers [6, 14]. Nevertheless, high hydrophobic property of pristine PVDF membranes lead fouling during the filtration of aqueous solutions. Due to the adsorption of macromolecules within the pores, the performance of existing membranes can significantly reduce and result in high operation and maintenance costs required for the filtration process [6, 15].

Consequently, various reports of hydrophobic membranes have focused on the development of hydrophilicity using different modification techniques in order to improve the filtration processes [14]. Surface coating [96-103], surface grafting [104-108] and blending with hydrophilic agents [64, 65], especially nanoparticles such as TiO_2, SiO_2, Al_2O_3, CNTs, graphene and HNTs [16] have been widely used in order to increase hydrophilicity as well as antifouling property of UF membranes.

4.1 Membrane Foulants and Fouling Mechanisms

Membrane fouling is attributed to a both reversible and irreversible adjustment in membrane properties. Deposition of foulants on the membrane surface determines reversible fouling, whilst membrane pore-plugging by particles determines irreversible fouling [109].

The characteristics of foulants can be determined by several factors such as water composition, main constituents, water chemistry, membrane properties, temperature, mode of operation and hydrodynamic conditions. Therefore, membrane performance is potentially influenced by any factors that can change the hydrodynamic characteristics of membrane modules and the chemical characteristics of feed water. Consequently, the combined physical and chemical effects will determine the severity of fouling and the effective strategies required to control it [110]. Membrane fouling is divided into four categories:

1. Colloidal fouling
2. Biofouling
3. Organic fouling
4. Inorganic fouling [111].

4.1.1 Organic Fouling

The deposition of organic foulants in the internal structure and external areas of the membrane can cause fouling. The adsorption of organic foulants can be considered as major fouling mechanism. Polysaccharides, amino sugars, polyhydroxy aromatics, and proteins are strong foulants in natural organic matter (NOM) fractions [11]. NOM can be defined as a mixture of various particles, dissolved organic and inorganic constituents such as proteins, viruses, pesticides, herbicides, salts etc. presented in aqueous solutions [112, 113].

The organic fouling mechanism comprises membrane pore-blocking, pore-plugging and cake layer formation as shown in Figure 4.1 [11].

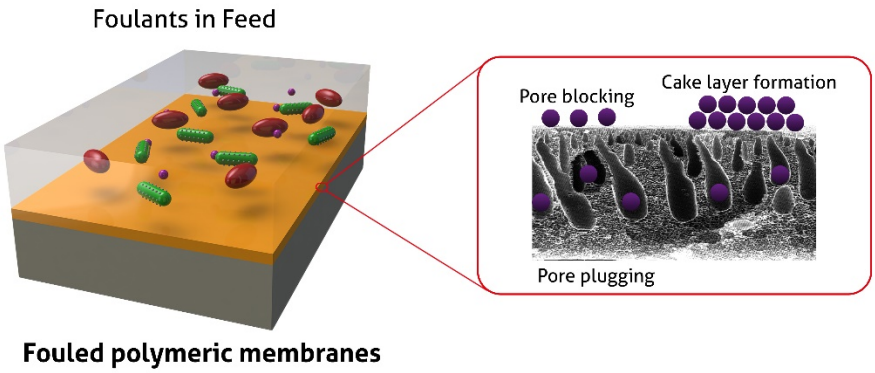


Figure 4.1 Schematic representation of organic fouling mechanism [11].

Bowen et al. explained the consecutive steps of membrane blocking in flux decline during MF as follows:

1. The smallest pores are blocked by all particles arriving to the membrane.
2. The inner surfaces of bigger pores are covered.
3. Some particles arriving to the membrane cover other already arrived particles while others directly block some of the pores.
4. Cake starts to be built [114].

Lee et al. investigated NOM fouling mechanism in MF/UF processes by employing chemicals and morphological analyses. The results indicated that membrane types determine the mechanisms of NOM fouling. For MF, it was found that pore plugging, pore blockage and cake formation were responsible for fouling that reduced pore size and increased rejection. In the case of UF, internal pore adsorption reduced the internal pore diameter and enhanced rejection, whilst in NF the fouling mechanism was mostly governed by cake deposition and concentration polarization [109, 115].

4.1.2 Biofouling

The involvement of biologically effective organisms defines the biofouling phenomenon which is a dynamic process of bacterial colonization, deposition and development. Consequently, the microbial biofilms on membrane surfaces can be formed [116, 117]. Figure 4.2 shows the schematic representation of the major stages occurring during biofilm formation on the membrane surface [118]. Organic and inorganic components may be eliminated by pre-treatment. However, biofouling have been considered as

"Achilles heel" of the process [13] which give rise a reduction of permeability, membrane lifetime and high operation expenses [12, 13].

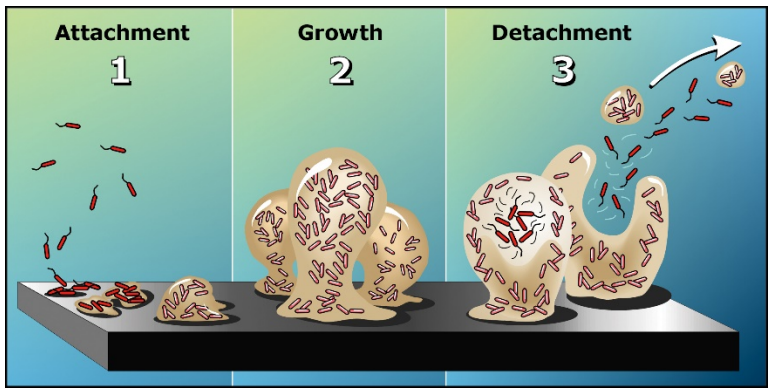


Figure 4.2 Schematic representation of biofilm formation on solid surface [118].

Roughness, which mainly influenced by membrane structure such as pore size and porosity, affects bacterial adhesion, and rougher surface facilitates bacterial adhesion. Hydrophobicity also strongly affects bacterial adhesion, and more hydrophobic surface facilitates bacterial adhesion [119]. Saeki et al. investigated the effect of hydrophobicity of polymers used in the preparation of water purification membranes on the dynamics of biofilm formation. It was found that uniform, flat, and thin biofilms were rapidly formed on the hydrophobic surface of PVDF. In contrast, the hydrophilic surface of poly(vinyl alcohol) (PVA) prevented bacterial adhesion and biofilm formation [120].

4.1.3 Inorganic Fouling

Inorganic fouling refers to the accumulation of inorganic solutes on the membrane surface which cause a decrease in membrane flux. The precipitation of inorganic ions is caused by the maximum amount of phosphorous and calcium and, to a lesser extent, aluminum and iron ions, which increase membrane scaling during permeation. Calcium can generate a more compact fouling layer on membrane surface, which in turn, decreases water flux [11]. A schematic illustration of bulk and surface crystallization from inorganic fouling is shown in Figure 4.3 [11] and Figure 4.4 [121].

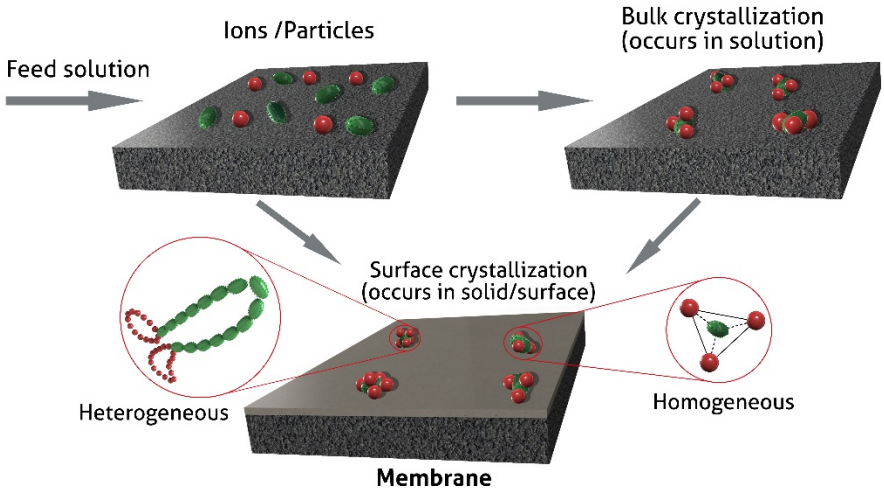


Figure 4.3 Schematic illustrations of bulk and surface crystallization from inorganic fouling [11].

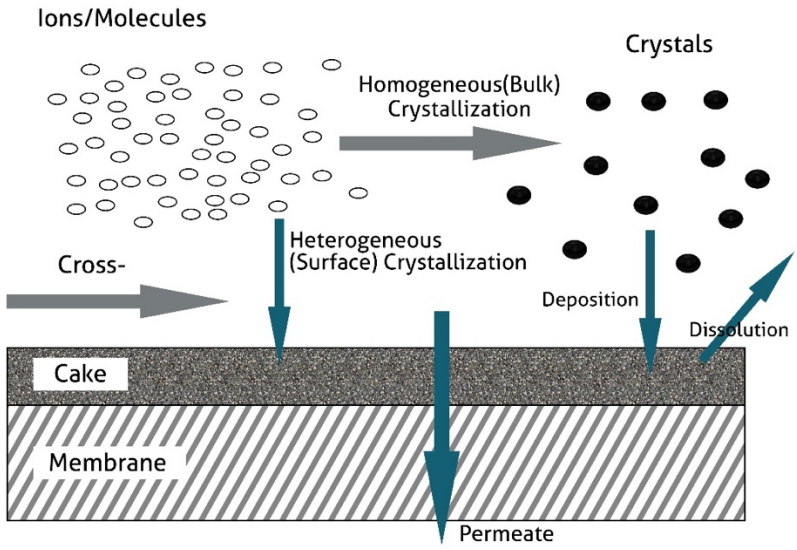


Figure 4.4 Schematic representation of inorganic scaling mechanism [121].

4.2 Mitigation of Membrane Fouling

The contact angle formed between the liquid-gas tangent and membrane-liquid boundary determines hydrophilic-hydrophobic properties of the membrane. A contact angle less than 90˚ determines hydrophilic behavior, whilst a large contact angle higher than 90˚ indicates that the membrane surfaces are hydrophobic as presented in Figure 4.5 [41].

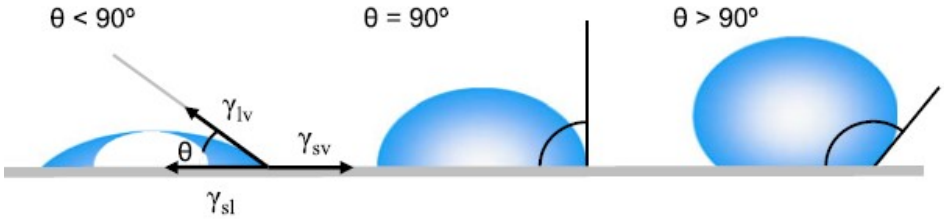


Figure 4.5 Illustration of contact angles formed by sessile liquid drops on a smooth homogeneous solid surface [41].

Most commercial membranes for pressure-driven processes are made from rather hydrophobic polymers with high thermal, chemical and mechanical stability, such as PVDF, PES, PS, PAN and PTFE. Usually these materials are known as hydrophobic and, as a result, they are prone to adsorption of various solutes from feed water [7-9]. The major reason for hydrophobic membrane fouling with organic compounds and microorganisms is that there are almost no hydrogen bonding interactions in the boundary layer between the membrane interface and water. The repulsion of water molecules away from the hydrophobic membrane surface is a spontaneous process with increasing entropy and, therefore, foulant molecules have a tendency to adsorb onto the membrane surface and dominate the boundary layer. In contrast, the membrane with a hydrophilic layer possesses a high surface tension and is able to form hydrogen bonds with the surrounding water molecules to reconstruct a thin water boundary between the membrane and bulk solutions. This layer can prevent or reduce pollutants adhering to the membrane surface [118, 122]. The antifouling membranes not only significantly reduce the adsorption of proteins, but are also able to prevent microbial attachment [97].

4.2.1 Surface Modification of PVDF Membranes

Surface modification methods are divided into two groups including surface coating [123], surface grafting [105, 108, 124, 125]. Surface coating can be considered as an easy technique to improve the membrane hydrophilicity by coating or depositing a thin functional hydrophilic layer onto the membrane surface. Because of the weak physical adsorption interaction between PVDF membrane and coated layer, the coated layer is prone to wash away during the process. Because of the instability of the coated layer, surface grafting technique can be applied instead of surface coating. Figure 4.6 illustrates the route of surface modification including surface coating and surface grafting [6].

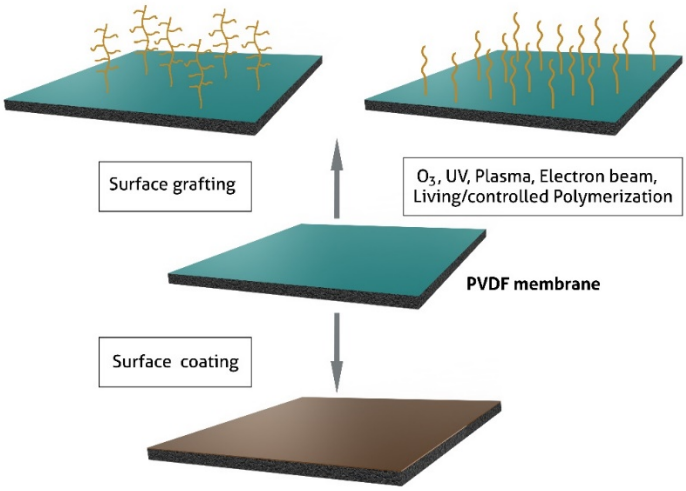


Figure 4.6 Schematic of surface modification of PVDF membrane [6].

In the case of surface coating, the membrane is dipped into the polymer-containing mixture to gain fouling resistance of existing membranes [7]. Surface coating is a simple but effective method for membrane surface modification, and it has been widely adopted to the surface properties of RO, NF, UF and MF membranes. Poly(vinyl alcohol) (PVA), chitosan and poly(ether block amide) (PEBAX) are hydrophilic polymers that are extensively used for hydrophilic modification of PVDF membranes [14] .

PVA can be used as a hydrophilic surface for membranes owing to its good hydrophilicity, biocompatibility, mechanical strength, thermal stability. Additionally, a PVA-coated surface has shown enhanced biofouling resistance [126]. Du et al. coated a PVDF FSM with dilute PVA aqueous solution and also performed a solid-vapor interfacial cross linking. It was found that surface hydrophilicity, PWF and also fouling level were all improved on account of PVA layer. Moreover, the researchers proposed that alkaline treatment could be used to remove the cake layer from membrane surfaces [98].

Boributh et al. [101] used a chitosan mixture for coating of PVDF FSM in order to increase the hydrophilicity and prevent biofouling. In other work, Shi et al. modified the PVDF dual-layer HFM by coating it with dopamine and grafting polyethyleneimine. The researchers obtained the hydrophilic and antibacterial membrane through quaternisation reactions. The PWF before and after bovine serum albumin (BSA) contamination was measured, and the flux recovery rate of the modified membrane was as high as 94%. The antibacterial tests showed that the hydrophilic and antibacterial PVDF membrane

possessed excellent antibacterial efficiency and resistance to bacterial adhesion [127]. However, during long-term operation of membrane processes, the coated layer can become separated from the membrane surface [128].

Surface grafting appears as a promising way for modifying the membrane surface through the covalent bonding interaction between the grafted chains and membrane. In contrast with surface coating, covalent attachment of graft chains on the membrane surface offers a long-term chemical stability of grafted chains. However, grafting may block membrane pores and decrease its permeability [129, 130]. Surface grafting can be carried out by UV photo-grafting [131], plasma treatment [132, 133], electron beam [134] and living/controlled polymerization grafting [135].

Rahimpour et al. modified PVDF FSMs using the dip-coating technique and UV irradiation, using benzophenone as the photoinitiator. They used acrylic acid (AA) and 2-hydroxyethylmethacrylate (HEMA) as acrylic monomers and 2,4-phenylenediamine (PDA) and ethylene diamine (EDA) as amino monomers at different concentrations to improve the hydrophilicity, thus reducing the fouling tendency. After modification, the hydrophilicity, fouling resistance and flux recovery of PVDF membranes were all enhanced [104]. Zhang et al. investigated the graft polymerization of N-vinyl-2-pyrrolidinone onto the PVDF-based microporous membrane, containing a small quantity of PES performed under UV irradiation. The grafting rate increased with irradiation time and the contact angle of the modified membrane surface decreased from 86◦ to 32◦ after 10 min of irradiation [105].

Plasma polymerization can be defined as an electrical ionization of a monomer resulting in the initiation of reactive monomer fragments. The degree of cross-linking of plasma polymers is higher compared to other commercialized polymers [136]. PVDF membranes with PEG and then dipped in a PEG/CHCl3 solution for the argon plasma method. The researchers revealed that the PWF decreased with the increase in surface PEG graft concentration, whilst the mean pore size remained almost unchanged. In addition, the PEG-g-PVDF membrane showed an excellent fouling resistance [106].

Liang et al. fabricated an extremely hydrophilic PVDF membrane with a post-fabrication technique. Using this approach, super-hydrophilic SiO2 nanoparticles are irreversibly bound to the poly(methacrylic acid) (PMAA) graft-copolymerized PVDF membrane surface using a dip-coating method. Both modifications considerably improved the

hydrophilicity of the membranes. The developed membrane also formed a tightly bound hydration layer on the membrane surface resulting in an antifouling performance [137].

Compared with the less active initiating ability of UV and plasma applied to a PVDF membrane, high energy irradiation is another efficient way to activate PVDF membrane and initiate the grafting copolymerization of functional monomer on its surface [6].

Atom transfer radical polymerization (ATRP) and reversible addition-fragmentation chain transfer polymerization (RAFT) are extensively used to graft chains onto the PVDF membrane surface [138]. ATRP can be linearly controlled by adjusting the concentration of the consumed monomer, the density of introduced initiator, the grafting time and the grafting temperature. Examples of copolymers prepared using this method, include grafting copolymers of PVDF with PMAA side chains (PVDF-g-PMAA), poly(oxyethylene methacrylate) side chains (PVDF-g-POEM) and poly(ethylene glycol methacrylate) side chains (PVDF-g- PEGMA) [139, 140]. Chen et al. applied RAFT polymerization technique to graft polymerize brushes of poly(methyl methacrylate) PMMA and PPEGMA from PVDF surfaces. PVDF surfaces were exposed to aqueous LiOH, followed by successive reductions with $NaBH_4$ and DIBAL-H to obtain hydroxyl functionality. Azo-functionalities, as surface initiators for grafting, were immobilized on the PVDF surfaces by esterification of 4,40-azobis(4-cyanopentanoic acid) and the surface hydroxyl groups. It was found that the CA value of membranes were decreased through the surface grafting method of PEGMA and MMA [141].

4.2.2 Blending Modification of PVDF Membranes

Blending with hydrophilic materials can be considered as the most practical way that can be adapted to a large-scale production of membranes. The hydrophilic PVDF membrane with other desirable properties can be obtained simultaneously during the membrane preparation process without any pre-treatment or post-treatment procedures, which is usually adopted in surface coating or surface grafting techniques. Most of the surface grafting techniques focused on the FSMs, which limited its application in the modification of HFMs; while blending some additives with PVDF and subsequent spinning hollow fiber would integrate both phase inversion preparation and hydrophilic modification procedure together using a single-step process [6].

Nanotechnology have been used in various application areas, and also have been studied by various investigators in desalination industry [16, 27, 33, 142-154]. According to

membrane structure and location of nanomaterials, nanocomposite membranes can be classified into four categories:

- Conventional nanocomposite
- Thin-film nanocomposite (TFN)
- Thin-film composite (TFC) with nanocomposite substrate
- Surface located nanocomposite

The typical structures of these membranes are illustrated in Figure 4.7 [155].

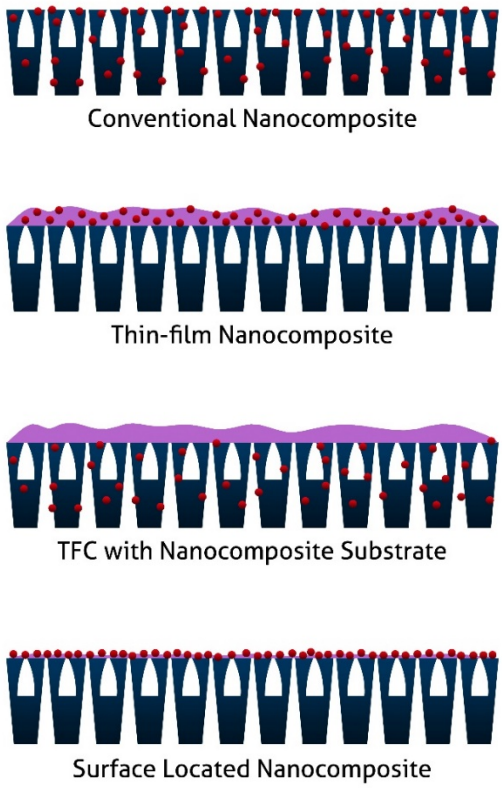


Figure 4.7 Typical types of nanocomposite membranes (The red spheres represent nanoparticles, nanotubes, nanofibers or nanosheets) [155].

Conventional nanocomposite membranes are mainly used in MF/UF methods because of the typical porous structure. Fabrication of nanocomposite membranes involves the dispersion of nanoparticles in dope solution before the phase inversion approach, by which FS and HF membranes can be fabricated as shown in Figure 4.8 [155].

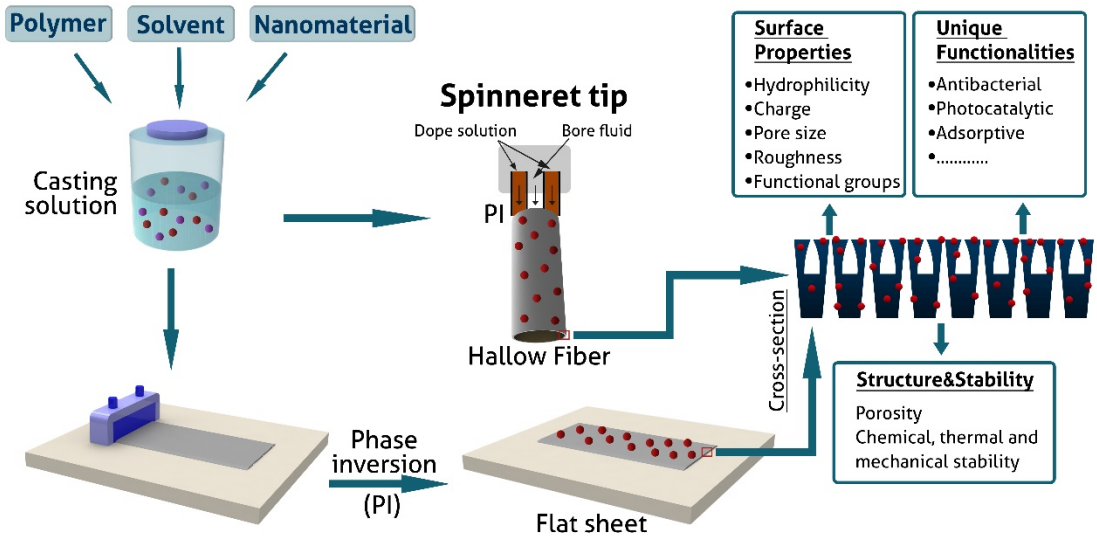


Figure 4.8 Fabrication of conventional nanocomposite membranes through the PI process and the main effects of nanofillers on final products [155].

It is proposed that the addition of nanoparticles into the polymeric materials can lead novel interfacial areas between polymers and particles and subsequently improve the desired properties of the existing nanocomposites by quantum size control. Besides, nanomaterials can control membrane properties through the attached functional groups and their hydrophilic properties [16].

Blending with particles, and adding precursors are two methods to obtain nanocomposite membranes. The inorganic nanoparticles are usually highly polar, which have poor interfacial compatibility with many commercial polymers for membrane fabrication. Compared with the bulk materials, the nanomaterials have a high specific surface area, which enables better contact and interaction with feeds during membrane processes. However, they are also prone to aggregation, to reach an energy-favorable state within the blending system with poor compatibility.

Another common blending process involves adding the precursors to casting solutions and generating nanoparticles during the fabrication of membrane. Compared with the nanoparticle blending process, this approach normally provides uniform distribution of inorganic components and flexible regulation of interfacial properties [156].

By using sol–gel method, integration of inorganic materials with polymers may increase chemical, mechanical and thermal stability of the matrix material [157, 158]. Moreover, the hydrophilicity of the standard material can be significantly improved [159, 160].

4.2.2.1 Dispersion of Nanoparticles in Polymers

The morphology of the added inorganic nanomaterials determines the size of the interphase between the fillers and polymer chains and then stabilizes the nanocomposite membrane by a possible molecular-level synergic effect between the organic and inorganic constituents [161]. A key parameter for the successful implementation of nanocomposite membrane is to increase the dispersion of the inorganic nanofiller in polymer matrix through the establishment of specific interaction between the two phases [33, 162]. Examples of surface interaction between particles in liquid phase are shown in the Table 4.1 [33].

Table 4.1 Examples of surface interaction between particles in liquid phase [33].

Surface Interaction	Generation mechanism
Van der Waals interaction	Short-ranged electromagnetic force between molecule and/or atoms
Overlap of electric double layer	Electrical interaction by the overlap of adsorbed polymer layer on particles
Steric interaction of adsorbed polymer	Short-ranged interaction by the overlap of adsorbed polymer layer on particles
Bridge force	Formation of the bridge of polymer binder and/or surfactant between particles
Hydration force	Overlap of hydrogen-bonded water molecule on hydrophilic surface on particle

One of the most important problem of adding inorganic materials to polymer matrix is the agglomeration occasion which provokes the instability of polymer solution and non-uniform distribution of particles in the membranes [163, 164]. The natural characteristic of nanoparticles and bad compatibility with hydrophobic PVDF bulk is responsible for the agglomeration phenomenon [14]. The agglomeration of nanoparticles within polymer matrix is generally cause a reduction in mechanical properties [27].

Sonication and surface modification methods have been used to prevent agglomerations Since the intra-nanoparticles interaction is very strong, it is hard to break the intra-particle interactions with conventional mixers and sonicators [156, 165]. Thus, the surface treatment can be considered as more effective method for the dispersion of nanoparticles in order to fabricate nanocomposite materials with outstanding properties. With development in nanotechnology, combination of modified nanoparticles into polymeric materials has received great attention [166-168].

The functionalization of nanoparticles is performed with silane coupling agents like 3-methacryloyloxypropyl trimethoxysilane (MAPTMS) and 3-aminopropyltriethoxysilane (APTES). These agents are used to decrease the hydrophilicity and surface energy of the nanoparticles and subsequently to prevent agglomerations enhancing matrix interactions [27, 28].

4.2.2.2 Inorganic Nanoparticles

The incorporation of metal oxide nanoparticles including SiO_2 [169-174], Al_2O_3 [164, 175-178], TiO_2 [56, 168, 179-192], ZnO [193-195], ZrO_2 [196, 197] with polymerix UFMs has been revealed to enhance hydrophilicity, PWF, antifouling property, mechanical and thermal stability of membranes [198, 199].

SiO2 nanoparticles were commonly used owing to their mild reactivity, chemical properties, mechanical properties and nontoxic nature [169], and also good compatibility with organic solvents [200]. Nanoporous SiO_2 enhances PWF through offering an inner water channel to let the passage of water molecules, subsequently increased water flux [201]. Yu et al. prepared PVDF-SiO_2 composite HF UFM via sol-gel process using tetraethoxysilane (TEOS) followed by the wet-spinning process [169]. Wu et al. chemically functionalized SiO_2 nanoparticles using silane coupling agents, which were then further used to immobilize PEG molecules on their surface. The results demonstrated that the novel membrane possessed antifouling property [173].

Al2O3 is a highly stable inorganic material that is environmentally friendly, considerably abrasive, and oxidation/reduction resistant [202]. Yan et al. investigated the effects of the nanosized Al2O3 content in the polymer solution on the membrane performances. The porosity and crystallization of the membrane did not influence from Al2O3 nanoparticles. In addition, the hydrophilicity, mechanical properties and PWF performance enhanced at the concentration of 2 wt.% [178].

TiO2 has gained great interest owing to its stability, chemical resistance, photocatalytic functionality as well as antibacterial properties. Most importantly, blending with TiO2 nanoparticles can destroy bacterial colonization and mitigate the biofouling issue of membranes [75, 202-205]. Yu et al. fabricated PVDF-TiO2 nanocomposite HF UFM using sol-gel and blending techniques. As a result, the sol-gel method was found to be more effective in dispersion of nanoparticles strengthening matrix interactions [186]. Song et al. investigated PVDF-PEG-TiO2 membranes to achieve bigger pore size and high porosity. The results showed that TiO2 nanoparticles lead to enhance the rejection of HA but decrease the flux because of the smaller pore sizes. In addition, due to the photocatalytic property the novel membrane showed the self-cleaning property [185]. Razmjou et al. modified TiO2 nanoparticles using the APTES agent in order to ensure the stability of TiO2 in polymer solution. The results indicated that the functionalization of particles resulted in better distribution within membrane even though the concentration was high [163]. In another study, Yuliwati et al. studied the effects of LiCl.H2O, TiO2 nanoparticles on PVDF HF ultrafiltration membrane by blending modification method. It was found that at the concentration of 1.95 wt.% TiO2, porosity, hydrophilicity and PWF, of the composite membrane were all improved [94].

In order to study the effects of multi-nanoparticles, Han et al. prepared PVDF/SiO_2/TiO_2/Al_2O_3 composite HFM by wet spinning method. Higher break strength, improved PWF and best porosity were obtained at the concentration of 1 wt.% TiO_2, 1wt.% SiO_2, 1 wt.% Al_2O_3 [206]

4.2.2.3 Carbon Nanotubes

CNTs are one-dimensional nanomaterials and an allotrope of carbon, known for their excellent surface adsorption, chemical, mechanical and thermal properties. It was first reported in 1991, and found to be the one-dimensional counterpart of the zero dimensional spherical fullerene, having the same hexagonal carbon lattices [148]. Theoretical and experimental results have shown unusual mechanical properties of CNTs with Young's modulus as high as 1.2 TPa and tensile strength of 50–200 GPa [207, 208]. These characteristics make CNTs amongst the strongest and stiffest materials on earth [209].

Single-walled carbon nanotubes (SWCNTs) and multi-walled carbon nanotubes (MWCNTs) are two forms of CNTs which differ by the quantity of carbon atom cylindrical arrays arranged around the hollow nanotube core. The properties of each of

the two types of CNT vary depending on the atomic configurations of the nanotube cylinders [210]. The large-scale fabrication of SWCNTs blended membranes doesn't find to be cost effective because of the high price of SWCNTs. On the other hand, MWCNTs shows better water permeability and the price of this membrane might be significantly lower than those produced from SWCNTs [211].

Through using MWCNTs in polymers, polymeric materials can show superior properties including high thermal and electrical conductivity as well as high mechanical characteristics. In addition, MWCNTs can improve the interaction of nanoadditives with polymer matrix owing to their large aspect ratio. Nevertheless, their uniform dispersion can be difficult because of the Van der Waal's force between nanotubes [212, 213]. State-of-the-art developments in the utilization of CNTs for water treatment as well as membrane fabrication and CNT functionalization for better adsorption capacity have been reviewed by various researchers [211, 214-218].

In order to improve the adhesion of CNTs to the polymeric matrix, CNTs have been functionalized with chemical agents or applied an acid treatment. By bringing functional groups to CNTs, it is expected that the nanotubes can disperse more uniformly [219-225]. The procedure for acid and silane treatments of CNTs performed by Kim et al. [226] is given in Figure 4.9.

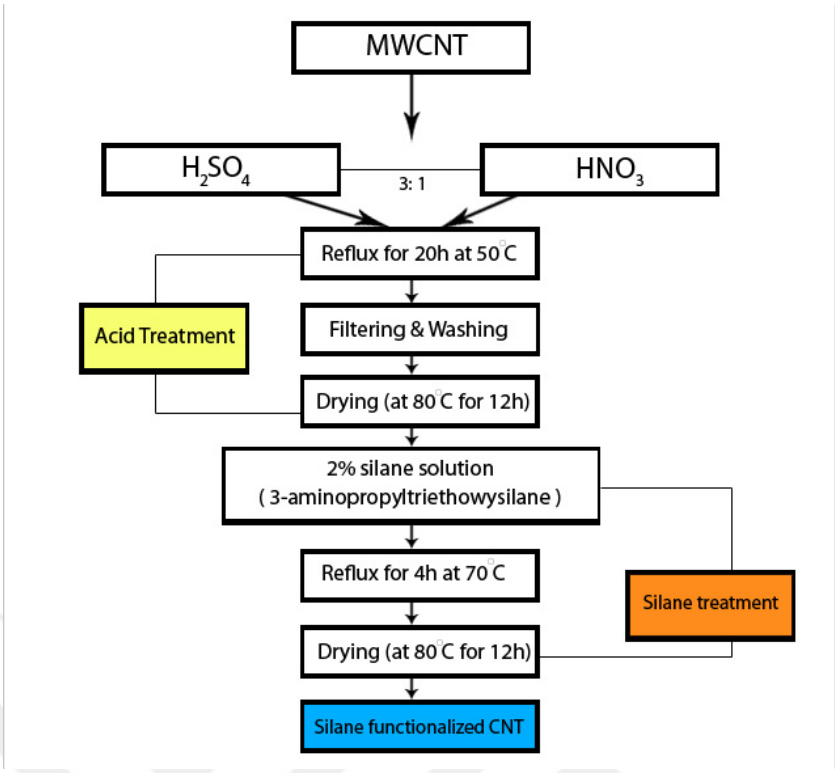


Figure 4.9 Flow chart of oxidization and silanization process [226].

Ma et al. applied acid treatment to eliminate impurities of MWCNTs and introduce hydrophilic groups on the surface of MWCNTs. The results showed that hydrophilicity of the hybrid PVDF/OMWCNTs membrane was enhanced. Accordingly, the water flux increased by 11 times and BSA rejection increased 22.2% at 1 wt.% OMWCNTs [221]. Nevertheless, acid treatment may cause a structural damage to the MWCNTs wall. In order to solve this problem, MWCNTs is coated with polydopamine (Pdop) to improve their hydrophilic property. Sianipar et al. evaluated that various properties of the Pdop-coated MWCNT blend membrane such as, PWP, hydrophilicity, antifouling performance and mechanical strength were improved compared with acid-treated MWCNTs blend membrane [227].

Zhao et al. [228] prepared hyperbranched poly(amine-ester) functionalized MWCNTs/PVDF composite membranes in order to evaluate the dispersion of $MWCNT_{HPAE}$ in a PVDF membrane and investigate the hydrophilicity, permeability, structure and antifouling performance of the hybrid membranes [228]. Yu *et al.* [166] prepared APTES-modified MWCNTs to enhance their compatibility with PVDF matrix. It was found that APTES modified MWCNTs/PVDF nanocomposite membranes showed outstanding morphology and pore structure. In addition, the hydrophilicity, BSA rejection

and the mechanical strength were all improved. Esfahani et al. investigated the novel and complementary effects of TiO_2 nanoparticles and MWCNTs on the performance of a UFM. The results showed that the presence of an equivalent mixture of both nanoparticles gave a flexible response under two different fouling conditions [229].

Zhao et al. prepared a UFM from PVDF/GO and PVDF/MWCNTs in order to compare their properties. It was found that PVDF/GO composite membranes had larger pores, a lower roughness, and performed worse in terms of hydrophilicity, rejection and PWF, compared with PVDF/MWCNTs blend membrane [230]. Zhang et al. integrated OMWCNTs and GO into the PVDF matrix which revealed synergistic impacts on the microstructure and performance of membranes [231].

4.2.2.4 Halloysite Nanotubes

Clay particles have been used as a performance enhancing additive in polymeric membranes owing to their natural abundance and low cost [232-236]. Lai et al. prepared PVDF/nanoclay FSMs and HFMs to study the improvement to abrasion resistance. The results indicated that the addition of nanoclay suppressed finger-like void formation increasing the mechanical strength and abrasion resistance [237, 238].

Berthier was explained halloysite for the first time in 1826 by Berthier as a dioctahedral 1:1 clay mineral of kaolin group [239]. The chemical composition of halloysite resembles to kaolinite containing water molecules ($Al_2Si_2O_5(OH)_4.nH_2O$) [240]. When n=2 hydrated HNT is named HNT-10 Å and in the case of n=0, HNT-10 Å transform to HNT-7 Å at 30-110°C with the loss of water molecules [241].

The tubular aluminosilicate clay called HNTs have received great attention due to its extraordinary properties such as tubular nanostructure, large aspect ratio, natural abundance, functionality, biocompatibility, and mechanical characteristics. In addition, they are relatively inexpensive ($4/kg) and global supply exceeds thousands of tons per year which means that true mass-scale industrial applications can be readily achieved, unlike the gram-scale yielding of CNT with a very high price ($500/kg) [17-19, 242]. More importantly, the unique tubular microstructure and hydrophilic group of HNTs are similar to those of CNTs. Therefore, HNTs may have potential to replace expensive CNTs as hydrophilic additives [243].

A schematic diagram of the structure of halloysite-(10 Å) is shown in Figure 4.10 [244] and comparison of the properties of HNTs and CNTs is shown in Table 4.2 [17, 241, 245].

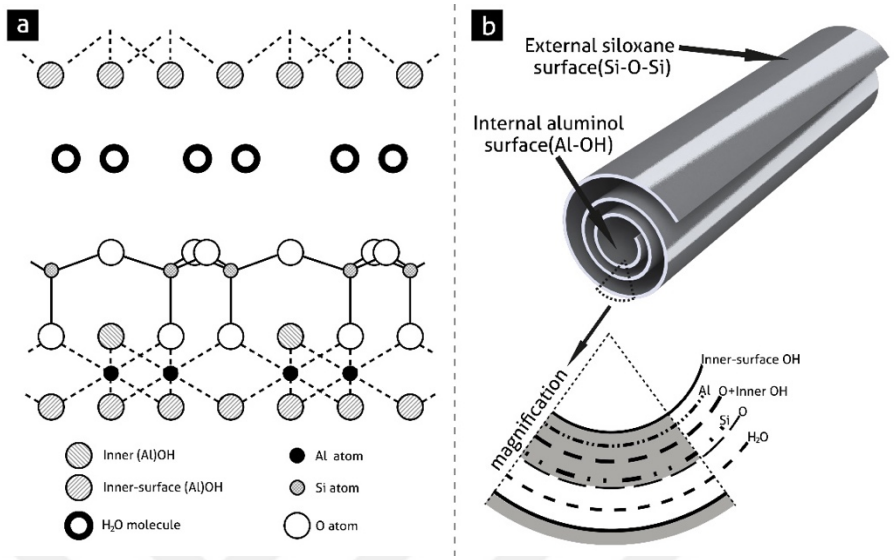


Figure 4.10 Schematic diagram of (a) crystalline structure of Halloysite-(10 Å), (b) structure of halloysite particle [244].

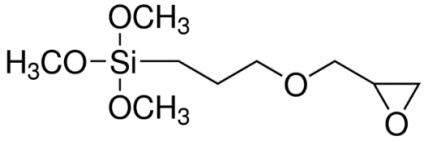
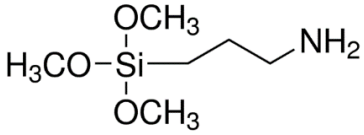
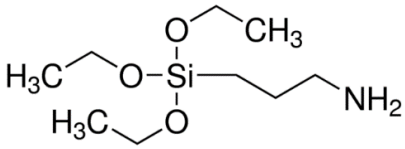
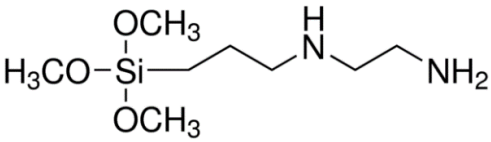
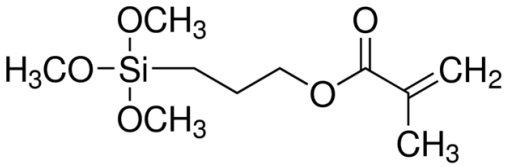
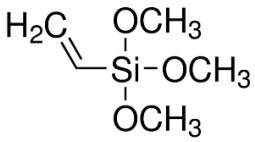
Table 4.2 Comparison of the Properties of HNTs and CNTs [17, 241, 245].

Properties	**HNTs**	**CNTs**
Chemical formula	$Al_2Si_2O_5(OH)_4.nH_2O$	C
Length	0.2-2 µm	1-5 µm
Outer diameter	40-70 nm	2-10 nm
Inner diameter	10-40 nm	1-3 nm
Biocompatibility	Biocompatible	Health hazard
Water wettability	Hydrophilic	Hydrophobic
Surface chemistry	SiO_2 outside, $Al(OH)_2$ inside	Graphene layers
Surface charge (pH 2-9)	Negative	Not charged
Specific surface area (m^2/g)	100-150	15-350
Elastic modulus (TPa)	0,14	1,09-1,25
Density (g/cm^3)	2,14-2,59	1,8
Thermal stability (°C)	400	500-700

Owing to the many hydroxyl groups on the HNTs surface, membranes blended with HNTs exhibit good hydrophilicity and antifouling properties and have some potential applications in desalination and wastewater treatment [246-254]. By incorporation of

HNTs into the membrane, mechanical, thermal stability and also permeation performance can be improved. More importantly, antifouling, antibacterial and photocatalytic properties can be gained by introducing functional groups on the surface of HNTs [255]. Silane treatments have been widely used surface modification method in order to graft HNTs [244]. Organosilanes were found to be effective agents for surface modification of clays, rendering the surface less hydrophilic by reducing the number of Si–OH groups at its surface in order to increase their dispersion in a polymer matrix [256, 257]. The grafting reactions can occur in either toluene or water/alcohol mixtures. Various silanes used for HNTs shown in Table 4.3 [244, 257-263].

Table 4.3 Chemical composition of silanes used for modification of HNTs [244, 257-263].

Name	Chemical composition
3-Glycidoxypropyltrimethoxysilane (GPTS)	
3-Aminopropyltrimethoxysilane (APS)	
3-Aminopropyltriethoxysilane (APTES)	
3-(2-Aminoethylamino)propyltrimethoxy silane (AEAPS)	
3-Trimethoxysilypropylmethacrylate (MAPTS)	
Vinyltrimethoxysilane (VTMS)	

Yuan et al. grafted HNTs with APTES to investigate the effect of thermal pretreatment conditions and HNTs structure on the reaction mechanism which involves grafting and oligomerization. Grafting occurs between hydrolyzed APTES and the surface hydroxyl groups, including the aluminol groups at internal surface of lumen and the aluminol and silanol groups at edges or external surface defects. Oligomerization occurs when there is

sufficient water physically adsorbed on the surface of halloysite for complete hydrolysis of APTES. The results demonstrated that the thermal pretreatment and evacuation pretreatment affects the loading of hydrolyzed APTES into the lumen of HNTs. The related modification mechanism is represented schematically in Figure 4.11 [244].

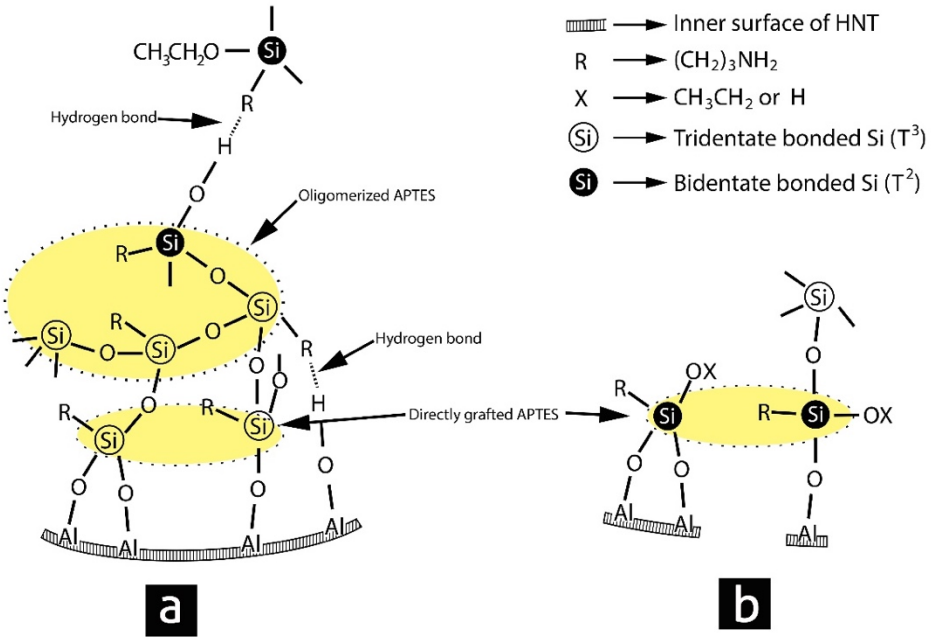


Figure 4.11 Schematic representation (a) of the proposed mechanism of the formation of cross-linked network, and (b) of the grafting between bidentate bonded Si and AlOH groups [244].

Zeng et al. modified HNTs using a process that involved grafting APTES and prepared a PVDF/HNTs blend UFM for oil/water separation. The results indicated that the blend membranes exhibited good hydrophilicity, with a higher PWF and lower contact angle compared with the pristine PVDF membrane, because of the large number of hydrophilic groups in APTES-HNTs [175]. In their next study, the researchers fabricated a PVDF NF membrane by adding APTES-modified HNTs as shown in Figure 4.12 [264].

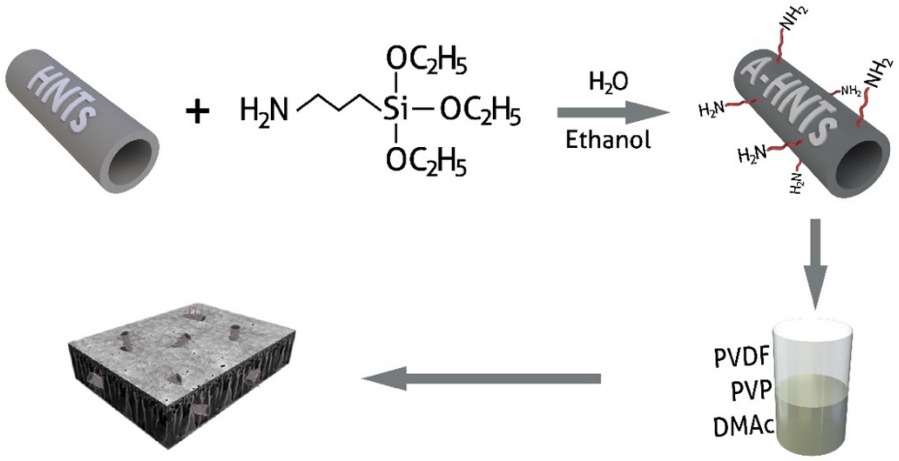


Figure 4.12 Preparation process of PVDF/A-HNTs nanofiltration membranes [264].

Zang et al. used HNTs as an additive for the preparation of PES UFMs to investigate the antibacterial property of the hybrid membrane [246, 253, 254]. Copper (Cu) represents a more promising metal for antibacterial applications due to its excellent antimicrobial properties, low toxicity, and low cost. Their research group modified HNTs with silane coupling agent in order to make HNTs have the capability of loading Cu ions [251] and silver (Ag) ions [254]. Chen et al. modified HNTs with chitosan and then loaded with Ag nanoparticles [253]. Chitosan molecule contains nitrogen atoms, which have a lone pair or lone pairs of electrons that can bind Ag ion through an electron pair sharing to form a complex [265]. Besides, chitosan molecule contains a large number of reactive hydroxyl groups therefore the surface hydrophilicity can be enhanced [145, 146].

Zhao et al. synthesized a nanocomposite membrane containing AgNPs, HNTs and reduced graphene oxide (RGO) to fabricate a blend UFM. It was found that the water flux, antifouling property and antibacterial performance of hybrid membrane were improved [247].

Moslehyani et al. modified HNTs by N-β-(aminoethyl)-ɣ-aminopropyltrimethoxy silane (AEAPTMS) in order to immobilize of silver lactate (SL) on the surface of HNTs and fabricated hybrid PVDF UFM. The resulted membrane showed more than 99% bacterial rejection and significant improvement in permeation flux [266].

Dextran is a type of natural polysaccharide, which has strong hydrophilic properties. Yu et al. grafted dextrans onto the HNTs and used modified HNTs as an additive to improve the hydrophilicity of UFMs. Zhao et al. functionalized HNTs with carboxylic groups (-COOH) and then covalently immobilized lysozyme onto the surface of modified HNTs.

Lysozyme belongs to the hydrolase family, a group of enzymes which destroy the cell walls of microbes, making it a good candidate in antibacterial applications [248].

Zeng et al. loaded TiO_2 on the surface of HNTs by the sol-gel method [267] and prepared TiO_2-HNTs/PVDF blend membranes as illustrated in Figure 4.13. It was found that the hydrophilicity and antifouling performance of the blend membrane improved due to the loading of HNTs, TiO_2 was able to disperse more effectively in membrane matrix [268].

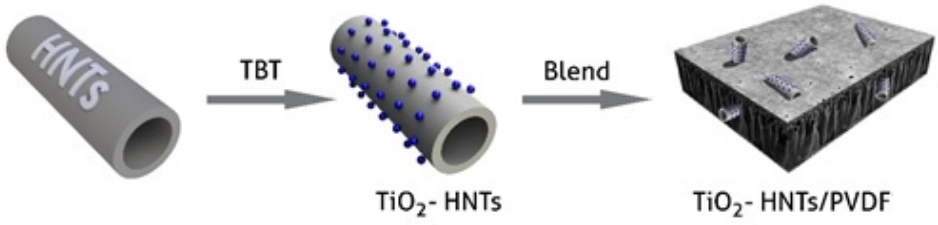


Figure 4.13 The schematic illustration of the preparation of TiO_2-HNTs/PVDF [268].

Table 4.4 provides a summary of PVDF UFMs blended with inorganic nanoparticles.

Table 4.4 Effects of nanoparticles on the performance of PVDF UF membranes.

Membranes	Optimum dosage (%)	Contact Angle (◦)	Porosity (%)	Pore Size (nm)	Tensile Strength (MPa)	Elongation at break (%)	PWF (L/m^2h)	BSA Rejection (%) or MWCO (Da)	Ref.
PVDF/TiO_2	5	35	85	43.6	2.23	59.01	266	93%	[181]
PVDF/SiO_2	3	53.4	84.2	99	2.39	160	301	90%	[169]
PVDF/Al_2O_3	2	57.42	55.31	-	19.92	7.34	100	35000 Da	[178]
PVDF/MWCNTs	1	53.4	88.7	36	-	-	620	89%	[230]
PVDF/MWCNTs-HPAE	2	73	58.41	-	-	-	-	93%	[228]
PVDF/OMWCNTs	6	54.7	86	75	0.78	7.48	1200	80%	[221]
PVDF/RGO-TiO_2	0.05	69.2	85.98	76.4	-	-	221	99%	[269]
PVDF/TiO_2-HNTs	3	52.9	65.4	93.9	-	-	354.2	70%	[268]
PVDF/HNTs-APTES	3	58	66.4	45.9	-	-	203	90%	[175]
PVDF/HNTs-SL	1	46.35	51	-	96.21	-	315.43	-	[266]

4.2.2.5 Boron Nitride

Boron nitrides (BN) consist of same amount of boron and nitrogen atoms. BN is not occurred in nature and can be produced synthetically from boron, boric acid (H_3BO_3) and boron trioxide (B_2O_3). In 1842, Balmain first synthesized BN using the reaction between molten H_3BO_3 and potassium cyanide (KCN) [270]. Three crystalline forms of BN are hexagonal BN (h-BN), diamond like cubic BN (c-BN), and wurtzite BN (w-BN). Among these structures, h-BN can be considered as the most stable phase under standard circumstances [271]. In addition, h-BN has a crystal structure analogue of graphite known as an important engineering ceramic [272]. Various nanostructures of h-BN such as BN nanotubes (BNNTs), BN nanosheets (BNNSs), BN spherical nanoparticles (BNNPs) can be produced with regard to its layered structure [25]. The properties of bulk h-BN and its nanostructures are given in Table 4.5 [271].

Table 4.5 Properties of low-dimensional and bulk h-BN materials [271].

BN structures		Elastic modulus (TPa)	Fracture strength (GPa)	Thermal conductivity ($Wm^{-1}K^{-1}$)	Specific surface areas (m^2g^{-1})
1D	BNNTs	0.5-1.3	33	180-300	212-254
2D	BNNSs	0.72-0.95	70-217	>600	2600
Bulk h-BN		0.811	-	390	<10

BNNPs have similar structures and superior physiochemical properties such as mechanical properties, better dispersion in polymer matrix, thermal conductivity, electrical-insulating properties, resistance to oxidation and chemical inertness compared to carbon nanomaterials [20, 21]. Due to these reasons, BN nanostructures have been widely used as a reinforcing agent in polymer matrix composites.

It has been seen that the thermal conductivity, elastic modulus, mechanical strength enhanced, and electrical insulating was provided in polymer composites of BN [23-26]. With regard to its mechanical, thermal, electronic properties, h-BN nanostructures have been used polymer matrix composites, hydrogen storage [273], field emitter [274], electrocatalyst [275], adsorbent material for removal of oils , organic solvents and dyes from water [276]. Lei et al. developed porous BNNSs with very high specific area as an advanced sorbent material for water purification and treatment. The results showed that the nanostructured BN absorbed up to 33 times of its own weight in contaminants [276]. Yu et al. fabricated porous BNNS/PVDF composite membrane by PI method for oil/water separation [21, 277]. The results revealed that a multifunctional PVDF/BNNS composite membrane showed an excellent performance in separation of oil/water and organic molecules, excellent durability, stability and recyclability properties. Besides, the developed membrane exhibited high water permeation performance than the pristine PVDF membrane [21].

CHAPTER 5

EXPERIMENTAL METHOD

5.

5.1 Materials

Commercial halloysite nanotubes (HNTs) ($Al_2Si_2O_5(OH)_4$) of 1,2 μm length, 40 nm outer diameter and 20 nm inner diameter were procured from Esan Eczacıbaşı Endüstriyel Hammaddeler Sanayi ve Ticaret A.Ş. (Turkey). Hexagonal boron nitride (h-BN) nanoparticles were obtained from BORTEK (Turkey). Surface modification of nanoparticles was carried out using 3-aminopropyltriethoxysilane (APTES), procured from Sigma-Aldrich (USA), and ethanol (C_2H_6O) and acetic acid (CH_3COOH) procured from MERCK (Germany). Kynar® MG15 PVDF powder, procured from Arkema Inc., Philadelphia (USA), was used as the hollow fiber membrane matrix. PVP purchased from BASF Co., Ltd. (Germany) was used as pore forming additives to the membrane. N,N-dimethylacetamide (DMAc) (>99.6%), procured from Ak-Kim Kimya Sanayi ve Ticaret A.Ş. (Turkey) was used as a solvent. Glycerol procured from MERCK (Germany) was used as a non-solvent additive. Sodium hypochlorite solution (NaOCl) (15%), obtained from Ak-Kim Kimya Sanayi ve Ticaret A.Ş. (Turkey), was used to post treat membranes. MWCO measurement was carried out with feed solution containing sodium azide and dextrans, with molecular weights ranging between 0-2320000 Da procured from Sigma-Aldrich (USA). Deionized water (DIW) was used in bore liquid, coagulation and washing bath.

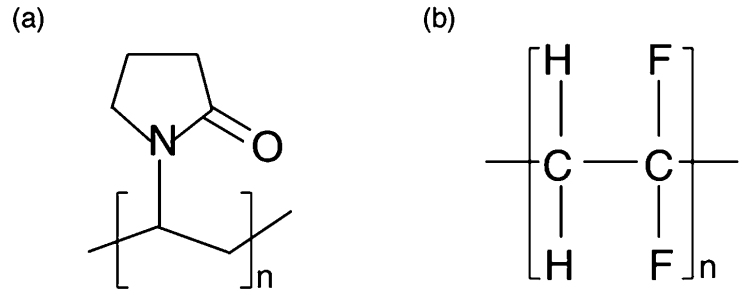


Figure 5.1 The molecular structure of (a) PVP and (b) PVDF polymers [278].

5.2 Surface Modification of HNTs with Silane Coupling Agent

HNTs were dried at 110 °C for 12 h in a vacuum furnace in order to reduce the moisture ratio and increase silylation efficiency [244, 279]. Dried HNTs were kept in a desiccator. The organosilylation of HNTs was performed as follows: 0.4-mL of APTES was added to 20-mL ethanol/water solution (95:5), which was adjusted to a pH 5.0 with acetic acid. (Figure 5.2). The mixture was stirred mechanically at room temperature for 5 min to delay hydrolysis reaction. Next, 5 g of HNTs were added to the solution, which was then transferred to a three-necked round flask. The prepared solution was refluxed at 80 °C under a nitrogen atmosphere for 3 h with rigorous stirring. (Figure 5.3). The precipitates were washed repeatedly with ethanol/water solution for 15 min by centrifugation with NÜVE NF 800R centrifuge (Figure 5.4). The product was then dried at 60 °C overnight (Figure 5.5) [280, 281]. The synthesis procedure for A-HNTs is illustrated in Figure 5.6.

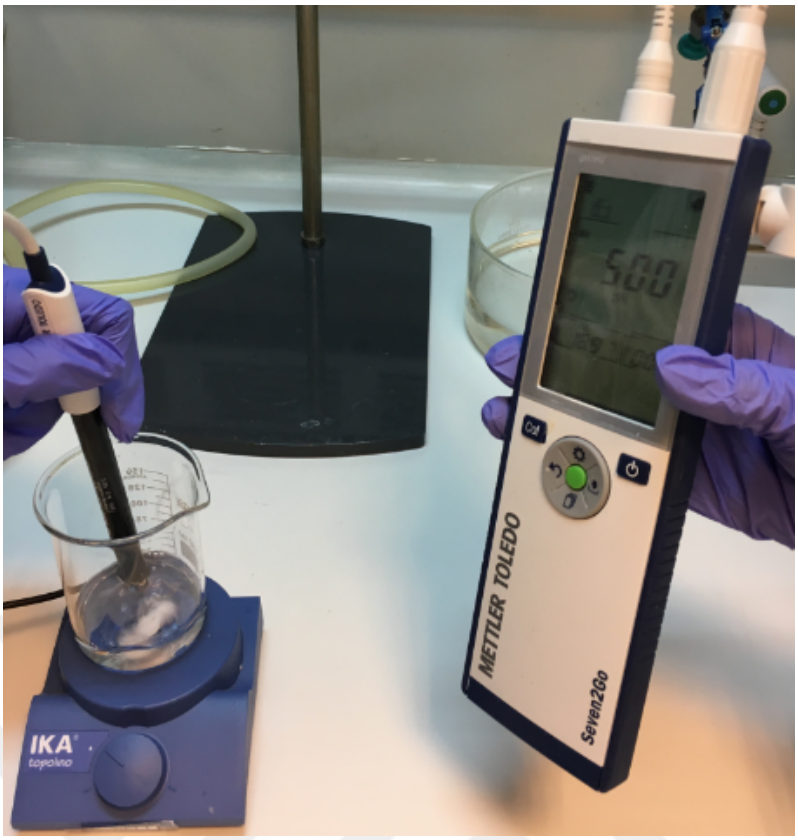


Figure 5.2 Hydrolysis reaction of APTES.



Figure 5.3 Reflux system of silanization reaction.

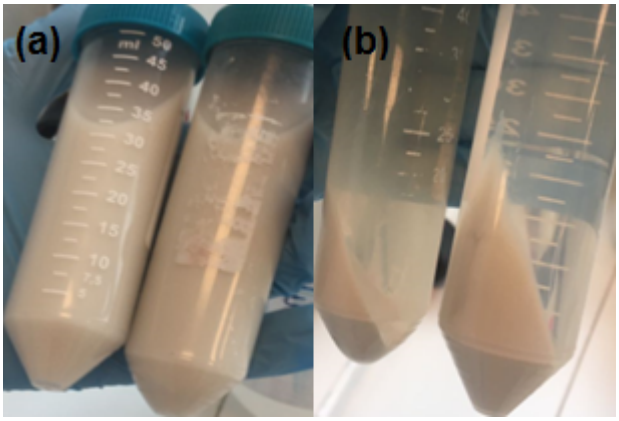


Figure 5.4 (a) Centrifugation of the solution, (b) Precipitate A-HNTs after centrifugation.

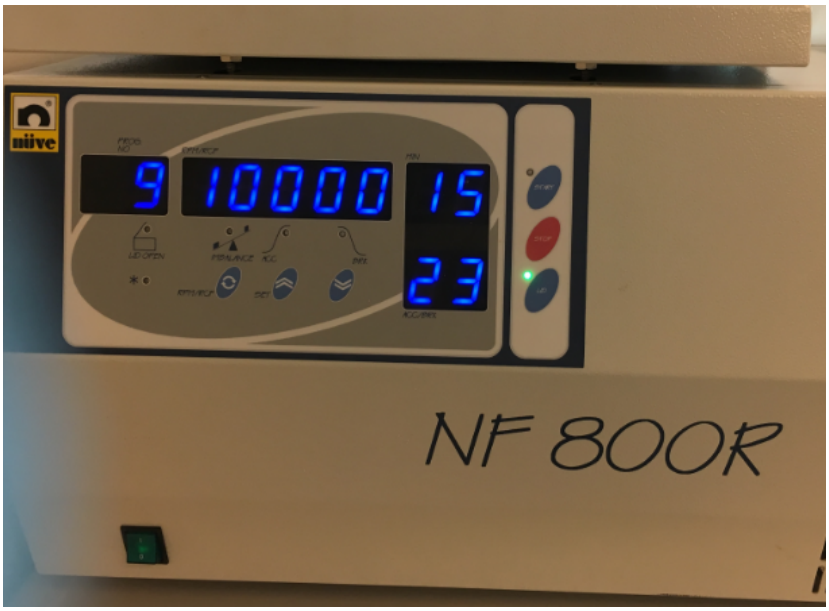


Figure 5.5 NÜVE NF 800R Centrifuge bench.

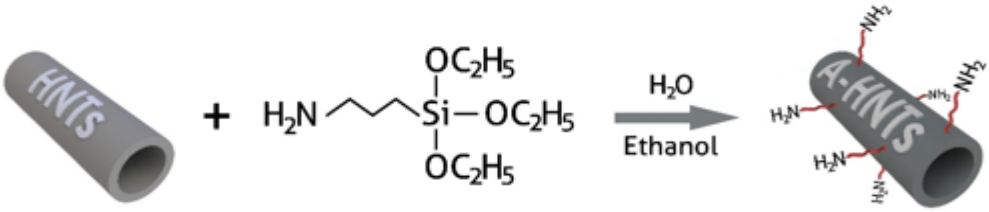


Figure 5.6 Schematic representation of A-HNTs synthesis [175].

5.3 Surface Modification of h-BN with Silane Coupling Agent

2 g h-BN and 25-mL ethanol were added into a beaker and the solution was stirred mechanically for 5 min. And then 0.1-mL APTES was added into the mixture (Figure 5.7). The prepared solution was refluxed at room temperature for 12 h under N_2 purging and magnetic stirring (Figure 5.8) in three-necked flask. After reflux process, the precipitate was transferred to the centrifuge tube for centrifugation and was washed with 30-mL ethanol for 5 times (Figure 5.9). The silane modified h-BN was dried at 80 °C for 3 h.

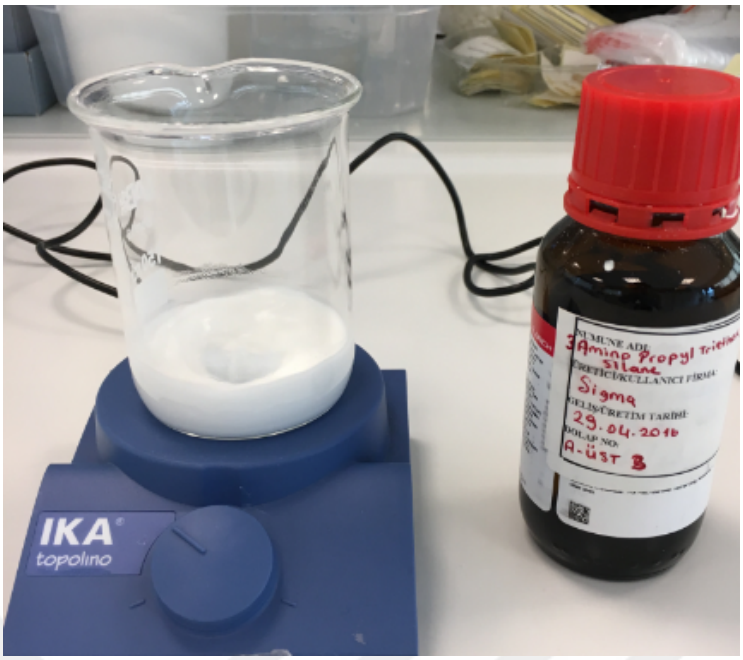


Figure 5.7 Mixing of h-BN with ethanol.

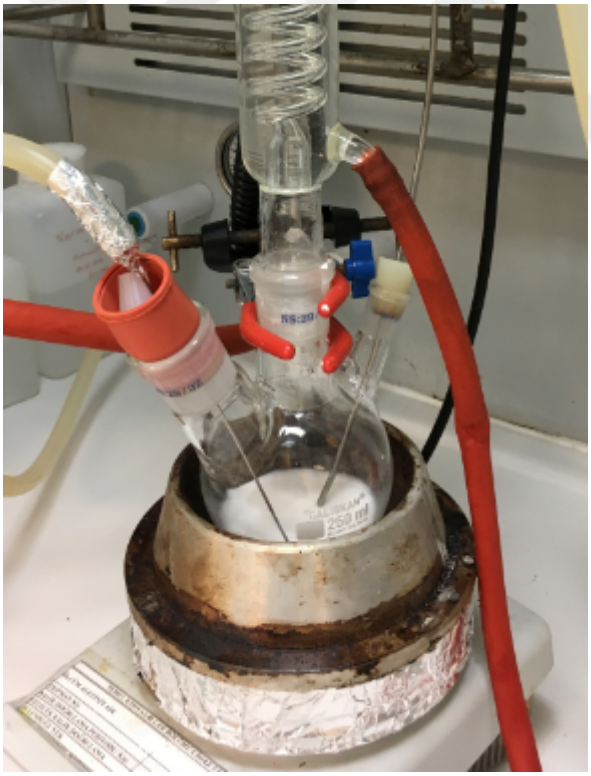


Figure 5.8 Reflux system of silanization reaction.

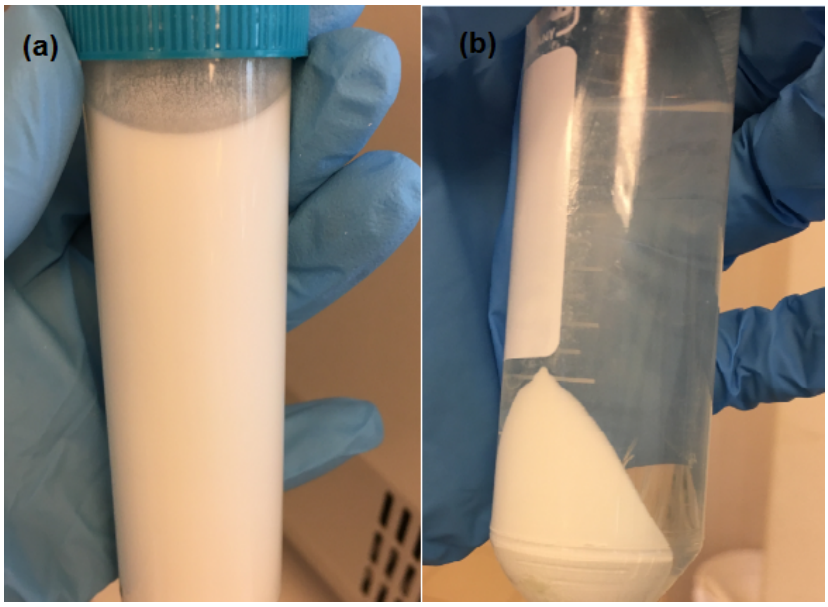


Figure 5.9 (a) Centrifugation of the solution, (b) Precipitate A-BN after centrifugation.

5.4 Preparation of Polymer (Dope) Solution

The modified HNTs and h-BN with different concentrations (0, 0.2, 0.4, 0.6) were first dispersed in 200 g DMAc using BANDELIN RK51H ultrasonic bath for 1 h. (Figure 5.10).

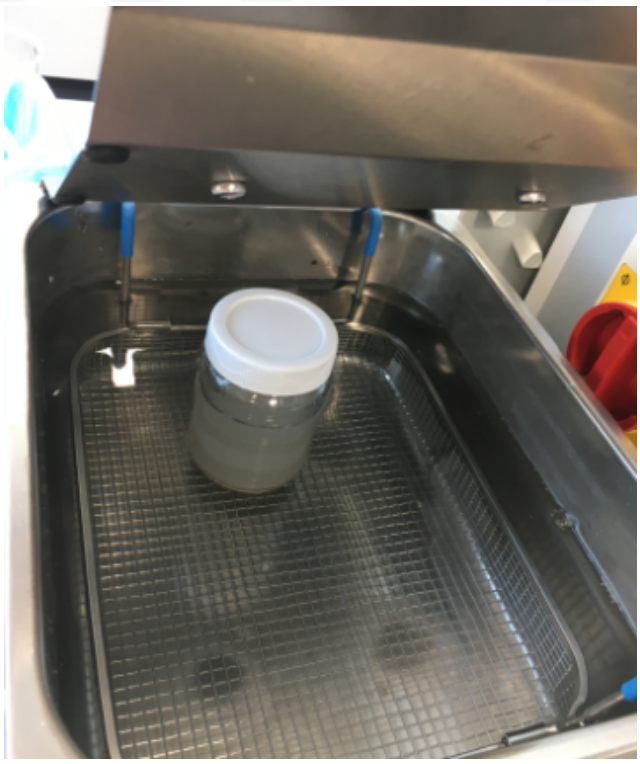


Figure 5.10 Sonication of nanoparticles by ultrasonic bath.

The first chosen dope and bore liquid compositions of hollow fiber membranes are given in Table 5.1. The membranes without nanoparticles were described as pristine membrane. The dope solutions were prepared as follows: First, the required quantity of DMAc, non-solvent, and PVP powders were weighed and poured into the dope tank within the BENCHMARK B2000 water bath. After the dissolution of PVP at 85 °C, PVDF with 18 wt.% was added into the tank and continuously stirred with IKA EUROSTAR 60 overhead stirrer overnight to obtain a homogenous solution. Dope samples were taken in a glass bottle and kept in oven at 85 °C for 1 h to remove air bubbles in the solution. Before the spinning process, the dope solutions were degassed with 1 bar N_2 gas for an hour in order to eliminate the air accumulated during mixing step, as dope solutions containing air bubbles could lead to breaking the fiber during the operation.

Table 5.1 Dope and bore liquid compositions of hollow fiber membranes.

	DOPE (wt.%)					**BORE (wt.%)**	
	PVDF	**PVP-K30**	**PVP-K90**	**DMAc**	**HNTs**	**DMAc**	**DIW**
Pristine (1)	18	5	2	75	-	75	25
0.2 wt.% A-HNT	18	5	2	74.962	0.036	75	25

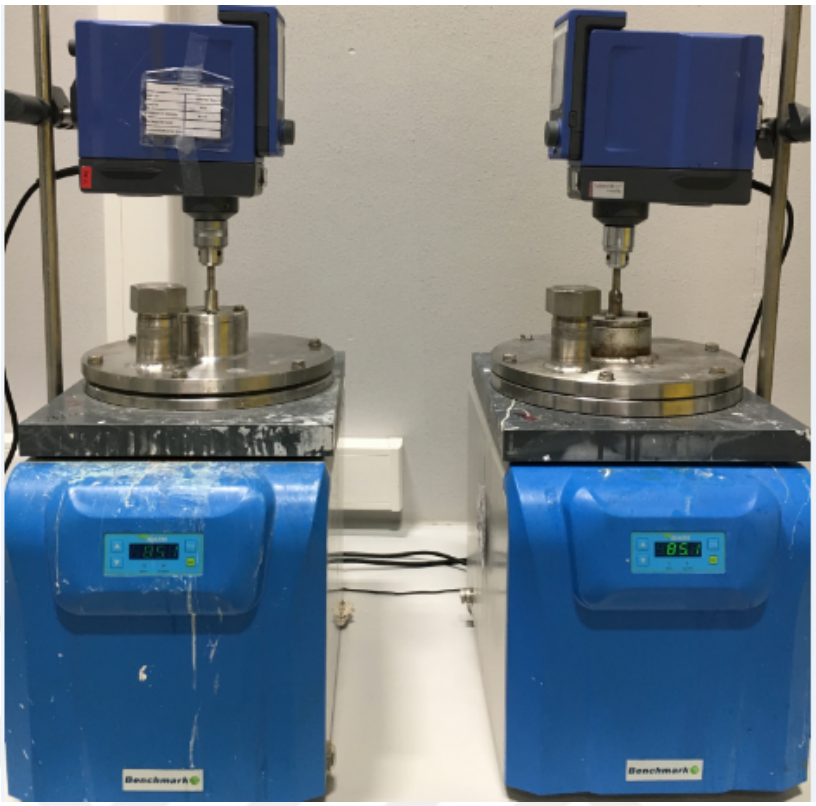


Figure 5.11 Preparation of dope solutions.

The final chosen dope and bore compositions for preparing hollow fiber membranes are given in Table 5.2. As bore liquid, 60% DMAc, 35% deionized water (DIW) and 5% non-solvent composition was used for all membranes. Prepared bore liquid was spontaneously heated because the reaction of mixing water with glycerol is exothermic. Prepared bore liquid is shown in Figure 5.12. Different dope concentrations of A-HNT and A-hBN (0, 0.2, 0.4, 0.6 wt.%) were prepared as follows: Primarily, solvent DMAc, non-solvent and dispersed nanoparticles were mixed with IKA EUROSTAR 60 overhead stirrer for 10 min. As following, PVP K30 and PVP K90 were poured into solution and intensively stirred for 30 min at room temperature (Figure 5.13). Prepared polymer solution was transferred into pilot scale dope tank with mixer and mixed for minimum 3 h at 85 °C (Figure 5.14). After the addition of PVDF powder, the spinning solution was continuously mixed overnight. Lastly, it was degassed using N_2 gas for an hour in order to eliminate the air accumulated during mixing step. Because dope solutions containing air bubbles could lead to break of the fiber during the operation.

Table 5.2 Dope and bore liquid compositions of hollow fiber membranes.

	DOPE (wt.%)							BORE (wt.%)		
	PVDF	**PVP-K30**	**PVP-K90**	**DMAc**	**Non-solvent**	**HNT**	**h-BN**	**DMAc**	**Non-solvent**	**DIW**
Pristine (2)	18	7.5	7.5	61	6	-	-	60	5	35
0.2 wt.% A-HNT	18	7.5	7.5	60.964	6	0.036	-	60	5	35
0.4 wt.% A-HNT	18	7.5	7.5	60.928	6	0.072	-	60	5	35
0.6 wt.% A-HNT	18	7.5	7.5	60.892	6	0.108	-	60	5	35
0.2 wt.% A-BN	18	7.5	7.5	60.964	6	-	0.036	60	5	35
0.4 wt.% A-BN	18	7.5	7.5	60.928	6	-	0.072	60	5	35
0.6 wt.% A-BN	18	7.5	7.5	60.892	6	-	0.108	60	5	35



Figure 5.12 Preparation of bore liquid consisted of solvent/deionized water/non-solvent.

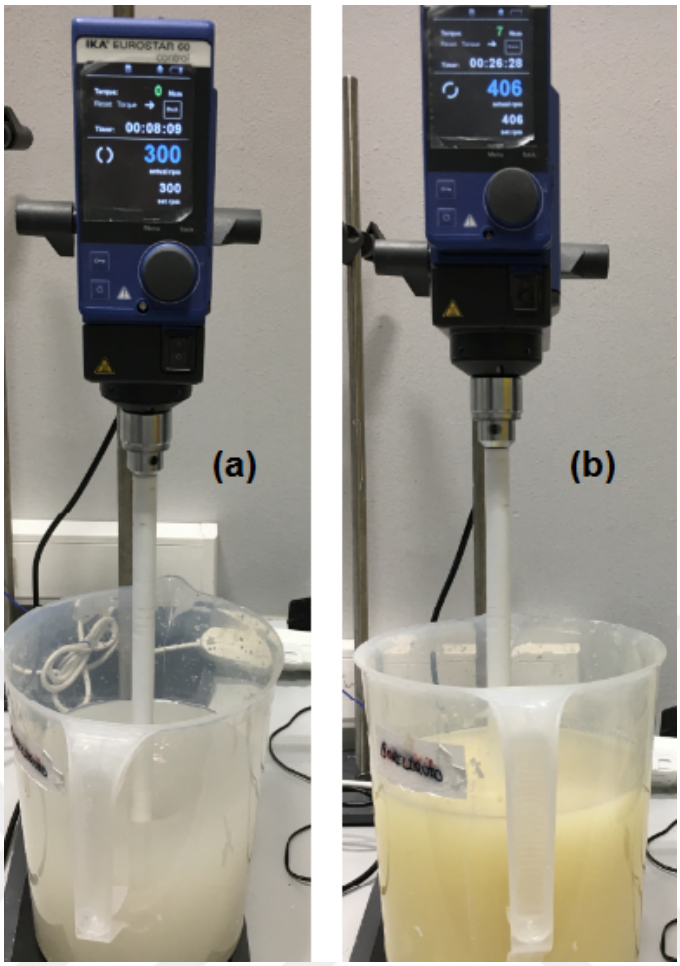


Figure 5.13 (a) Solvent, non-solvent, nanoparticle mixture, (b) Polymer mixture.

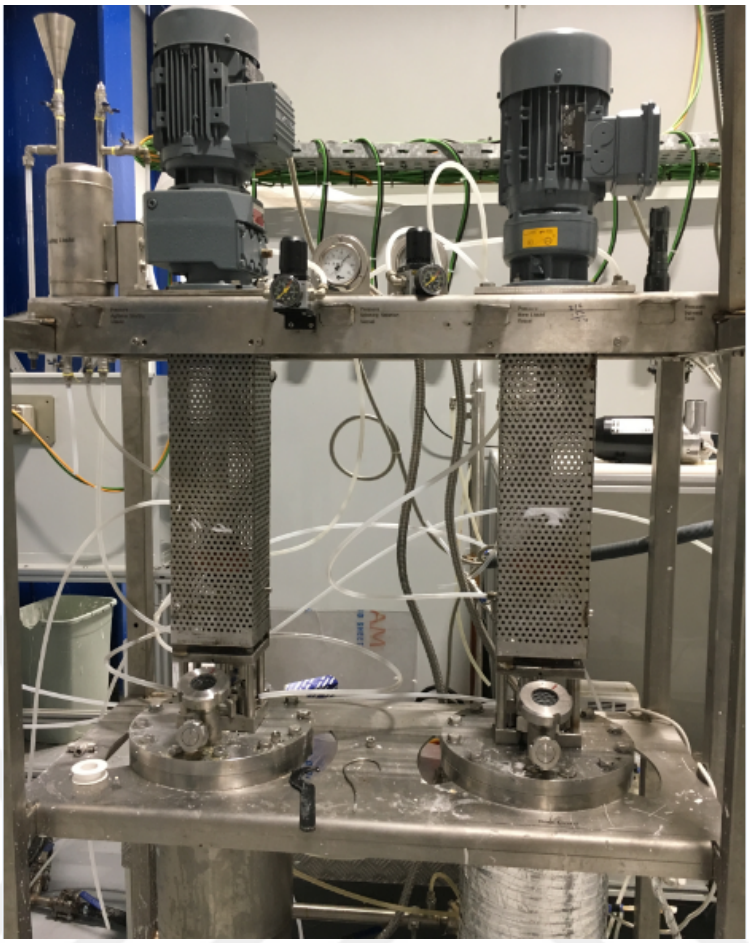


Figure 5.14 Pilot scale dope tanks with rotator.

5.5 Viscosity Measurement of Dope Solutions

Before the spinning process, viscosity values of dope solutions were calculated using (MALVERN KINEXUS PRO+) a rheometer to determine the processing conditions of the spinning. An approximately 1.2-mL dope solution was loaded on a stainless steel active hood cartridge using a plastic spatula. (Figure 5.15). After determination of zero gap length with the help of software, dynamic viscosity (η) with a shear rate of 1 s^{-1} at 85 °C was measured in centipoise (cP) (mPa.s).

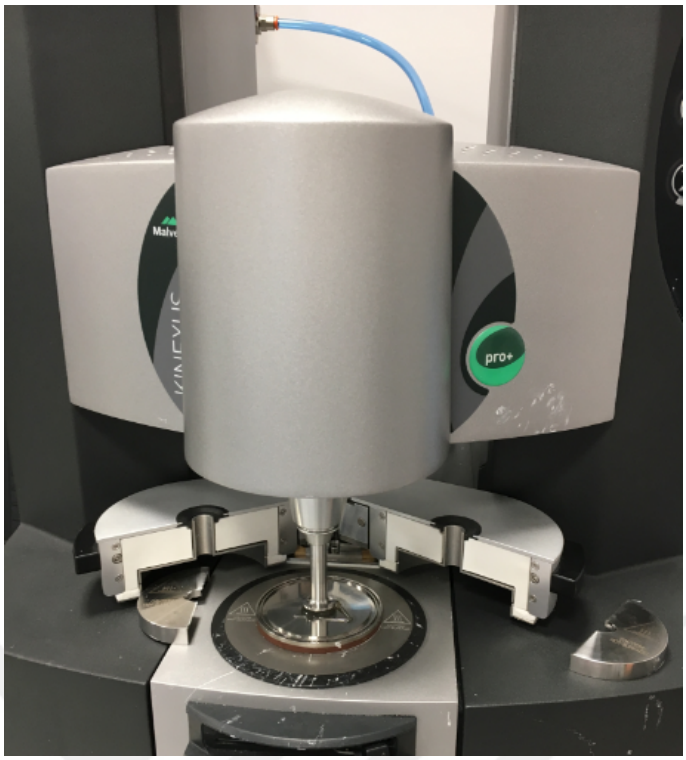


Figure 5.15 Viscosity measurement.

5.6 Spinning of Hollow Fiber Membranes

PVDF-based hollow fiber UF membranes were fabricated using the dry-jet-wet spinning method, as described in [53]. . Pilot scale membranes were produced using a custom-made extrusion line via the immersion precipitation method. Operation conditions such as speed of extrusion (pump) and stretching (line), outer and inner diameter of desired fibers can be controlled by the PLC screen located on the pilot machine. Before the spinning process, the coagulation bath should be swamped with hot water at 60 °C. Dope tank pressure was adjusted to 5-10 bar and “pump polymer off”, “pump bore liquid off” button was activated on PLC screen. It takes time to dope material to provide static balance, so the dope solution and bore liquid should be drained through spinning line for a time in order to achieve a constant flow as shown in Figure 5.16. The distance between the spinneret and the coagulation bath (air gap) was adjusted to 5 cm. When the dope solution meets with bore liquid, hollow fiber structure forms. At first, the pump speed was arranged to 10 m/min and hollow fiber was passed through coagulation bath, driving roll, rinsing bath respectively. The purpose of the rinsing bath is removing excessive solvent within fibers. Hollow fibers were collected on the winder rinsing with fresh water feed. Hollow fiber fabrication system and schematic illustration of the spinning set up are shown in Figure 5.17 and Figure 5.18.



Figure 5.16 Flow of dope solution.

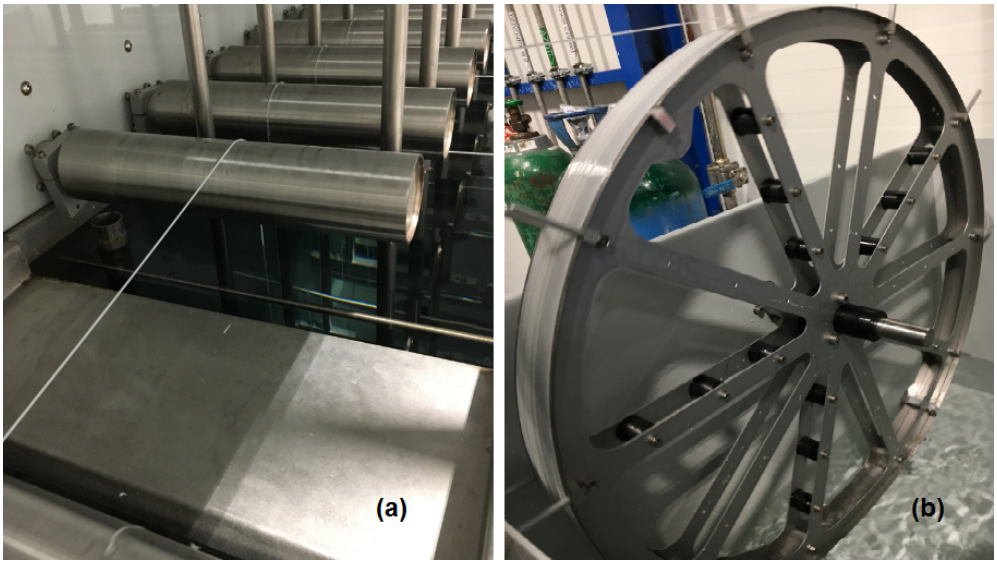


Figure 5.17 (a) Spinning line, (b) Take-up of hollow fiber fabrication.

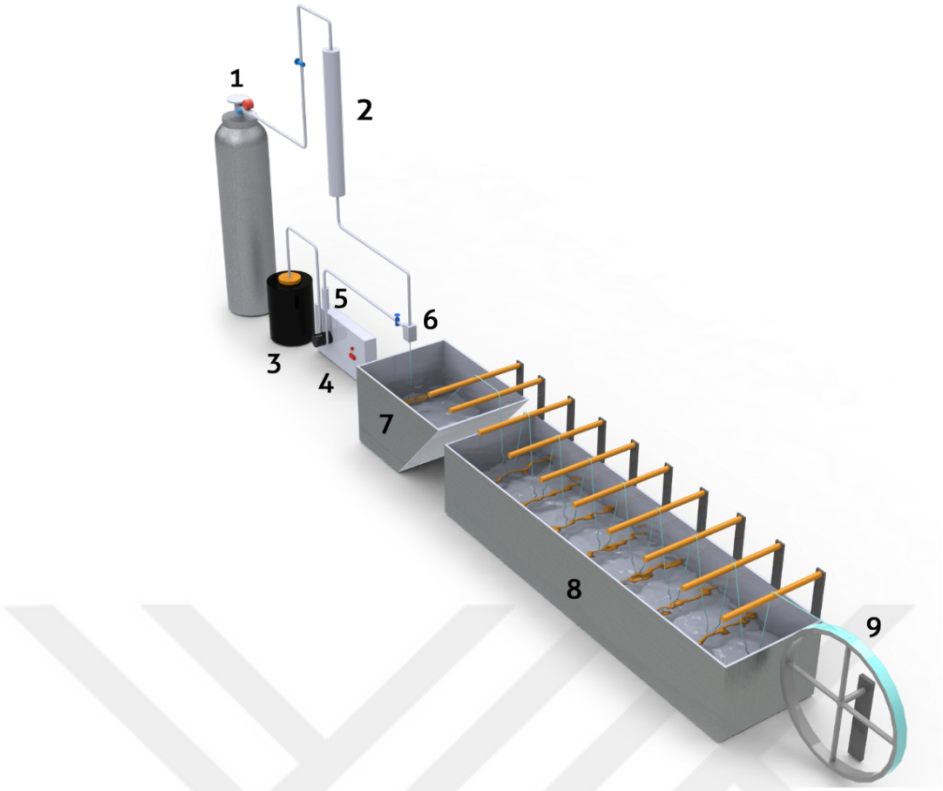


Figure 5.18 Schematic illustration of the pilot scale spinning set up. (1: N_2 gas cylinder, 2: dope tank, 3: bore liquid tank, 4: gear pump, 5: flow meter, 6: spinneret, 7: coagulation bath, 8: washing bath, 9: winder).

5.7 Post Treatment of Hollow Fiber Membranes

At first, hollow fiber membranes were immersed in the water bath at 60 °C for 1 h to remove the residual solvent within membrane and then they were put into 100.000 ppm.h sodium hypochlorite (NaOCl) solution in order to remove PVP from the membrane structure. NaOCl post treatment of hollow fiber membranes is shown in Figure 5.19. Post treated membranes were rinsed with hot water for 1 h to remove NaOCl trapped inside the fibers and the DMAc from the production. Water should be refreshed four times and hollow fibers were stored in deionized water.

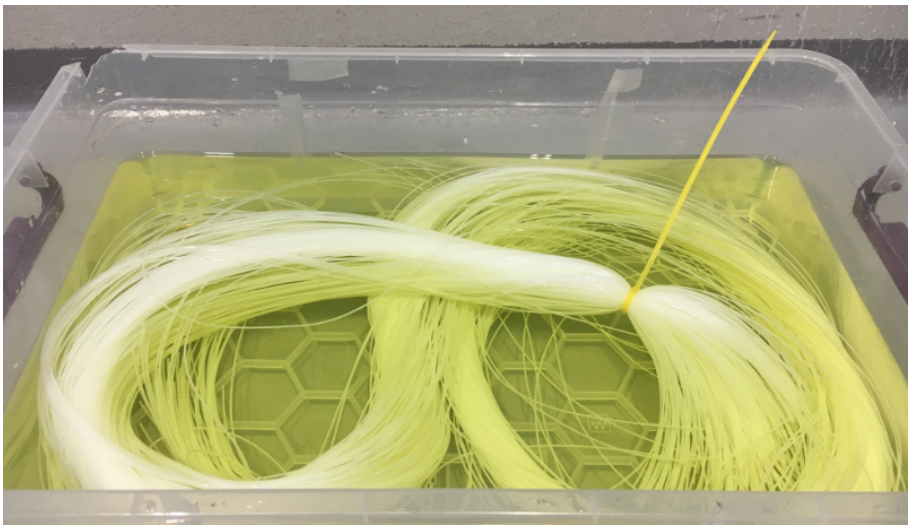


Figure 5.19 NaOCl post treatment of hollow fiber membranes.

5.8 Preparation of Hollow Fiber Test Modules

HF test modules were prepared 4 times for each sample and then averaged to determine the PWP and MWCO values of the membrane. Schematic illustration of the HF test modules is shown in Figure 5.20. Five hollow fibers with an effective length of 20 cm were passed through a polyurethane pipeline with a diameter of 1.2 cm and a length of 35 cm. Two pieces of t-fittings were placed at the end of the two pipelines, after which two pieces of pipelines were put at the end of the t-fittings. The shell sides of the two ends of the mini modules were glued through the t-fittings with epoxy resin and plugged as shown in Figure 5.21. Test modules were left for 2 h for curing before the test. Finally, the end of one pipeline was cut from the plug.

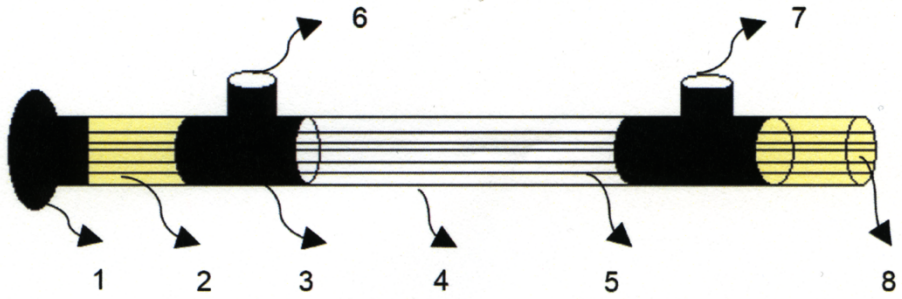


Figure 5.20 Schematic illustration of HF test modules (1: plug, 2: glue, 3: t-fitting, 4: pipeline, 5: HF membranes, 6: pipe input, 7: air vent outlet, 8: pipe outlet).

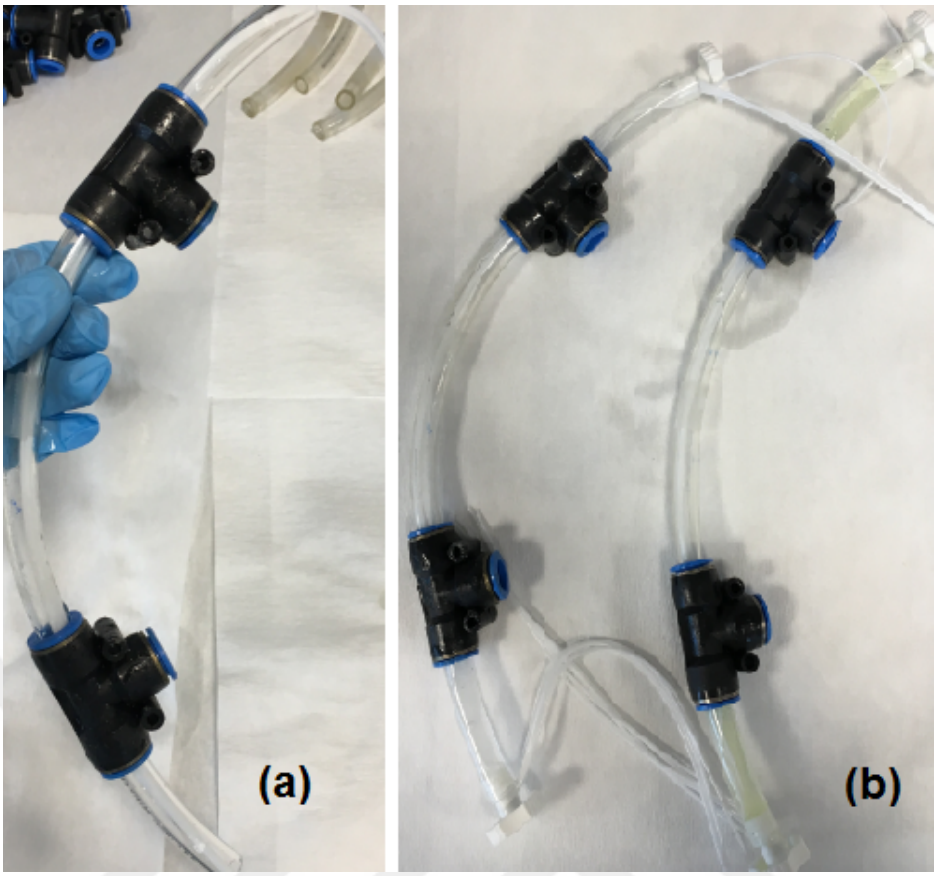


Figure 5.21 (a) Preparation of HF test modules, (b) Glued and plugged HF test modules.

CHAPTER 6

CHARACTERIZATION

6.1 Characterization of Nanoparticles

6.1.1 Fourier-transform Infrared Spectroscopy (FT-IR)

The FT-IR spectrometer was employed to record the characteristic peaks of HNTs and h-BN. The FT-IR measurements were performed with THERMO SCIENTIFIC NICOLET iS10 spectrometer as shown in Figure 6.1. FT-IR spectra were conducted between 1200 and 3800 cm^{-1} with 8 cm^{-1} resolution.



Figure 6.1 THERMO SCIENTIFIC NICOLET iS10 FT-IR Spectrometer.

6.1.2 Thermogravimetric Analysis (TGA)

TGA measurements were carried out to determine the thermal stability of the nanoparticles. TGA analyses were performed on a PERKIN ELMER TGA 4000 as given in Figure 6.2. Samples of 2-3 mg were heated from 30 °C to 800 °C at 10 °C/min under nitrogen atmosphere.

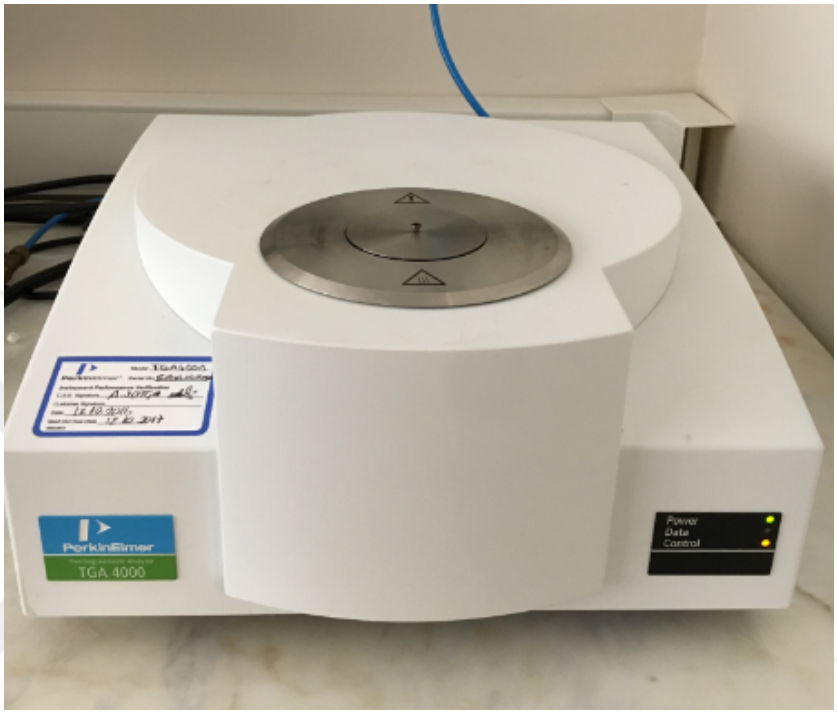


Figure 6.2 PERKIN ELMER TGA 4000.

6.1.3 X-ray Diffraction Analysis (XRD)

The X-ray diffraction analysis was applied to determine the crystallinity of APTES-HNTs. Powder X-ray diffraction measurements were performed at room temperature by GNR APD 2000 PRO XRD diffractometer with an acceleration voltage of 40 kV and an emission current of 30 mA. The data were collected using Cu Kα radiation (λ = 1.5418 Å) with a scan rate of 0.02° 2θ s^{-1} and a range of 0-70°.

6.2 Membrane Characterization Techniques

6.2.1 Light Microscopy

Light microscope was used to determine the structure and sizes (outer diameter, inner diameter) of hollow fibers. Light microscope images were taken with NIKON ECLIPSE

LV100ND motorized microscope as shown in Figure 6.3. Hollow fibers were cut and placed in a plastic holder (Figure 6.4).

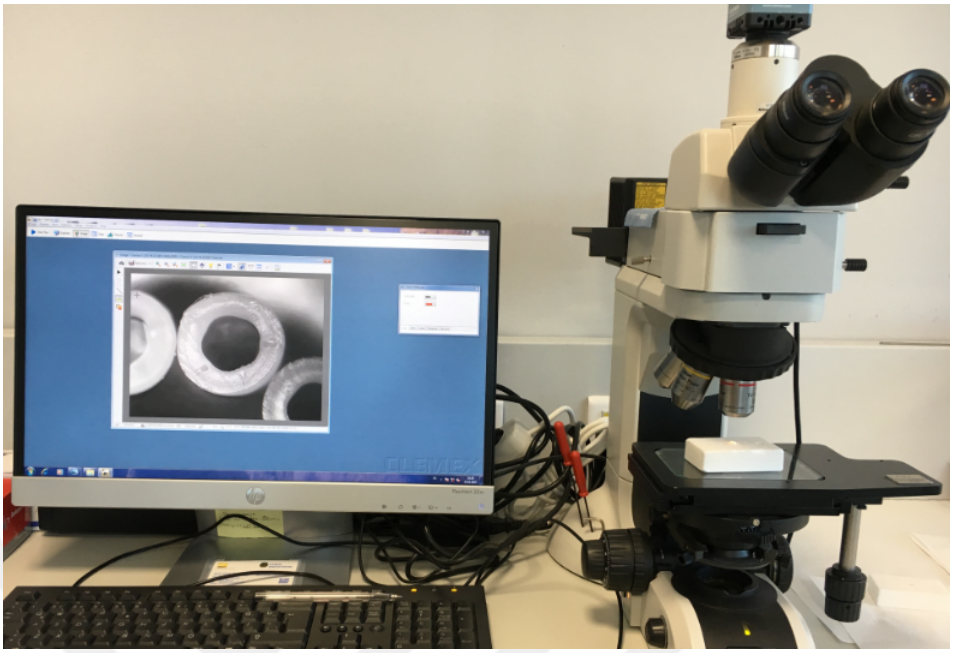


Figure 6.3 NIKON ECLIPSE LV100ND Motorized Microscope.



Figure 6.4 Installed hollow fibers for light microscopy.

6.2.2 Calculation of Pure Water Permeability Value

To determine the pure water permeability (PWP) performance of the membranes, a manual permeability measurement system was used. The permeability measurements were conducted at 25 °C with a feed pressure of 1.0 bar. Hollow fibers were tested in bundles of five fibers of 20 cm in length. The prepared hollow fiber test modules were pressured at 1.0 bar with deionized water for 20 min, followed by calculation of the PWP (J) was calculated with an excel program according to equation (6.1) below [282]:

$$J = \frac{Q}{S \times t \times \Delta P} \times F \quad (6.1)$$

where:

J: Permeability (L/m^2.h.bar)

Q: Volume of the permeated pure water (L)

S: Effective surface area (m^2)

t: Time (hour)

ΔP: Transmembrane pressure (bar)

F: Correction factor of pure water temperature ($1.03^{(T-25°C)}$)

T: Pure water temperature (°C)

$$S = 2\pi r \times L \times n \quad (6.2)$$

where:

r: Radius of fibers (m)

L: Length of fibers (m)

n: Number of fibers

PWP set up and schematic diagram for UF experimental equipment are shown in Figure 6.5 and Figure 6.6.



Figure 6.5 Pure water permeation set up.

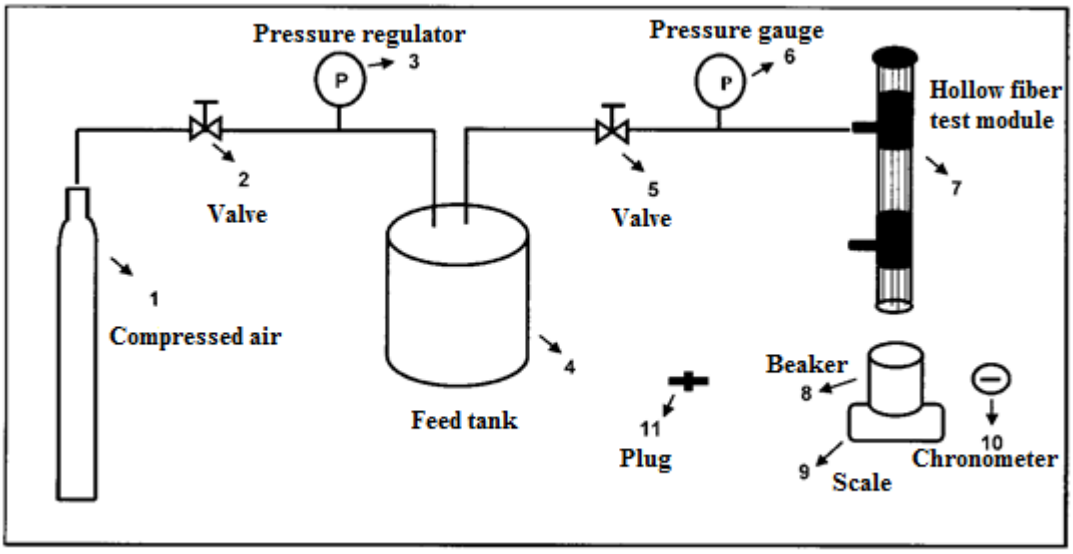


Figure 6.6 Schematic diagram for ultrafiltration experimental equipment.

6.2.3 Determination of the Molecular Weight Cut-off (MWCO) Values

The MWCO of hollow fiber membranes can be defined as the molecular weight at 90% rejection. It was tested using dextran solutions with different molecular weights, such as

below 500.000 Da. The feed solution was filtered from the HF test modules for 1 h before the sample was taken from the permeate solution (Figure 6.7). MALVERN water gel permeation chromatography (GPC) system was used to measure the MWCO in the feed and permeate solution (Figure 6.8). The rejection of membranes (R) was calculated according to the equation (6.3) [68] using the retention test calculation excel software:

$$R(a) = \frac{Cf - Cp}{Cf} \tag{6.3}$$

where Cf (mg/L) is the dextran concentration of the feed solution and Cp (mg/L) is the dextran concentration of the permeate solution with a diameter of a.

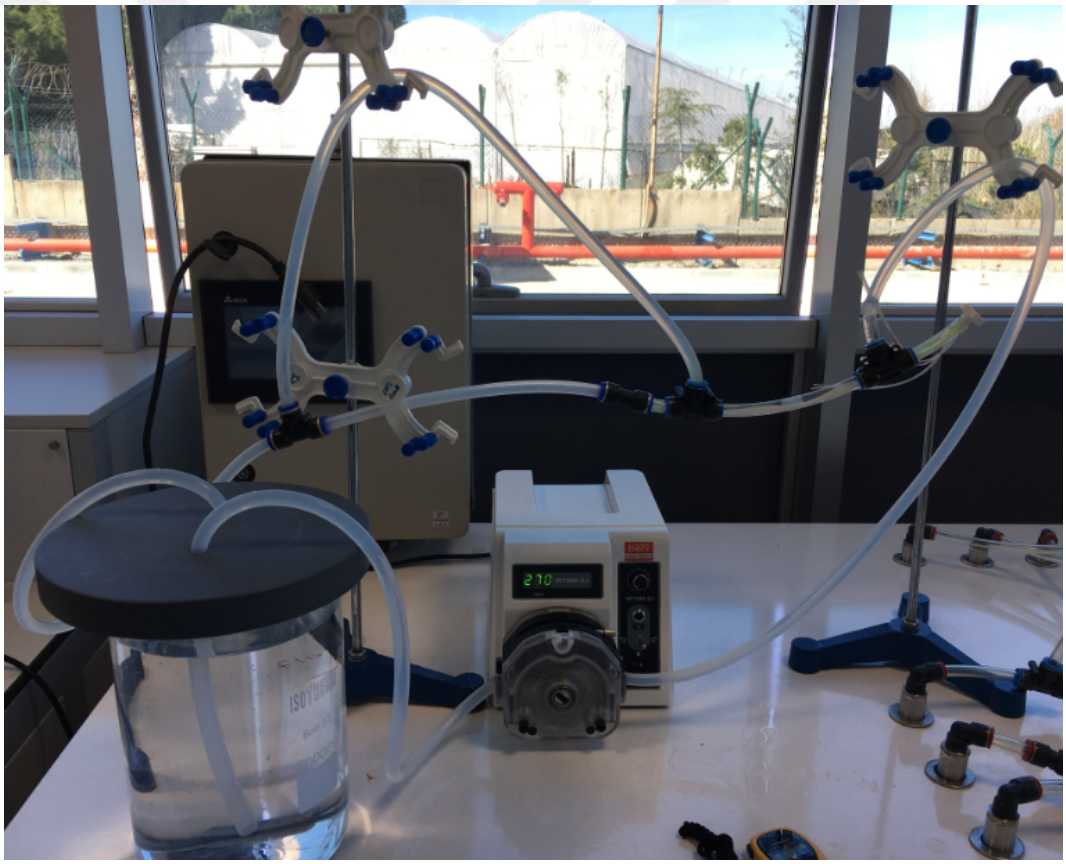


Figure 6.7 MWCO experimental set up.



Figure 6.8 MALVERN GPC device.

6.2.4 Tensile Test

Mechanical properties including tensile strength and maximum elongation percent of hollow fiber membranes, were determined by SHIMADZU AGS-X Tensile Tester as shown in Figure 6.9. A manual grip was used to compress the hollow fiber membrane by turning the valve. Tensile tests were performed four times and then averaged for each sample, for which the loading capacity was 8 mm/min using 150 mm long fibers. Tensile strength and percentage of maximum elongation were calculated from the program used by the tensile tester, with the stress-strain curve being drawn according to equations (6.4) and (6.5) below:

$$Tensile\ Srength = \frac{F}{Ao} \quad \text{(MPa)} \tag{6.4}$$

$$Elongation\ Percent = \frac{\Delta L}{Lo} \times 100 \quad (\%) \tag{6.5}$$

where:

F: force (N)

Ao: cross sectional area of the membrane before elongation (mm^2)

ΔL: displacement at maximum load (mm)

Lo: initial length of the membrane (mm)

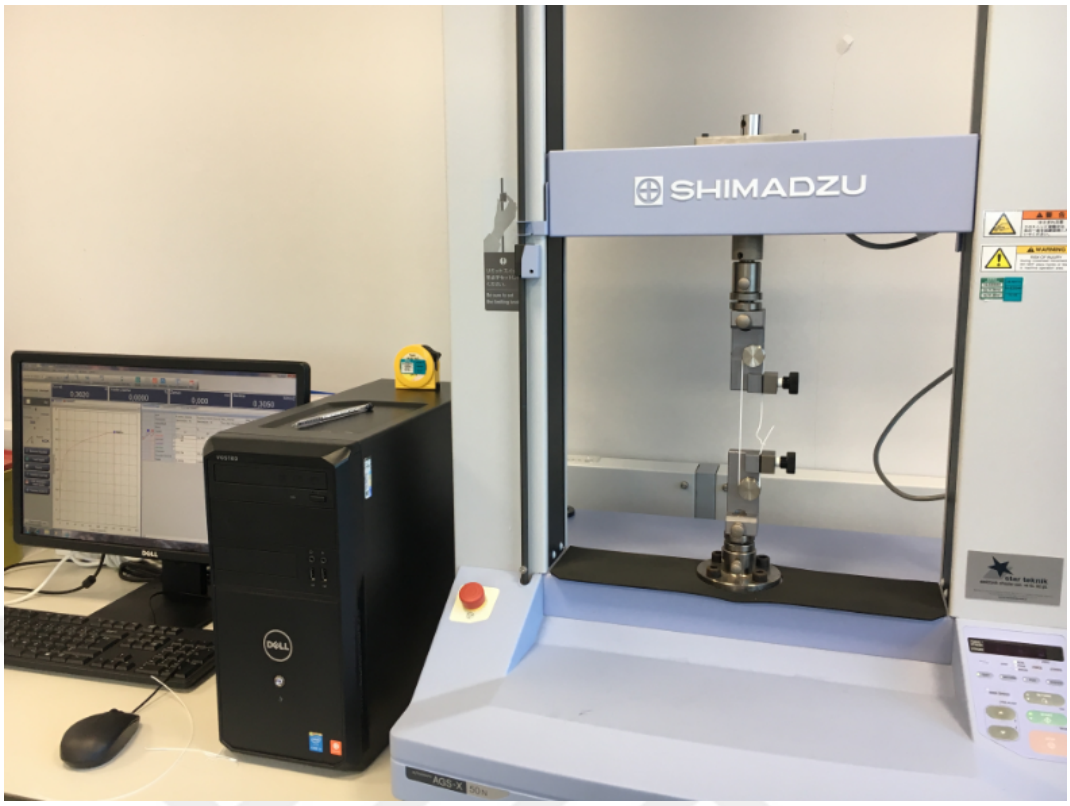


Figure 6.9 SHIMADZU AGS-X Tensile Tester.

6.2.5 Bubble Point Pressure Measurements

The bubble point test determines the maximum pore size in hollow fiber membranes. According to Laplace's equation, maximum pore size can be calculated as shown below [169]:

$$r_p = \frac{2\gamma}{\Delta P} cos\theta \tag{6.6}$$

where r_p is the radius of a given capillary-shaped pore, γ the surface tension at the liquid/air interface (71.96 x 10^{-3} N.m^{-1}), ΔP (Pa) is the transmembrane pressure and θ is the contact angle (°) [283].

To determine the bubble point pressure of the hollow fiber membranes, test modules containing five 50 cm-long fibers were prepared (Figure 6.10). Fibers were passed through a 10 cm-long tube before gluing the inside of the tube with an epoxy resin. After drying the modules for 2 h, a bubble point test was carried out in a bath of isopropyl alcohol (IPA)-water (50%) mixture by using the experimental setup shown in Figure 6.11. The pressure was gradually increased until the first bubble occurrence in the bath, which indicates the bubble point pressure of the membrane. Next, the pressure was rapidly

increased in order to burst the hollow fibers. The bubble point and burst pressures were recorded. The test was repeated 4 times for each membrane and then averaged.



Figure 6.10 Test modules for bubble point pressure measurement.



Figure 6.11 Bubble point measurement set up.

6.2.6 Contact Angle Measurements

The wettability of the membranes is determined by their hydrophobic and hydrophilic properties. The surface hydrophilicity of the hollow fiber membranes was characterized by a water contact angle (CA) (θ) measurement using an optical tensiometer ATTENSION THETA OPTICAL TENSIOMETER shown in Figure 6.12. The sessile drop method was applied in making the measurements. Previously dried membranes were taped onto the table and then 3 µl of deionized water was dropped onto the membrane surface. The CA between water and the surface of hollow fiber membrane were measured at 5 different locations of each sample and then averaged to minimize the experimental error.

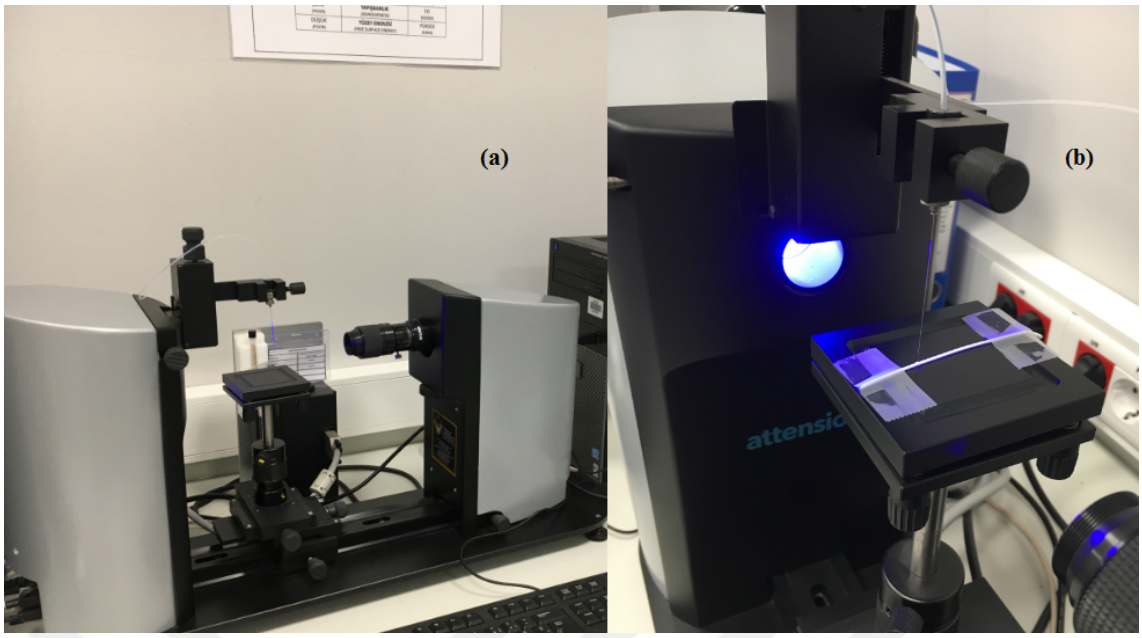


Figure 6.12 (a) Contact angle measurement device, (b) prepared sample for the measurements.

6.2.7 Scanning Electron Microscopy (SEM)

The surface and cross-section morphologies of the hollow fiber membranes were observed with a ZEISS ULTRA PLUS field emission scanning electron microscope (FESEM) given in Figure 6.13. Prior to the test, membranes were dried in NUVE EV 018 vacuum oven (Figure 6.14) overnight and then immersed in liquid nitrogen for few seconds followed by freeze-fracturing carefully. The samples were mounted using an aluminium holder with double-sided conductive carbon tape as shown in Figure 6.15. Samples were then coated with Gold (Au) 10-12 nm thick for several minutes using CRESSINGTON 108AUTO sputter coater to provide electrical conductivity. (Figure 6.16). The FESEM micrographs of cross-section, inner surface and outer surface of hollow fiber membranes were taken at 2.50 KV under various magnifications.

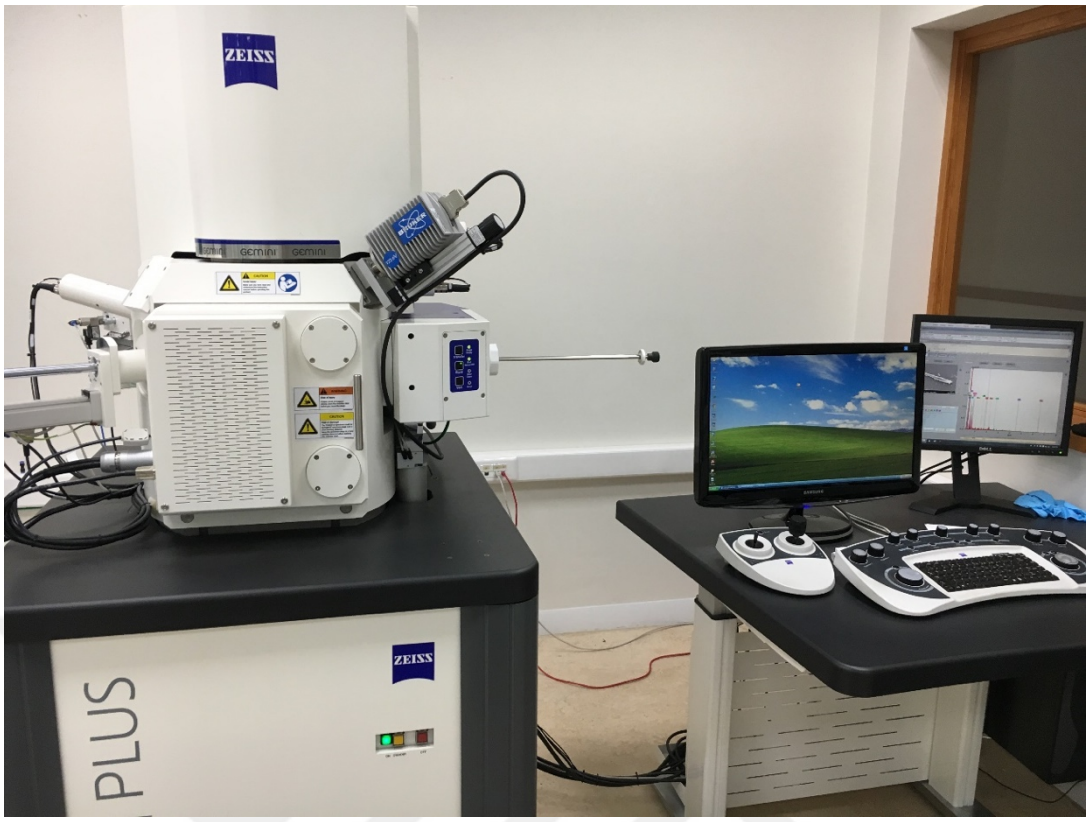


Figure 6.13 ZEISS FESEM.



Figure 6.14 NUVE EV 018 vacuum oven.



Figure 6.15 Prepared test samples.

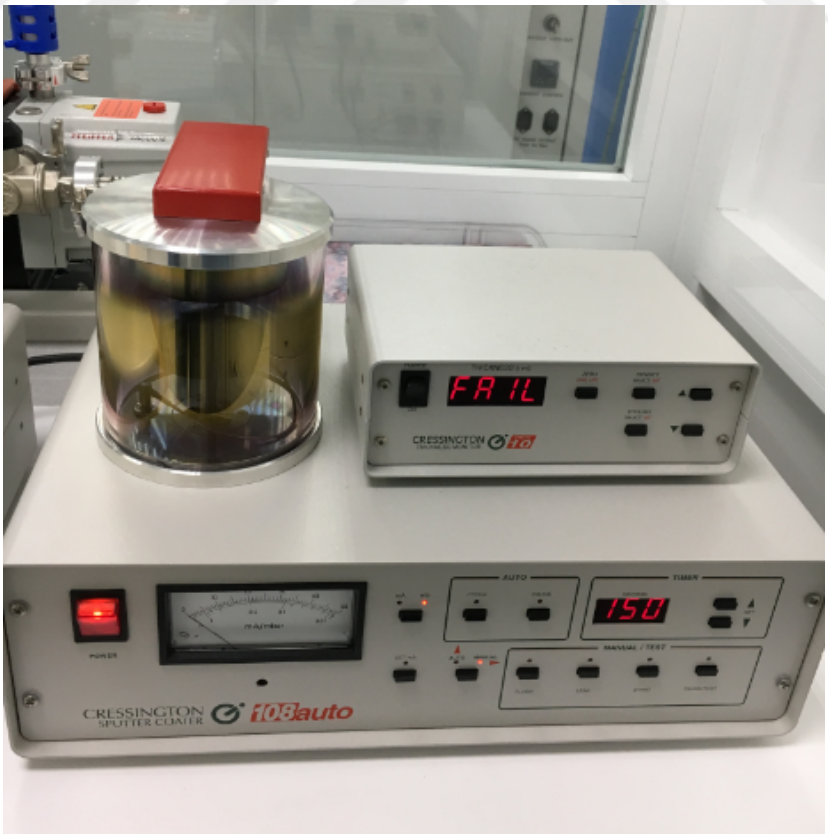


Figure 6.16 CRESSINGTON 108AUTO Sputter coater.

CHAPTER 7

RESULTS AND DISCUSSION

7.1 Characterization of Nanoparticles

7.1.1 FT-IR Spectra Results

FTIR spectra was used to determine the structure and functional groups of pristine HNTs, modified HNTs, pristine h-BN and modified h-BN. FTIR spectra of pristine HNTs and APTES-HNTs are given in Figure 7.1.

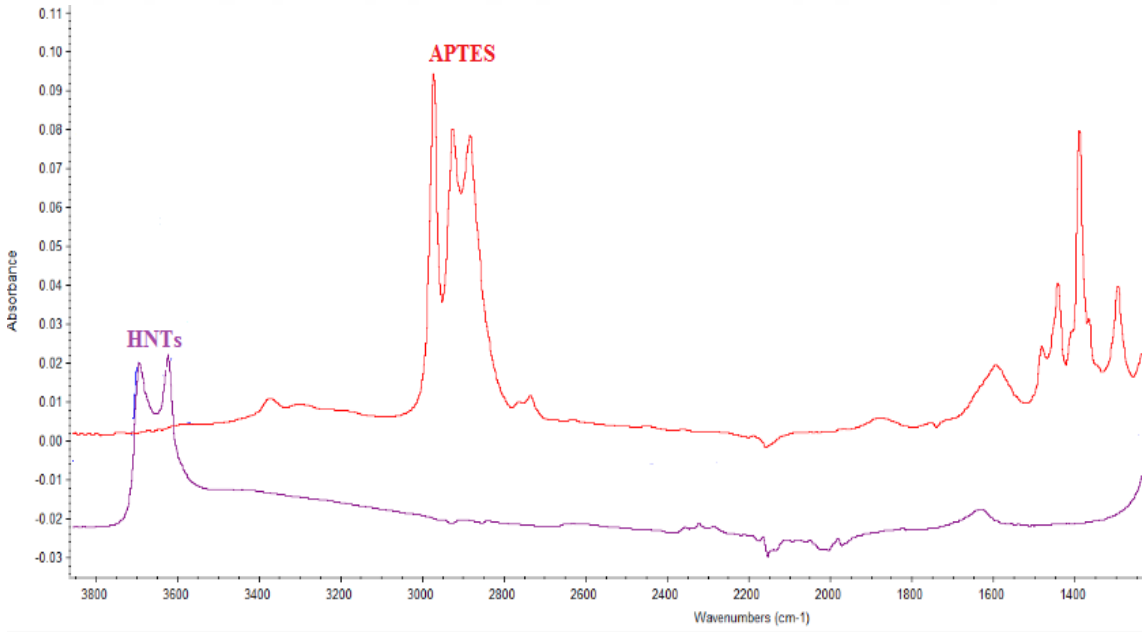


Figure 7.1 (a) FTIR spectra of APTES and HNTs.

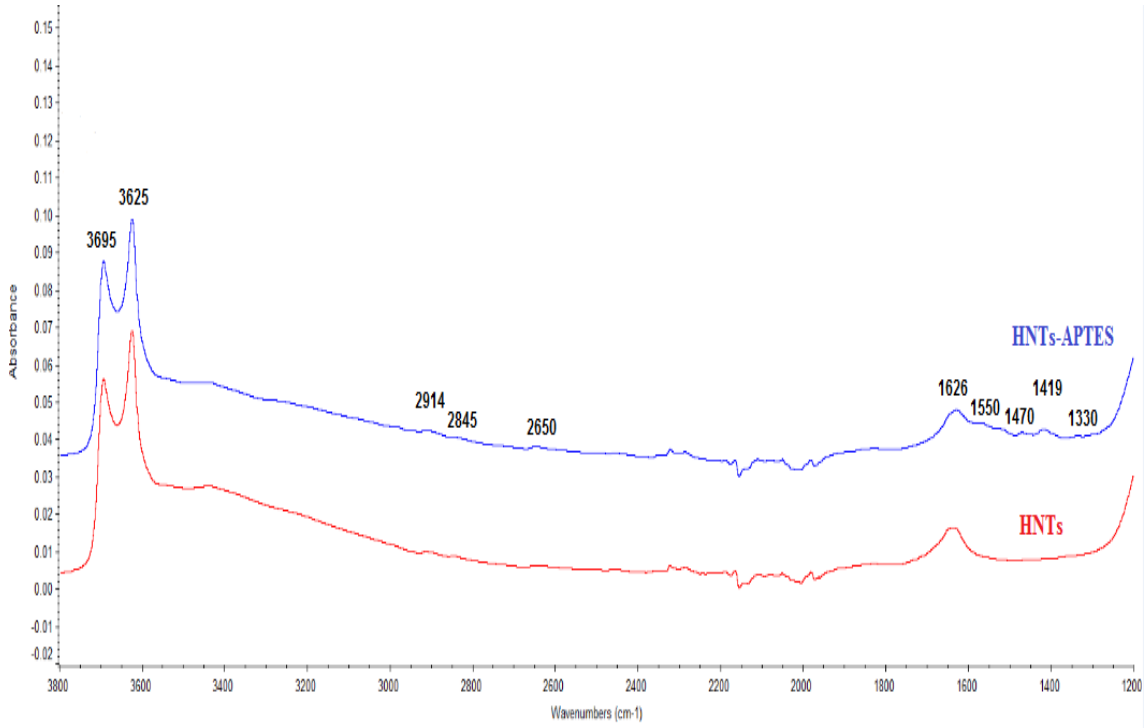


Figure 7.1 (b) FTIR spectra of HNTs and HNTs-APTES.

As shown in Figure 7.1 (b), the intense vibration bands at 3695, 3625 cm^{-1} indicate the Al—OH stretching vibrations of inner surface of HNTs, while the band at 1626 cm^{-1} was attributed to O—H deformation of water [244, 264, 284]. The FTIR spectra of HNTs-APTES confirmed that the crystalline structure of the modified HNTs was preserved. The peaks at 2914, 2849 cm^{-1} were assigned to the asymmetric and symmetric stretching of C–H_2. In addition, the bands at 1419, 1550 cm^{-1} correspond to the Si—CH_2 and N—H_2 groups of APTES [285]. Therefore, FTIR spectra confirmed the grafting of APTES on the surface of the HNTs.

FTIR results of pristine h-BN and modified h-BN are shown in Figure 7.2.

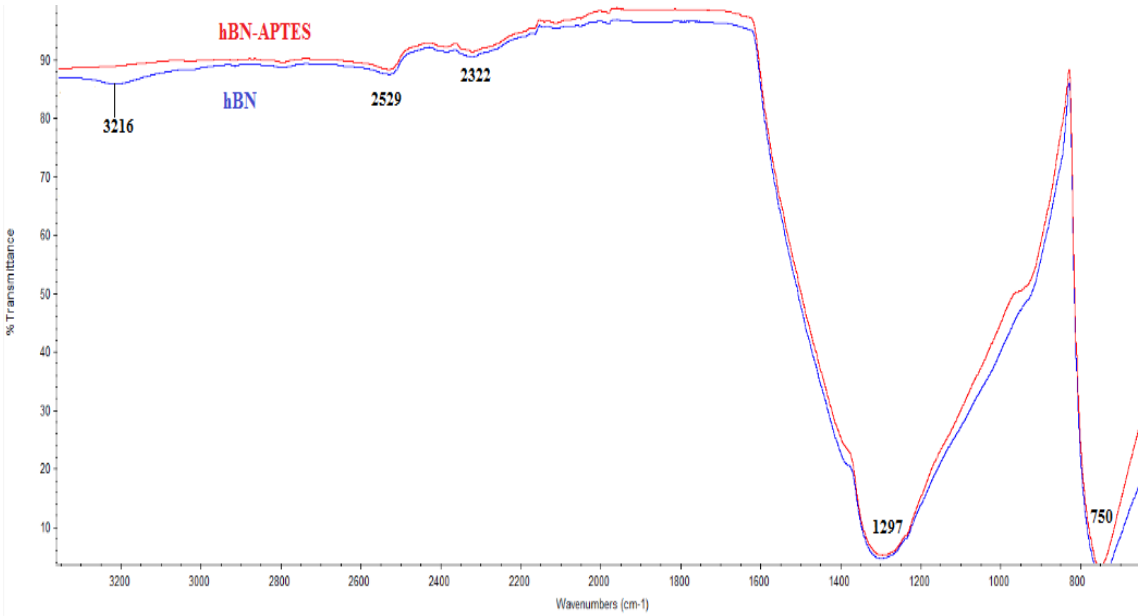


Figure 7.2 FTIR spectra of h-BN and hBN-APTES.

According to Figure 7.2, the peak at 3216 cm^{-1} which correspond to OH stretching was disappeared after the modification by APTES. The intense vibration bands at 1297, 750 cm^{-1} was assigned to B-N stretching and B-N-B bending vibrations, respectively [286, 287]. As a result of FTIR spectra, aminosilane modification of h-BN was successfully accomplished.

7.1.2 TGA Results

TGA was used to investigate the effect of silane modification of HNTs and h-BN on thermal properties. TGA results for raw HNTs and APTES modified HNTs are given in Figure 7.3 and Table 7.1.

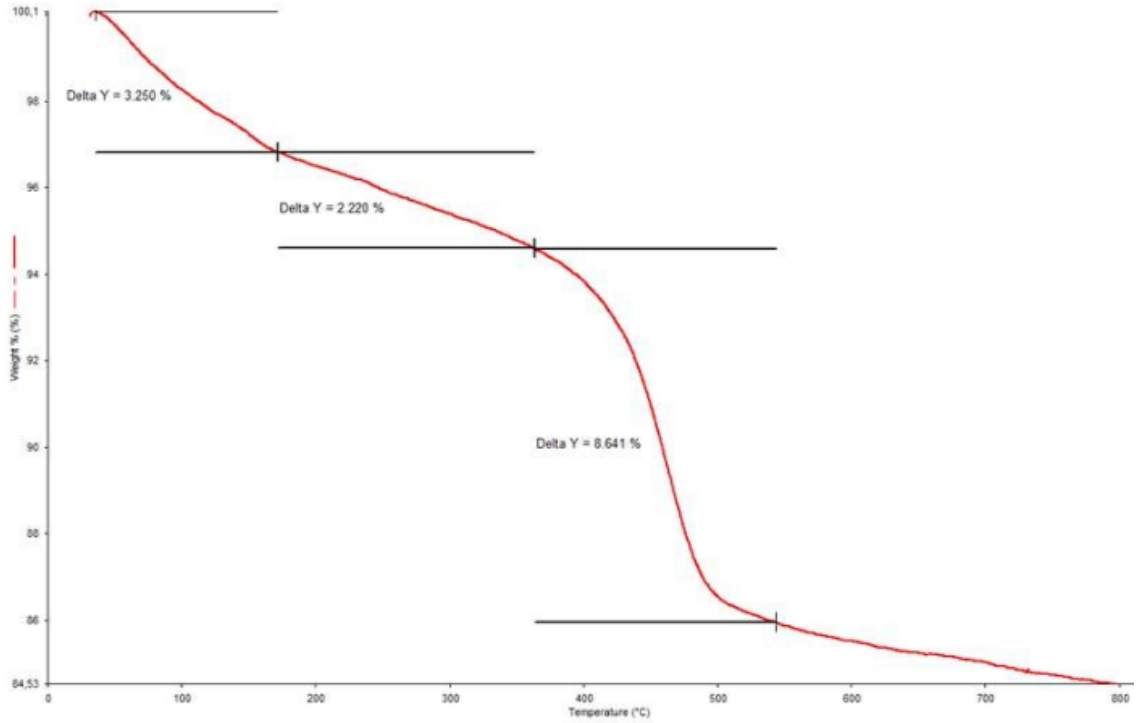


Figure 7.3 (a) TGA curve of raw HNTs.

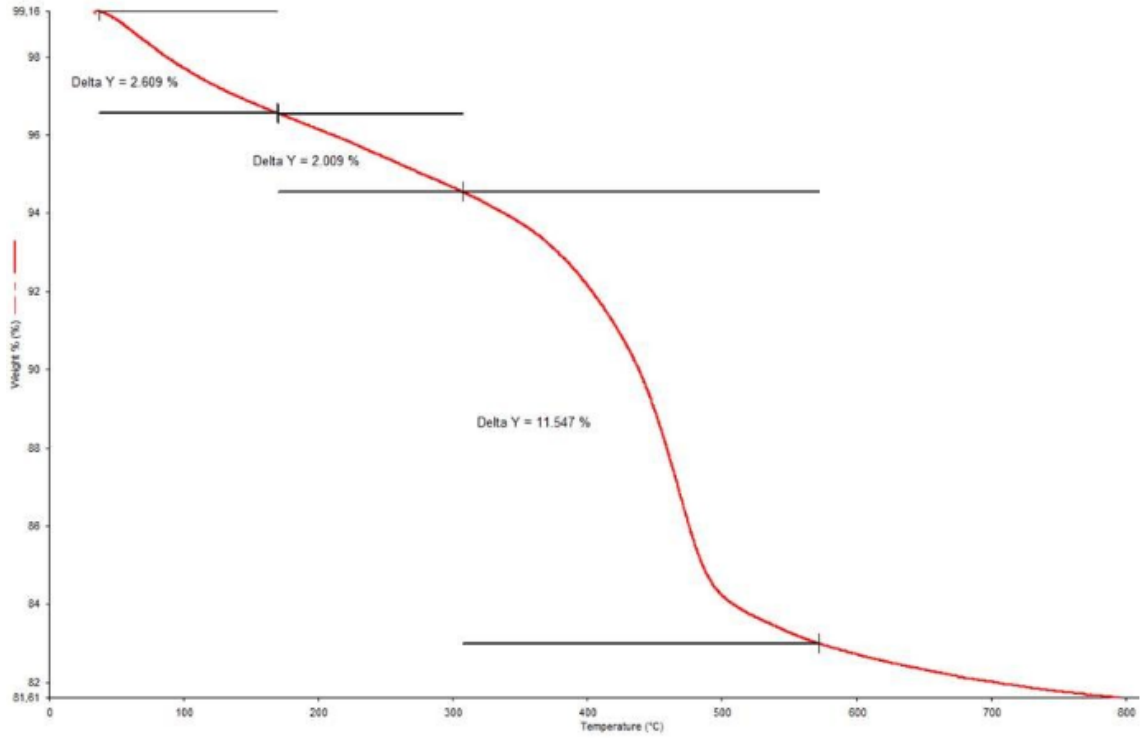


Figure 7.3 (b) TGA curve of modified HNTs.

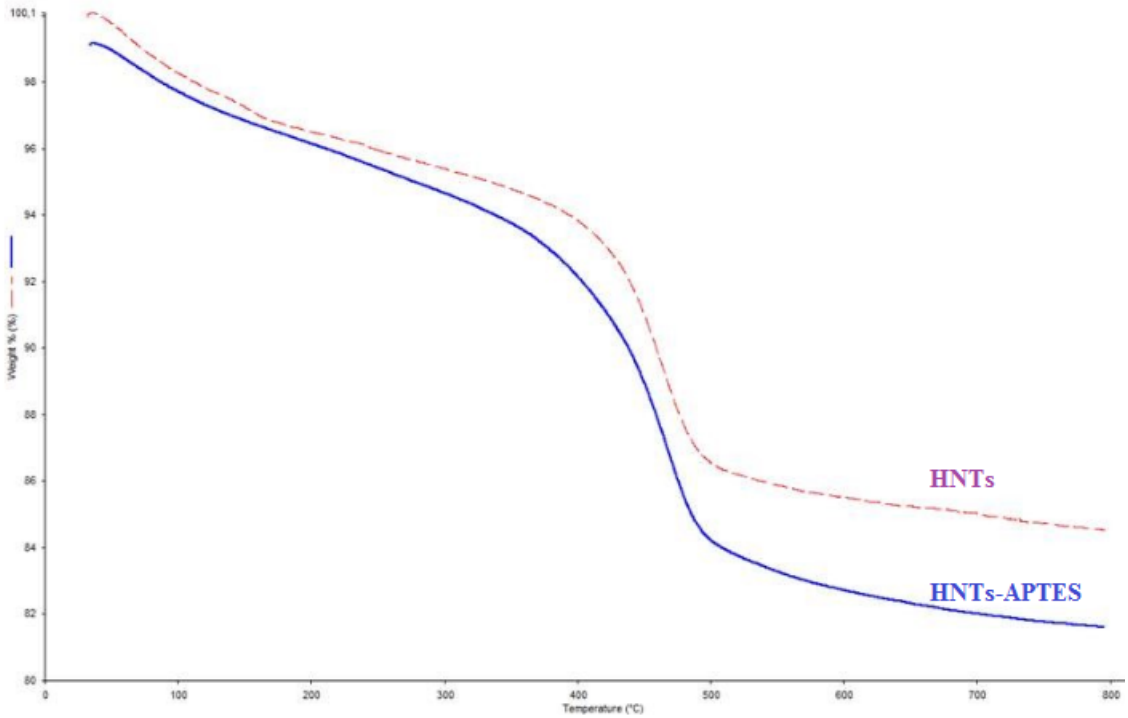


Figure 7.3 (c) TGA curves of raw HNTs and modified HNTs.

Table 7.1 TGA data for raw HNTs and modified HNTs.

	2nd		3rd		Total mass loss
	T (°C)	wt.%	T (°C)	wt.%	wt.%
Raw HNTs	172-362	2.22	362-544	8.64	14.11
HNTs-APTES	170-306	2.01	306-573	11.55	16.17

According to TGA data, for the raw HNTs and modified HNTs, the first mass losses in the range of 35-170 °C (Figure 7.3) were attributed to loss of physically adsorbed water from the surface and internal channel of the tubes. The second mass loss for raw HNTs in the range of 172-362 °C corresponded to the structural dehydroxylation of the aluminol groups (Al—OH) of HNTs. For the functionalized HNTs, the mass losses occurred at 170-306 °C and 306-573 °C, depending on the decomposition of Si and dehydroxylation of Al—OH groups, respectively [257, 288]. Because of the decomposition of the aminosilane functional groups of HNTs-APTES, more than 15 wt.% loss was observed. TGA results showed that APTES was successfully grafted on the surface of HNTs [175, 258, 261].

TGA results for raw h-BN and functionalized h-BN are given in Figure 7.4.

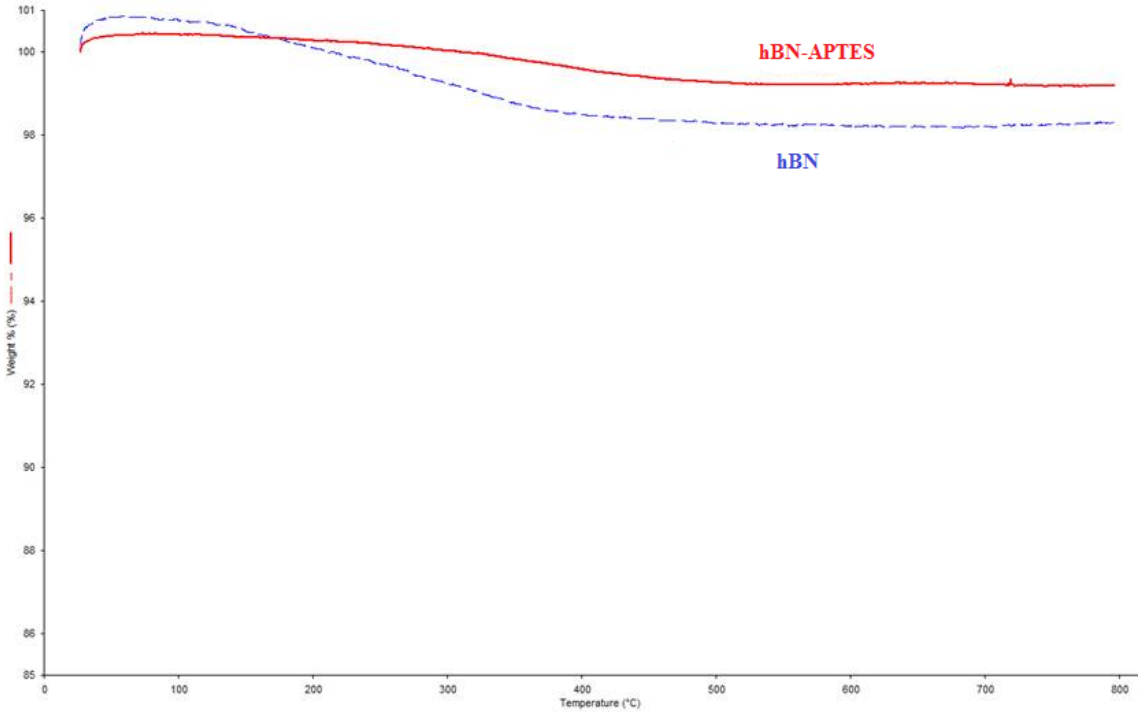


Figure 7.4 TGA results for the raw h-BN and modified h-BN.

The thermal stability of h-BN increased owing to the modification by APTES. The raw h-BN showed approximately 1 wt.% loss around 500 °C, whereas the modified h-BN showed less than 1 wt.% loss as given in Figure 7.4. Degradation of silane molecules occurred in the range of 200-500 °C.

7.1.3 XRD Results

The XRD analysis was conducted to investigate the influence of silane treatment on the crystalline structure of HNTs. Figure 7.5 shows XRD patterns of raw HNTs and APTES-HNTs.

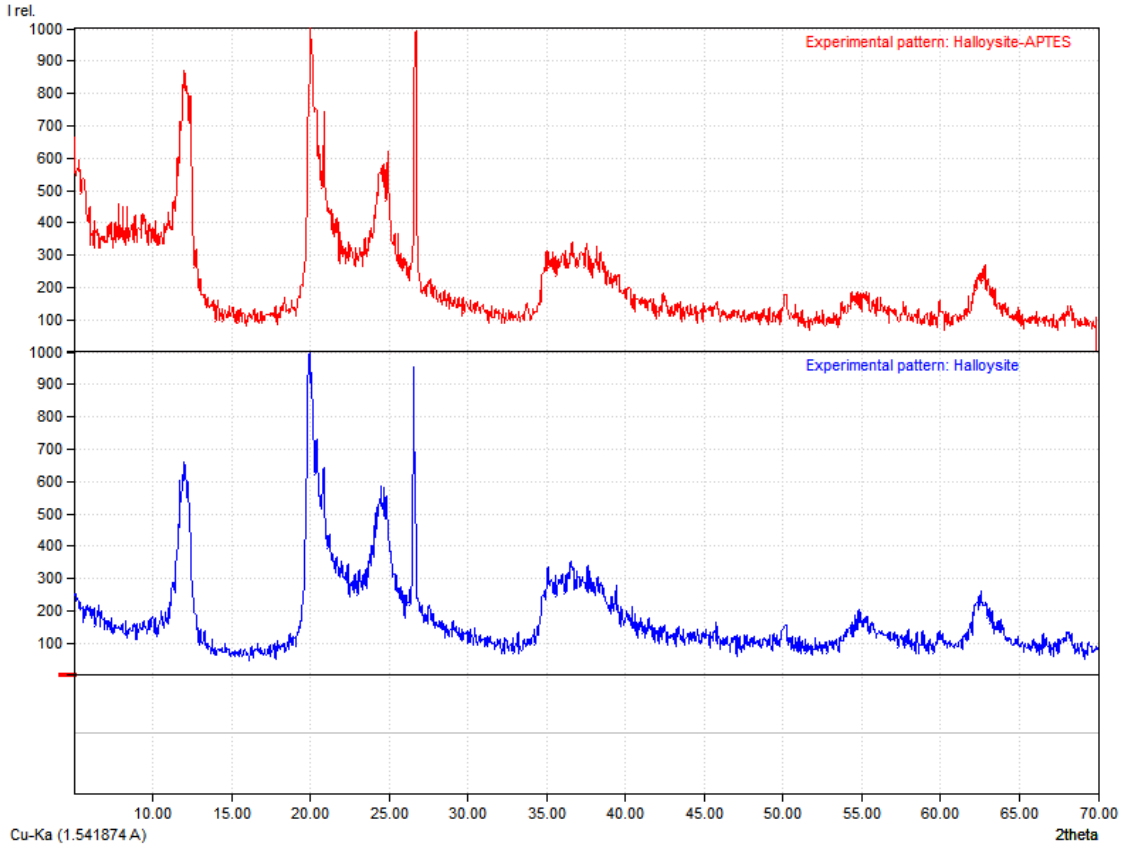


Figure 7.5 XRD patterns of HNTs and modified HNTs.

Raw HNTs showed characteristic peak at 2θ = 12°, according to the Bragg's law, (001) basal plane distance of about 7,35 A° indicates the presence of water molecules in the nanotubes. After the modification with APTES, the tubular structure of HNTs was conserved and the characteristic peaks did not change. This suggested that APTES was only grafted onto the hydroxyl groups of the surfaces and edges of the HNTs [289].

7.2 Membrane Characterization Results

7.2.1 Viscosity of Dope Solutions

During the PI process, the rheological property in the exchange of solvent and non-solvent is influenced by the viscosity of the polymer solution [282]. It was observed that the nanoparticles were homogeneously dispersed in the polymer solution without agglomeration phenomenon. For the formulation of Pristine (1) and 0.2 HNT (1), temperature depended viscosities are given between 30-80 °C in Figure 7.6. The viscosities of the first chosen dope solutions decreased with an increased temperature resulting hollow fiber membranes with a cellular morphology in the substrate and a regular finger like structure [58].

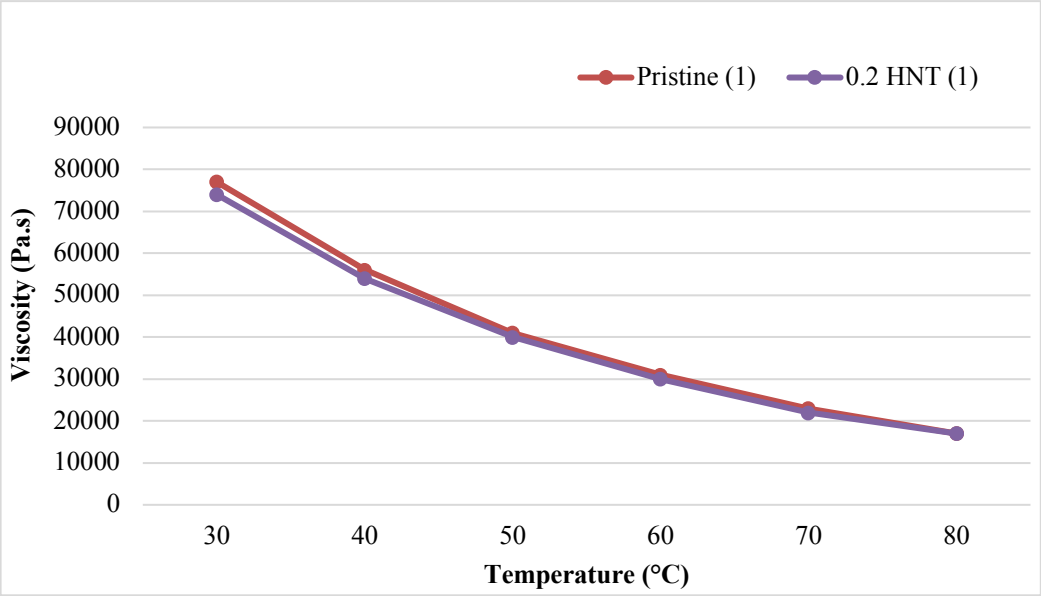


Figure 7.6 Dope solution viscosities according to temperature.

Dope solution viscosities with different concentrations of HNT and h-BN can be seen in Figure 7.7.

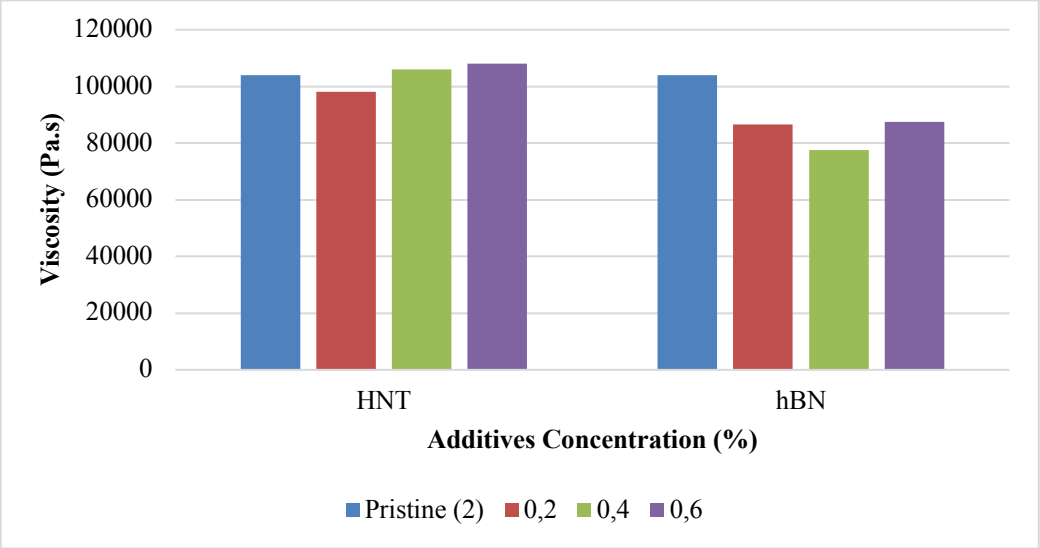


Figure 7.7 Dope solution viscosities.

When the HNT concentration was increased from 0.0 to 0.6 wt.%, the viscosity at 85 °C slightly increased from 104000 to 108000 cP (Pa.s), as shown in Figure 7.6. However, the addition of h-BN to the polymer solution decreased the viscosity in comparison with HNTs. The findings showed that the viscosity of the Pristine (2) was found about 25% higher than Pristine (1) depending on the high concentration of PVP in the polymer solution.

7.2.2 Light Microscopy

The morphology, inner diameter (ID), outer diameter (OD) and thickness of the prepared hollow fiber membranes were determined by light microscopy with a magnification of 50x. The cross-section images of the Pristine (1) and 0.2 HNT (1) is given in Figure 7.8.

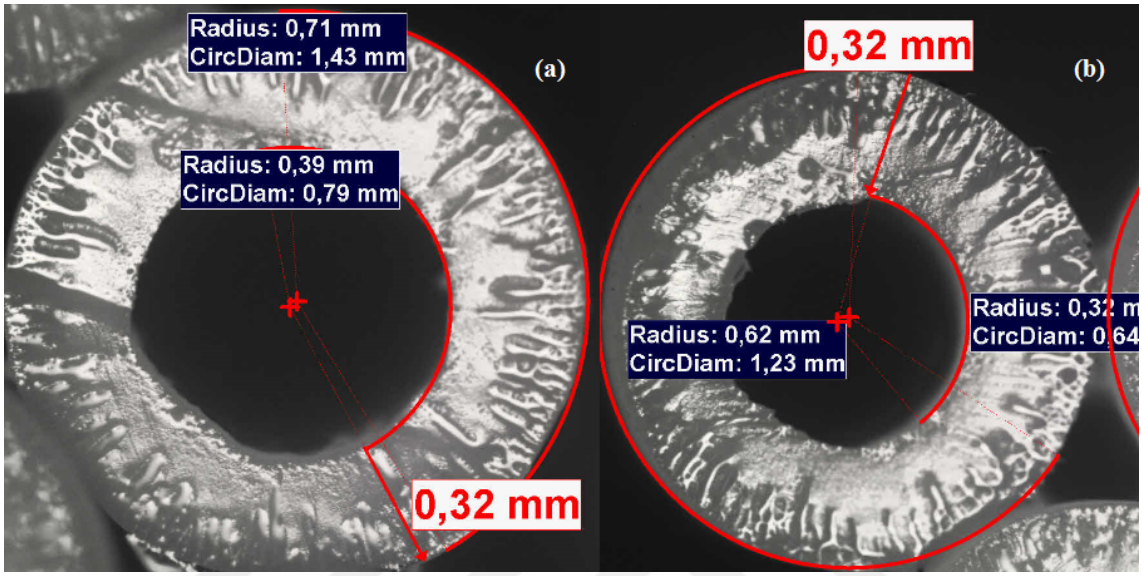


Figure 7.8 Cross section images of hollow fiber membranes (a) Pristine (1), (b) 0.2 HNT (1).

As seen in Figure 7.8, because of the low content of PVP in the polymer solution, finger-like macrovoids formed within the hollow fiber membrane structure.

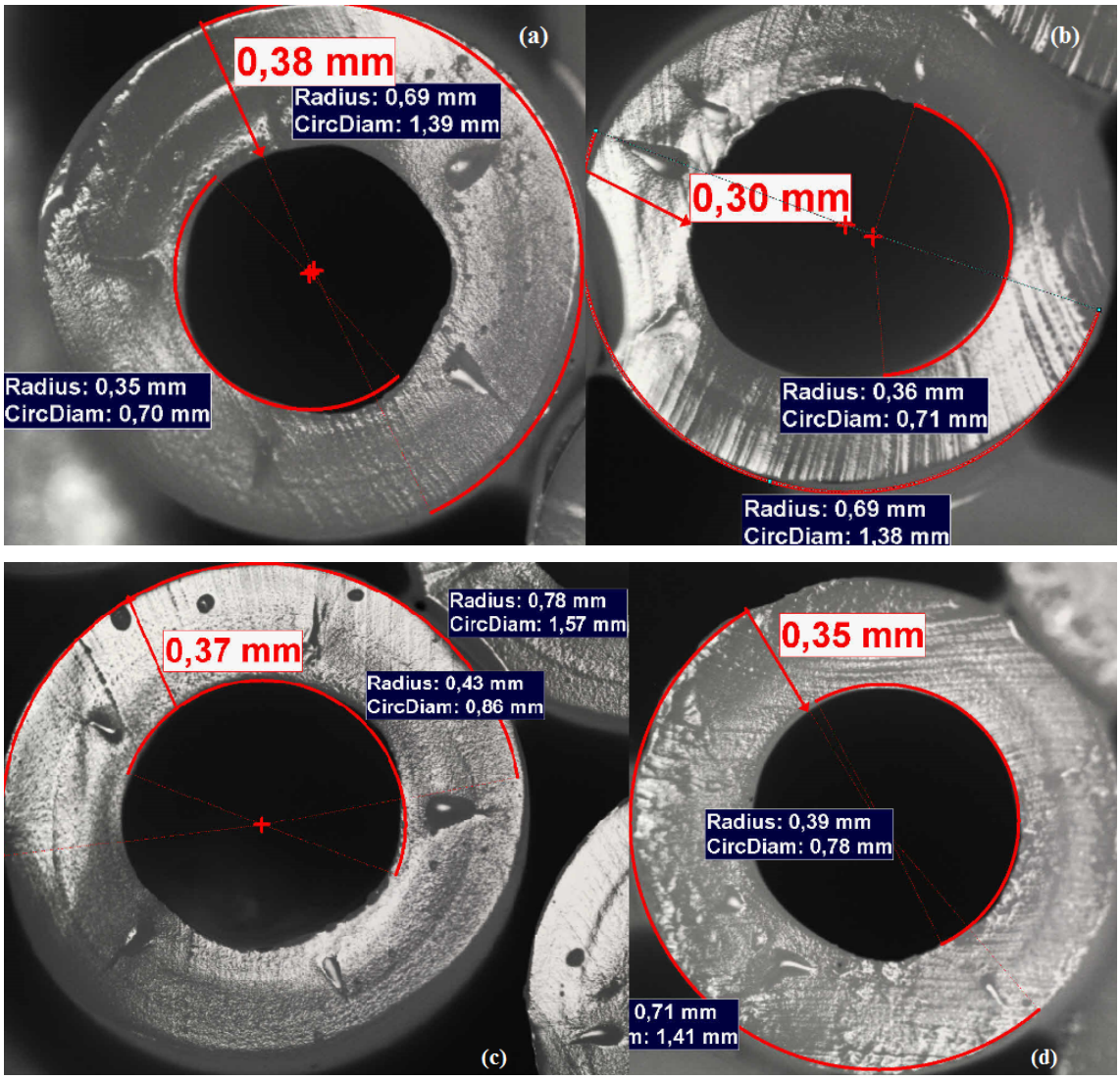


Figure 7.9 Cross sectional images of hollow fiber membranes (a) Pristine (2), (b) 0.2 HNT, (c) 0.4 HNT, (d) 0.6 HNT.

From the cross-sectional images, it can be clearly seen that the finger like membrane structure (Figure 7.9) replaced to dense structure containing few macrovoids (Figure 7.8) with an increase of the PVP content.

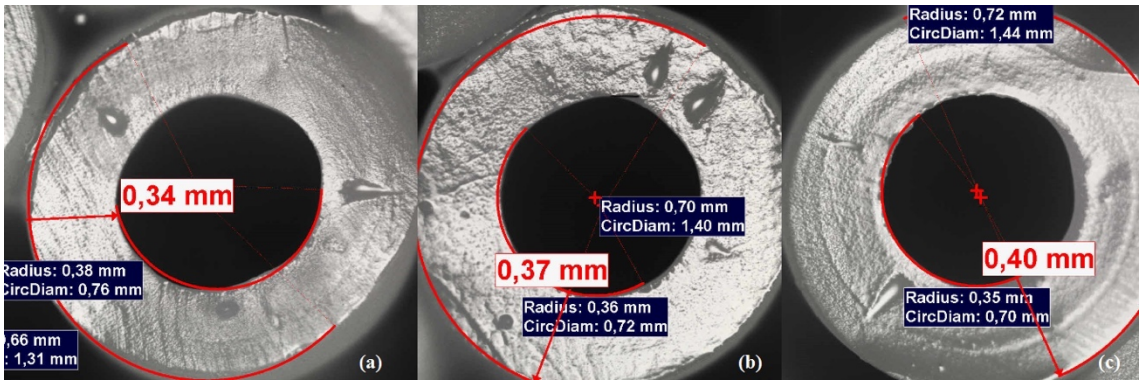


Figure 7.10 Cross sectional images of h-BN blended hollow fiber membranes (a) 0.2 h-BN, (b) 0.4 h-BN, (c) 0.6 h-BN.

It was observed that the amount and the location of the macrovoids within the membrane differed to composition of the nanoparticles.

7.2.3 Pure Water Permeability and MWCO Values of Hollow Fiber Membranes

The PWP primarily depends on the hydrophilicity and porosity of the membrane [290]. The PWP of novel PVDF membranes are shown in Figure 7.11.

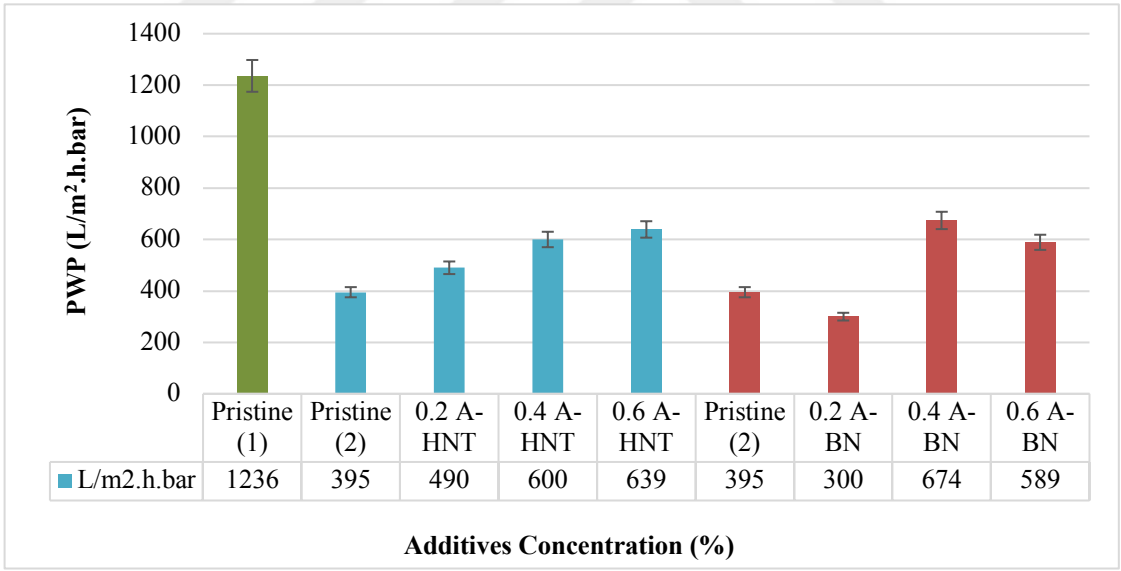


Figure 7.11 Pure water permeability of hollow fiber membranes.

The pristine (2) possessed 70% lower permeability performance compared with the Pristine (1) which contains a great deal of macrovoids within the membrane structure because of the low content of PVP in the formulation. Macrovoids in membranes may result in failure during high pressure operations. In order to eliminate the macrovoids,

high polymer concentrations, non-solvent additives and nanoparticles can be used in the dope solutions [72].

As expected, PWP results gradually increased with the increase of HNTs content in the dope solution. The pristine membrane showed 395 L/m^2.h.bar of PWP and with the addition of HNTs, the results increased rapidly. When the HNTs content was 0.6 wt.%, the PWP achieved the maximum at 639 L/m^2.h.bar, which increased by 62% compared with the standard PVDF membrane. HNTs' hydrophilic nature with many groups of (OH) and hollow tubular structure favor the transmission of water molecules, which serve to increase the PWP of membranes [253, 268]. Arthanareeswaran et al. revealed that nanoporous SiO_2 could enhance PWF by providing an inner water channel allowing water molecule passage [201]. Furthermore, hydrophilic nanoparticles result in higher porosity and bigger pore size within membrane [264]. At the content of 0.4 wt.% h-BN showed a peak value of 674 L/m^2.h.bar which is slightly higher than the HNT blended PVDF membranes. Additionally, PWP enhanced by 70% compared with the pristine membrane.

MWCO experiments were performed to determine the pore size of membranes. As shown in Figure 7.12, the Pristine (2) showed 20% lower MWCO than the Pristine (1) because of its smaller pore sizes.

MWCO values for HNTs and h-BN ranged from 68155 to 80020 Da and 68155 to 86736 Da, respectively. The results increased with the addition of nanoparticles, which is related to the increased pore size.

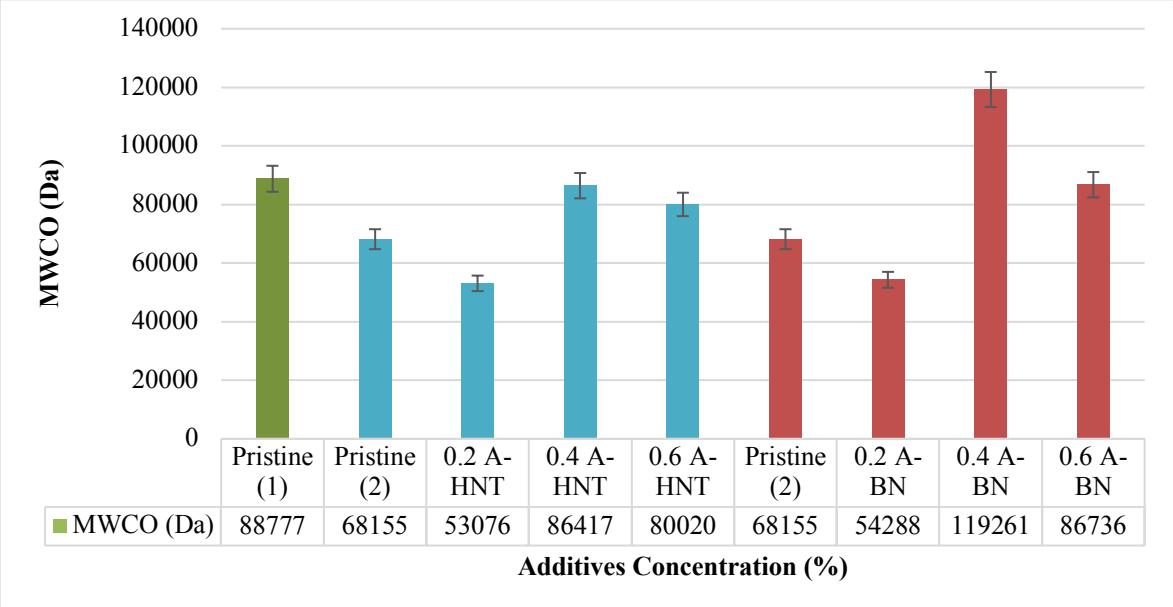


Figure 7.12 MWCO results of hollow fiber membranes.

7.2.4 Mechanical Properties and Bubble Point Pressure of Hollow Fiber Membranes

Mechanical properties are essential for membranes because failure of membranes may lead to reduction of separation performances [291, 292]. The mechanical characteristics of the prepared membranes with different concentrations of HNTs and h-BN are shown in Table 7.2.

Table 7.2 Tensile test and bubble point test results of the hollow fiber membranes.

Formulation	Tensile strength (MPa)	Elongation rate (%)	Bubble point pressure (bar)	Burst pressure (bar)
Pristine (1)	2.72 ±0.2	179±10	-	-
Pristine (2)	3.23±0.19	151±11	2.7±0.2	3.8±0.1
0.2 A-HNT	2.26±0.22	93±62	1.3±0.2	3.5±0.1
0.4 A-HNT	3.12±0.3	182±29	2.6±0.2	3.8±0.1
0.6 A-HNT	2.76±0.04	87±9	1.7±0.2	2.8±0.1
0.2 A-hBN	2.96±0.55	151±11	1.5±0.2	3.7±0.1
0.4 A-hBN	2.45±0.21	122±20	0.81±0.2	1±0.1
0.6 A-hBN	2.61±0.08	48±15	0.6±0.2	1±0.1

The mechanical properties of the prepared hollow fiber membranes were correlated with the membrane pore structure and outward-pointed macrovoids. The pristine (2) hollow fiber membrane showed the highest value of tensile strength and elongation rate at 3.23 MPa and 150%. With the addition of 0.2 wt.% HNTs, the tensile strength and elongation rate decreased 30% and 38%, respectively. At the 0.4 wt.% of the HNTs content, the tensile strength decreased from 3.23 MPa to 3.12 MPa, while the elongation rate increased from 151% to 182%. Thus, the mechanical properties of the hollow fiber membranes were the best at the 0.4 wt.% of the HNTs content. Lai et al. observed that the mechanical properties of the PVDF/nanoclay hollow fiber membrane weakened with lower nanoclay loading, but that the addition of a nanoclay wt.% higher than 5.08 increased tensile

strength from 3.8 MPa to 4.3 MPa. They also indicated that the incorporation of nanoclay to PVDF hollow fiber membranes caused an extra stiffness of the PVDF matrix [238]. Han et al. revealed that the reduction in the elongation rate results from the brittleness of inorganic particles in comparison with the flexibility of a polymer chain [206]. In this study, the maximum loading of HNTs was 0.6 wt.% to preserve PWP and MWCO performance of the novel membrane. Thus, additional studies should be carried out to enhance the mechanical properties of PVDF membranes reinforced with HNTs.

The incorporation of hBN to membrane first decreased and then increased the tensile strength and elongation percentage. At the loading of 0.6 wt.% hBN, the tensile strength and elongation rate decreased 20% and 50%, respectively. The results in this study are in accordance with the literatures. Majeed et al. reported that the utilization of nanofillers could improve the mechanical properties and separation performance of the membranes [293]. Yu et al. revealed that the inorganic nanoparticles in the dope solution could cause a decline in membrane elasticity decreasing the existing mechanical stability of membranes [186].

The tensile tests may not provide valuable information on the possible risks of exposure of the membranes to high pressures. Under certain assumptions, such as isotropy of the fiber, the tensile strength can be converted into a theoretical value for the burst pressure of the fiber when exposed to high internal pressures [283]. Bursting pressure is a mechanical performance parameter used to measure the point at which, the wall of the structure changes from an initial shape to a damaged shape. Increasing pressure after the bubble point results in the failure of the membrane [294]. As seen in Table 7.2, the maximum internal pressure for the pristine hollow fiber membrane showed the highest value at 3.8. The addition of 0.6 wt.% HNTs and h-BN decreased the burst pressure by 25% and 70%, respectively. These results are in accordance with the results obtained from the tensile test. Additionally, pore size results obtained by the bubble point technique according to Laplace equation are listed in Table 7.3

Table 7.3 Bubble point measurement for different hollow fiber membranes to determine the largest pore size of the fiber.

Formulation	Contact Angle (θ)	ΔP (bar)	Largest pore size (nm)
Pristine	72	2.7	164
0.2 A-HNT	59	1.3	570
0.4 A-HNT	55	2.6	356
0.6 A-HNT	53	1.7	510
0.2 A-hBN	61	1.5	465
0.4 A-hBN	57	0.81	969
0.6 A-hBN	54	0.6	1411

The maximum pore size for the pristine hollow fiber membrane is about 164 nm, while with the addition of 0.6 wt.% HNTs, the largest pore size increased to 510 nm. For the content of 0.6 wt.% h-BN, the maximum pore size reached the highest at 1411 nm.

7.2.5 Dynamic Contact Angle

The contact angle (CA) values of hollow fiber membranes according to different concentration of nanoparticles are given in Figure 7.13 and 7.14.

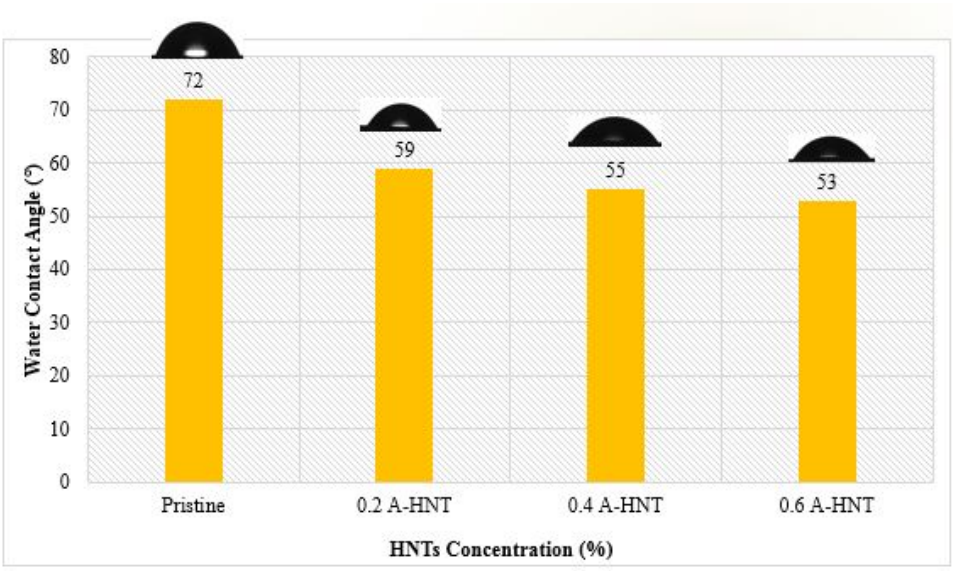


Figure 7.13 Water contact angle values and images of HNTs blended PVDF hollow fiber membranes.

The CA formed between the liquid-gas tangent and membrane-liquid boundary determine the hydrophilic-hydrophobic properties of the membrane [41]. Smaller contact angles are desired for high hydrophilicity which can be considered as one of the most important factors for water permeability and antifouling property of membranes influenced by the membrane surface morphologies [189, 231].

Owing to many hydroxyl groups on the HNTs surface, HNTs have an important impact on hydrophilicity, PWP as well as fouling resistance of polymeric UF membranes [175, 251, 254]. As shown in Figure 7.13, the CA value of the pristine PVDF membrane was 72° because of its hydrophobic nature. With the addition of HNTs, the CA of the modified membranes slightly decreased, improving the hydrophilicity, permeability and also antifouling property of UF membranes. At the content of 0.6 wt.% HNTs, the highest hydrophilicity was achieved with a CA value of 53°.

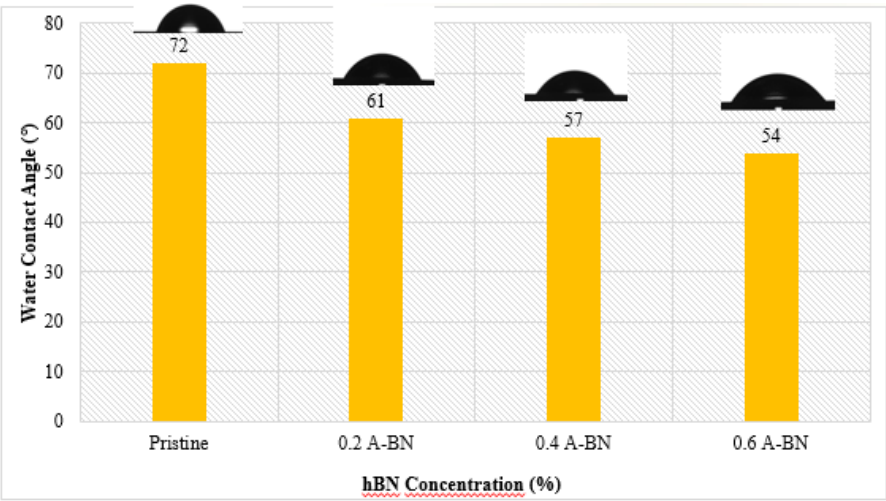


Figure 7.14 Water contact angle values and images of hBN blended PVDF hollow fiber membranes.

With the increase of hBN concentration, the CA of modified membranes slightly decreased, and 0.6 A-BN gave the best result of 54°. These findings are in agreement with the literatures that the hydrophilicity of PVDF UF membranes could be improved by blending with inorganic nanoparticles which is attributed to the change in membrane surface energy via surface functionalization of nanoparticles [153].

7.2.6 Morphologies of Hollow Fiber Membranes

The cross-sectional SEM images of the PVDF-based hollow fiber membranes with different concentrations of A-HNT are given in Figure 7. 15, 7.16, 7.17 and 7.18.

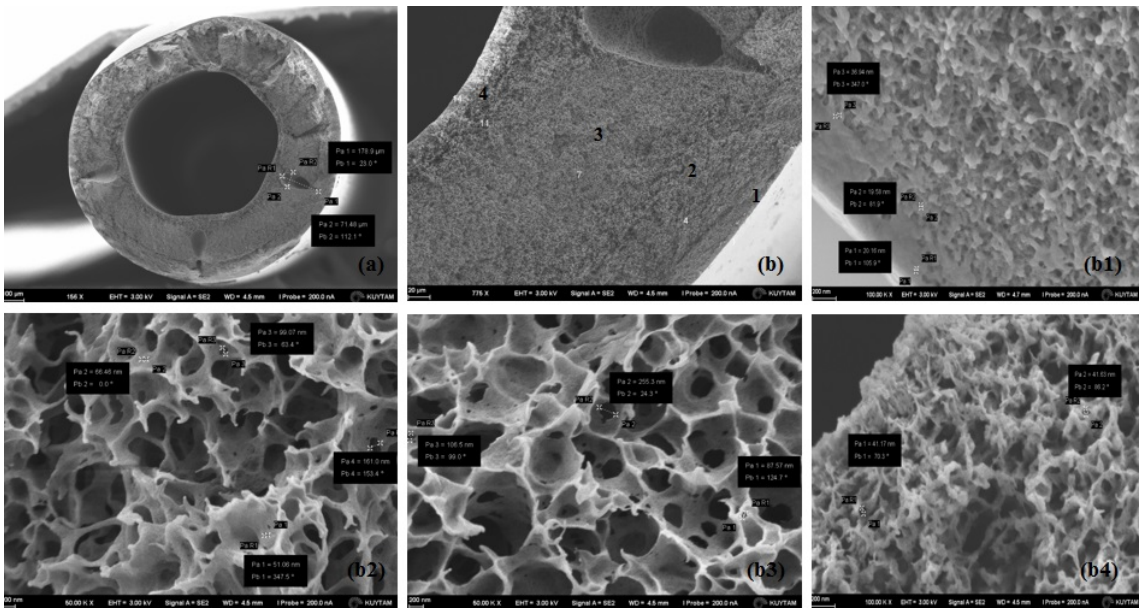


Figure 7.15 The cross-sectional images of the pristine hollow fiber membrane under different magnifications.

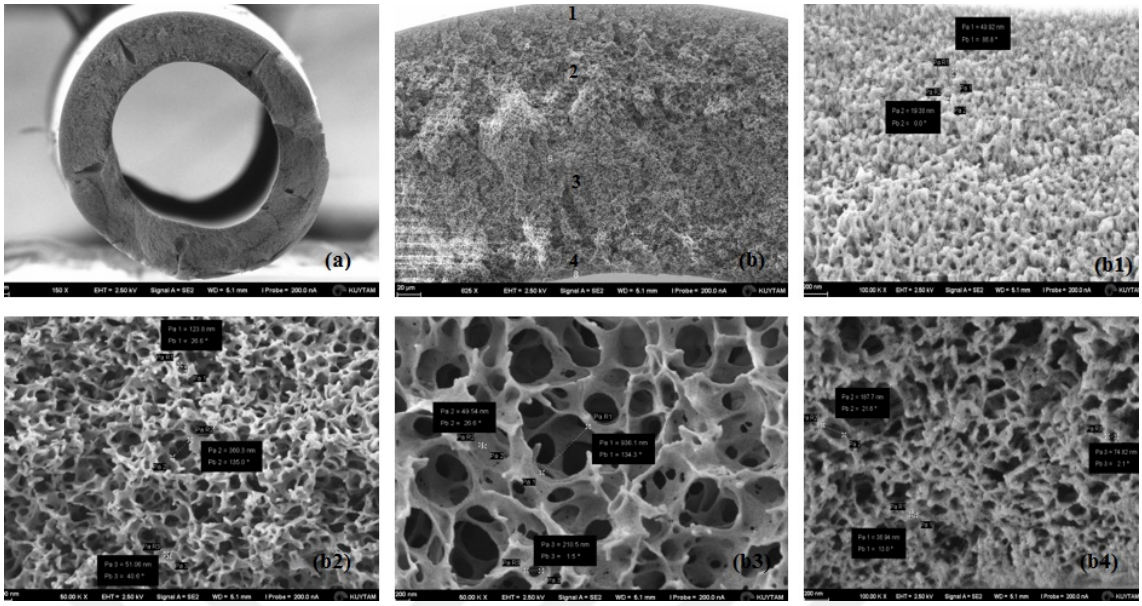


Figure 7.16 The cross-sectional images of the 0.2 A-HNT hollow fiber membrane under different magnifications.

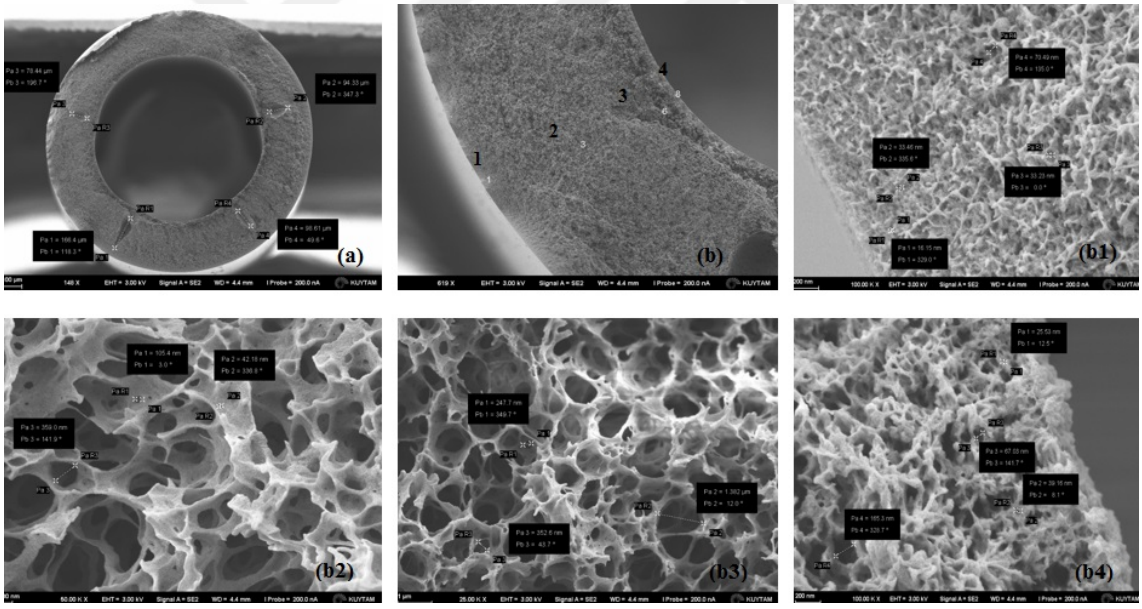


Figure 7.17 The cross-sectional images of the 0.4 A-HNT hollow fiber membrane under different magnifications.

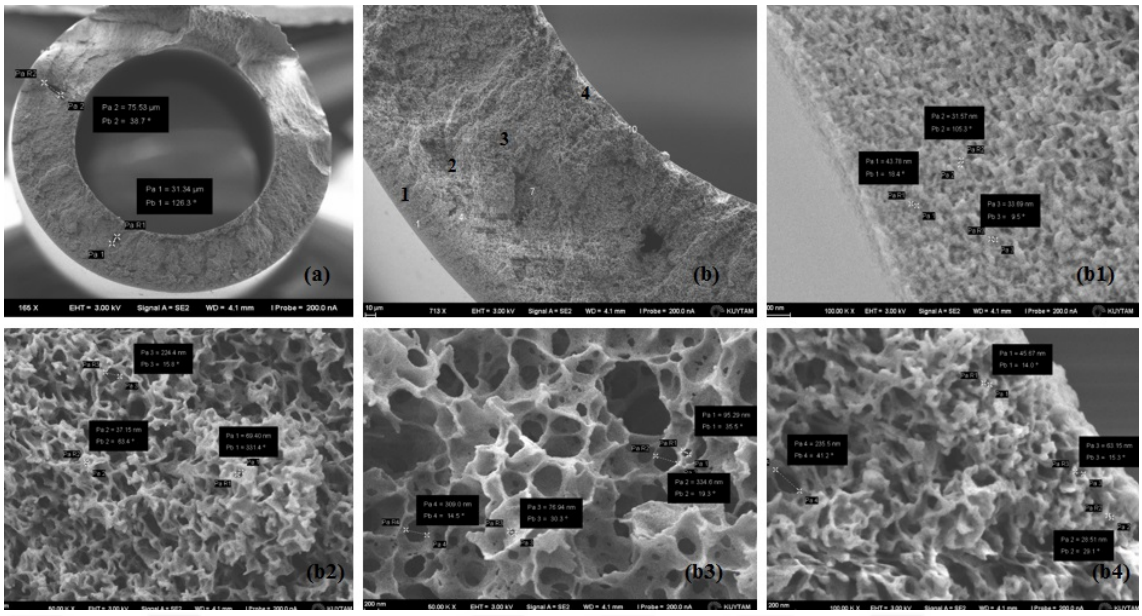


Figure 7.18 The cross-sectional images of the 0.6 A-HNT hollow fiber membrane under different magnifications.

In Table 7.4 presents the mean pore sizes and macrovoid lengths of HNTs blended hollow fiber membranes according to SEM images.

Table 7.4 Mean pore sizes and macrovoid lengths of the HNTs blended hollow fiber membranes.

Formulation	**1st layer (nm)**	**2nd layer (nm)**	**3rd layer (nm)**	**4th layer (nm)**	**Macrovoids (µm)**
Pristine	25	94	149	42	179
0.2 A-HNT	34	178	573	56	148
0.4 A-HNT	38	169	661	74	109
0.6 A-HNT	36	110	204	46	53

According to mean pore sizes, the cross-sections of the hollow fiber membranes consisted of four layers. As shown in Table 7.4, with the addition of HNTs, first the mean pore sizes of each layer increased but then decreased. The mean pore size of the selective layer for the pristine, 0.2 A-HNT, 0.4 A-HNT, and 0.6 A-HNT were 26 nm, 34 nm, 38 nm, and 36 nm, respectively. All the hollow fiber membranes consisted of ordered outward-pointed macrovoids due to the spinneret design, which is considered an important factor in determining molecular orientation and membrane morphology of the hollow fiber

membranes [50]. The number of outward-pointed macrovoids depends on the air-gap distance. Decreasing the air-gap distance results in a reduction in the number of macrovoids. Widjojo et al. revealed that the inward-pointed and outward pointed finger-like macrovoids develop due to surface instability, skin rupture or convective flow during rapid coagulation [295]. In this study, the same spinning parameters were selected for each compositions of the hollow fiber membranes. However, with a further increase in the content of HNTs, the average lengths of the macrovoids dramatically decreased. The suppression of outward-pointed macrovoids, which can be clearly observed in Figures 7.15, 7.16, 7.17, 7.18 (a), is related to the increase of viscosity.

The cross-sectional SEM images of the PVDF-based hollow fiber membranes with different concentrations of A-BN are given in Figure 7.19, 7.20 and 7.21.

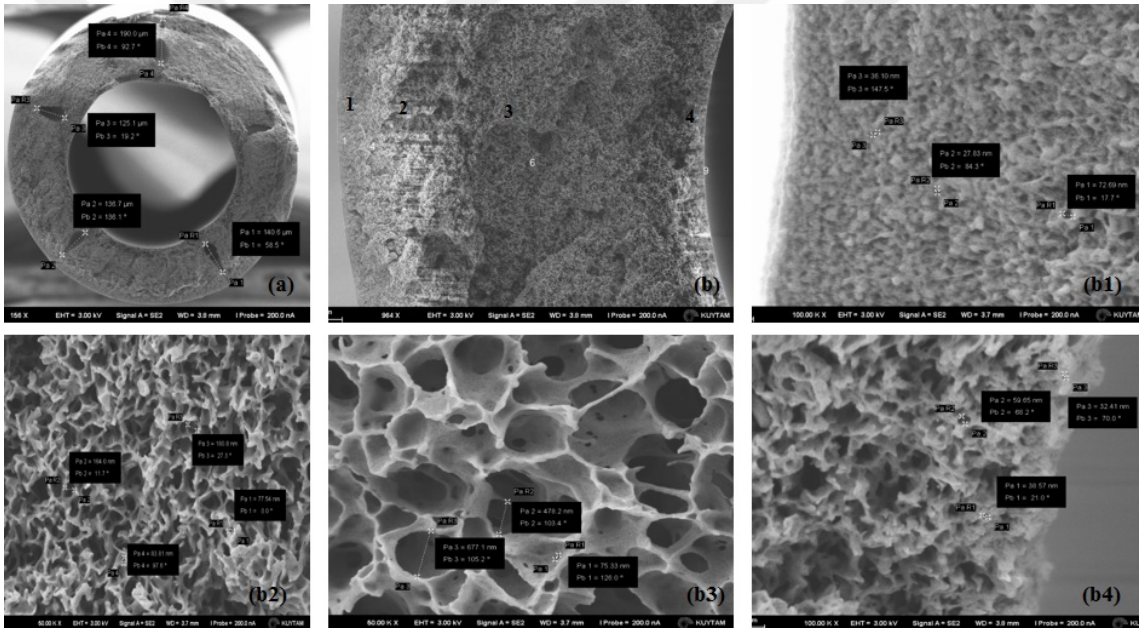


Figure 7.19 The cross-sectional images of the 0.2 A-BN hollow fiber membrane under different magnifications.

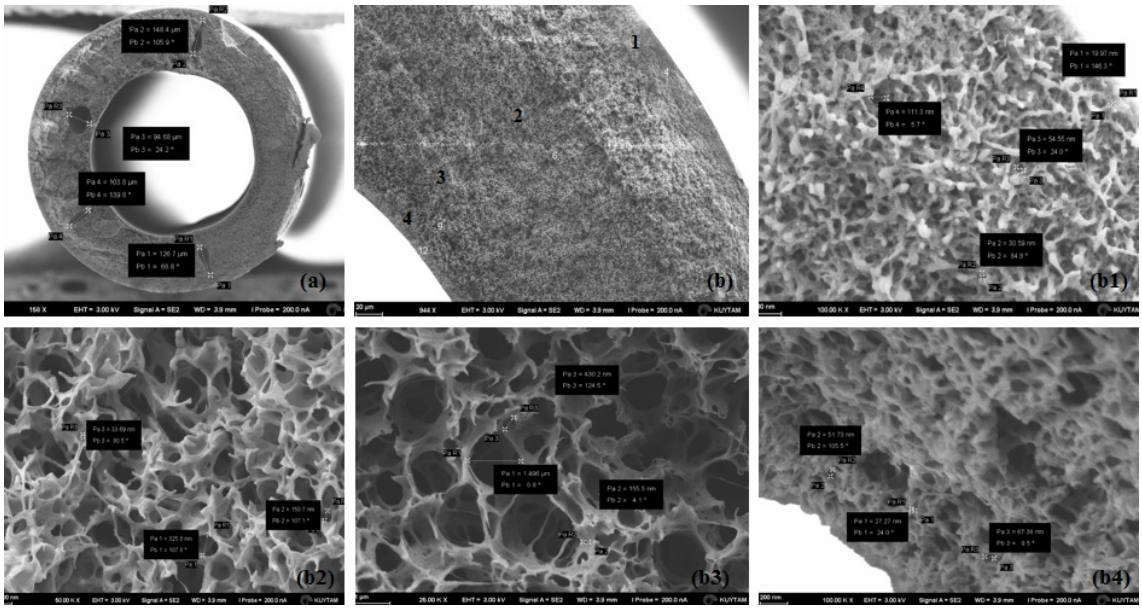


Figure 7.20 The cross-sectional images of the 0.4 A-BN hollow fiber membrane under different magnifications.

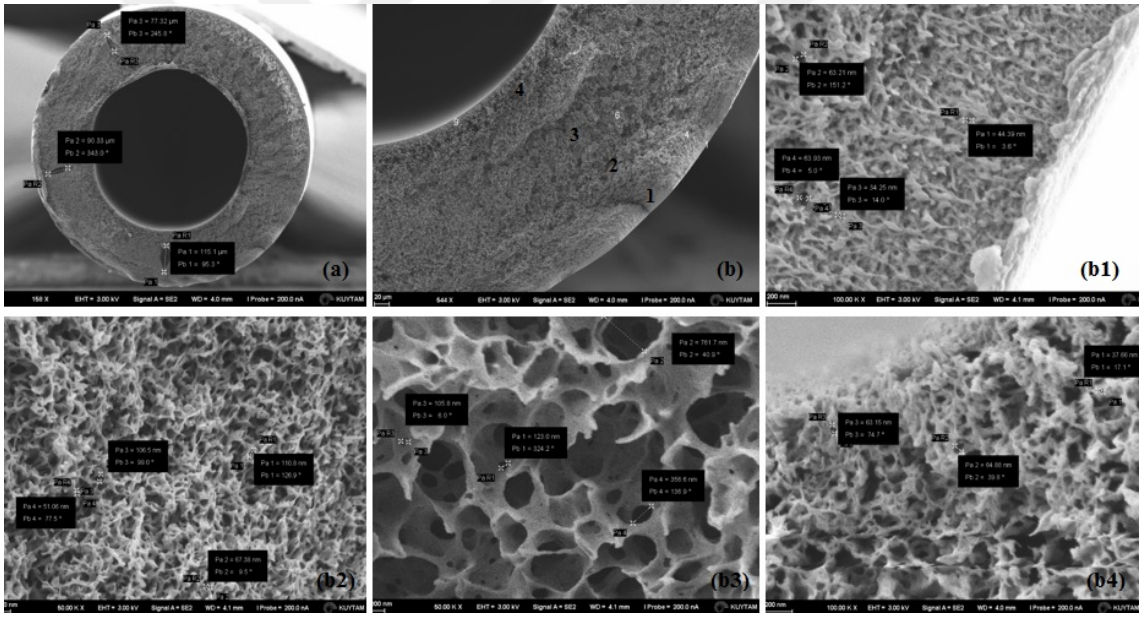


Figure 7.21 The cross-sectional images of the 0.6 A-BN hollow fiber membrane under different magnifications.

In Table 7.5 shows the mean pore sizes and macrovoid lengths of h-BN blended hollow fiber membranes according to SEM images.

Table 7.5 Mean pore sizes and macrovoid lengths of h-BN blended hollow fiber membranes.

Formulation	1st layer (nm)	2nd layer (nm)	3rd layer (nm)	4th layer (nm)	Macrovoids (µm)
Pristine	25	94	149	42	179
0.2 A-BN	45	126	410	44	134
0.4 A-BN	54	170	963	49	125
0.6 A-BN	47	83	337	55	94

As shown, first mean pore sizes dramatically increased up to 0.4 % content of A-BN, but then decreased. The selective layer for the pristine, 0.2 A-BN, 0.4 A-BN, 0.6 A-BN, possess 25, 45, 54, 47 nm of mean pore size, respectively. The addition of BN nanoparticles increases the thermodynamic instability in the gelation bath which promotes a rapid phase demixing, results in larger pores in low content of nanoparticles. However, an increase in viscosity of the dope solution may lead to decrease in pore sizes of the membrane [296, 297]. All hollow fiber membranes contain outward-pointed macrovoids within the cross sections as shown in Figure 7.19, 7.20, 7.21 (a). Table 7.6 clearly shows that the mean size of macrovoids gradually decreased with increasing the BN content. Peng et al. revealed that suppression of macrovoids can be achieved by adding high viscosity components such as nanoparticles [50]. The increase in dope viscosity hinders the demixing process, resulting in the suppression of macrovoids [169]. In addition, all hollow fibers have delamination free, sponge-like morphology with ticker dense layer which is quite desirable for enhancing membrane performance and also mechanical properties [298].

CHAPTER 8

CONCLUSIONS AND RECOMMENDATIONS

The feasibility of large-scale operation of pressure-driven membrane processes is influenced by membrane fouling. The desired membrane material properties are thermal, chemical, and mechanical stability and hydrophilicity. Nevertheless, membrane materials are usually fabricated from hydrophobic polymers. PVDF has been extensively used in UF membranes on account of its outstanding properties, such as high mechanical strength, thermal stability, and chemical resistance compared with other commercialized polymeric materials. However, the high hydrophobic property of PVDF membranes results in fouling and a decrease in water permeability. Therefore, many studies of hydrophobic membranes have focused on the improvement of hydrophilicity using various methods in order to increase the permeability, separation performance as well as antifouling property.

Among the various nanoparticles, tubular aluminosilicate clay, also known as HNTs, with its natural availability and unique combination of large aspect ratio, rich functionality, good biocompatibility, high mechanical strength, loading efficiency and low cost, has attracted great interest in hydrophilic modifications of UFMs. BNNPs have similar structures and superior physiochemical properties such as mechanical properties, better dispersion in polymer matrix, thermal conductivity, electrical-insulating properties, resistance to oxidation and chemical inertness compared to carbon nanomaterial. Due to these reasons, BN nanostructures have been widely used as reinforcing agent in polymer matrix composites. Nevertheless, BN has not been used in pressure driven membranes before.

Because of the hydrophilic nature and high surface energy of the NPs, silane modification is performed to provide a homogenous dispersion of nanofillers in a polymer matrix, which serves to enhance the interaction between nanoparticles and the polymer matrix.

In this study, HNTs and h-BN nanoparticles were functionalized by APTES as a silane coupling agent to improve their compatibility in the PVDF matrix, and pilot scale PVDF based HF UFMs formed of different concentrations of nanofillers (0, 0.2, 0.4, 0.6 wt.%) were fabricated via the dry-wet spinning method. FTIR, TGA and XRD analyses were applied to characterize the nanoparticles. Before the spinning processing viscosity measurements were carried out to determine the rheological property during the PI process. The performance of pristine and modified HFMs were determined through PWP measurements, MWCO experiments, contact angle measurements, tensile test, and bubble point test. Furthermore, SEM was used to observe the morphology of HFMs in terms of pore size distribution and the dispersion of nanoparticles within the membrane.

From the experimental results, the following conclusions can be drawn:

1. According to FTIR, TGA and XRD data, aminosilane modification of the HNTs and h-BN nanoparticles was successfully accomplished.
2. The rheometer measurements revealed that the viscosity of the Pristine (2) was found about 25% higher than Pristine (1) depending on the high concentration of PVP in the dope solution. Besides, the light microscopy images showed that due to the low concentration of PVP in the formulation Pristine (1), finger-like macrovoids formed within the HFM structure. Macrovoids in membranes may result in failure during high pressure operations. In order to eliminate the macrovoids, high PVP content, non-solvent additive and nanoparticles are used in the dope solutions.
3. From the SEM images, the addition of HNTs and h-BN within the membrane structure suppressed outward-pointed macrovoids related to the increase of dope viscosities. Moreover, the mean pore sizes of PVDF membranes increased because the addition of particles increases the thermodynamic instability in the gelation bath which promotes a rapid phase demixing.
4. The contact angle value of the pristine PVDF membrane was 72° because of its hydrophobic nature. The hydrophilicity of the PVDF HFMs were improved significantly with the addition of A-HNTs and A-hBN, due to the change in membrane surface energy by silane treatment of nanoparticles.
5. The PWP results gradually increased with the increase of nanoparticles depended on the hydrophilicity and porosity of the membrane. 0.6 A-HNT and 0.4 A-hBN achieved the maximum value at 639 and 674 $L/m^2.h.bar$, respectively which increased by 62% and 70% compared with the standard PVDF membrane.

The porosity and mean pore size of the membrane were slightly increased according to SEM images, MWCO results and bubble point test. The maximum pore size for the pristine HFM is about 164 nm, while with the addition of 0.6 wt.% HNTs, the largest pore size increased to 510 nm. For the content of 0.6 wt.% h-BN, the maximum pore size reached the highest at 1411 nm.

6. Mechanical properties are important for HFMs because failure of membranes may lead reduction of separation performances. The mechanical properties fluctuated, achieving the best tensile strength and elongation rate at 3.12 MPa and 182% respectively for 0.4 HNT. A similar trend was obtained for bubble point pressure test results. These findings are in accordance with the literatures that the utilization of inorganic nanoparticles in the dope solution could lead a decline in membrane elasticity decreasing the existing mechanical stability of membranes.

HNTs can provide novel properties such as antibacterial and catalytic performance when functional groups are introduced on their surfaces. Thus, they are seen to have the potential for incorporation into the UF membranes. Further studies should be carried out to improve the mechanical properties of PVDF HFMs reinforced with nanomaterials.

In this study, h-BN was used for the first time in pressure-driven membrane processes. It was found that, with the addition h-BN, the CA of the modified membranes decreased, developing hydrophilicity, permeability, membrane morphology as well as antifouling property of the PVDF UFM. These results are in accordance with the previous studies revealing the effects of inorganic nanoparticles on the performance of membranes.

REFERENCES

[1] Lalia, B.S., Kochkodan, V., Hashaikeh, R. and Hilal, N., (2013). "A review on membrane fabrication: Structure, properties and performance relationship", Desalination, 326:77-95.

[2] Mehwish, N., Kausar, A. and Siddiq, M., (2014). "Advances in Polymer-based Nanostructured Membranes for Water Treatment", Polymer-Plastics Technology and Engineering, 53(12):1290-1316.

[3] Gao, W., Liang, H., Ma, J., Han, M., Chen, Z.-l., Han, Z.-s. and Li, G.-b., (2011). "Membrane fouling control in ultrafiltration technology for drinking water production: A review", Desalination, 272(1–3):1-8.

[4] Le-Clech, P., Chen, V. and Fane, T.A.G., (2006). "Fouling in membrane bioreactors used in wastewater treatment", Journal of Membrane Science, 284(1–2):17-53.

[5] Van Der Bruggen, B., Vandecasteele, C., Van Gestel, T., Doyen, W. and Leysen, R., (2003). "A review of pressure-driven membrane processes in wastewater treatment and drinking water production", Environmental Progress, 22(1):46-56.

[6] Liu, F., Hashim, N.A., Liu, Y., Abed, M.R.M. and Li, K., (2011). "Progress in the production and modification of PVDF membranes", Journal of Membrane Science, 375(1–2):1-27.

[7] Hilal, N., Ogunbiyi, O.O., Miles, N.J. and Nigmatullin, R., (2005). "Methods Employed for Control of Fouling in MF and UF Membranes: A Comprehensive Review", Separation Science and Technology, 40(10):1957-2005.

[8] Sigal, G.B., Mrksich, M. and Whitesides, G.M., (1998). "Effect of Surface Wettability on the Adsorption of Proteins and Detergents", Journal of the American Chemical Society, 120(14):3464-3473.

[9] Xi, Z.-Y., Xu, Y.-Y., Zhu, L.-P., Wang, Y. and Zhu, B.-K., (2009). "A facile method of surface modification for hydrophobic polymer membranes based on the adhesive behavior of poly(DOPA) and poly(dopamine)", Journal of Membrane Science, 327(1–2):244-253.

[10] Kochkodan, V., Johnson, D.J. and Hilal, N., (2014). "Polymeric membranes: Surface modification for minimizing (bio)colloidal fouling", Advances in Colloid and Interface Science, 206:116-140.

[11] Ayyavoo, J., Nguyen, T.P.N., Jun, B.-M., Kim, I.-C. and Kwon, Y.-N., (2016). "Protection of polymeric membranes with antifouling surfacing via surface

modifications", Colloids and Surfaces A: Physicochemical and Engineering Aspects, 506:190-201.

[12] Baker, J.S. and Dudley, L.Y., (1998). "Biofouling in membrane systems — A review", Desalination, 118(1):81-89.

[13] Flemming, H.C., Schaule, G., Griebe, T., Schmitt, J. and Tamachkiarowa, A., (1997). "Biofouling—the Achilles heel of membrane processes", Desalination, 113(2):215-225.

[14] Kang, G.-d. and Cao, Y.-m., (2014). "Application and modification of poly(vinylidene fluoride) (PVDF) membranes – A review", Journal of Membrane Science, 463:145-165.

[15] Cui, Z., Drioli, E. and Lee, Y.M., (2014). "Recent progress in fluoropolymers for membranes", Progress in Polymer Science, 39(1):164-198.

[16] Goh, P.S., Ng, B.C., Lau, W.J. and Ismail, A.F., (2015). "Inorganic Nanomaterials in Polymeric Ultrafiltration Membranes for Water Treatment", Separation & Purification Reviews, 44(3):216-249.

[17] Lvov, Y. and Abdullayev, E., (2013). "Functional polymer–clay nanotube composites with sustained release of chemical agents", Progress in Polymer Science, 38(10–11):1690-1719.

[18] Du, M., Guo, B. and Jia, D., (2010). "Newly emerging applications of halloysite nanotubes: a review", Polymer International, 59(5):574-582.

[19] Yuan, P., Tan, D. and Annabi-Bergaya, F., (2015). "Properties and applications of halloysite nanotubes: recent research advances and future prospects", Applied Clay Science, 112–113:75-93.

[20] Farshid, B., Lalwani, G., Shir Mohammadi, M., Simonsen, J. and Sitharaman, B., (2015). "Boron nitride nanotubes and nanoplatelets as reinforcing agents of polymeric matrices for bone tissue engineering", Journal of Biomedical Materials Research Part B: Applied Biomaterials.

[21] Liu, D., He, L., Lei, W., Klika, K.D., Kong, L. and Chen, Y., (2015). "Multifunctional Polymer/Porous Boron Nitride Nanosheet Membranes for Superior Trapping Emulsified Oils and Organic Molecules", Advanced Materials Interfaces, 2(12):1500228-n/a.

[22] Liu, D., Lei, W., Qin, S. and Chen, Y., (2014). "Template-Free Synthesis of Functional 3D BN architecture for removal of dyes from water", Scientific Reports, 4:4453.

[23] Zhi, C., Bando, Y., Tang, C., Kuwahara, H. and Golberg, D., (2009). "Large-Scale Fabrication of Boron Nitride Nanosheets and Their Utilization in Polymeric Composites with Improved Thermal and Mechanical Properties", Advanced Materials, 21(28):2889-2893.

[24] Yin, J., Li, J., Hang, Y., Yu, J., Tai, G., Li, X., Zhang, Z. and Guo, W., (2016). "Boron Nitride Nanostructures: Fabrication, Functionalization and Applications", Small, 12(22):2942-2968.

[25] Meng, W., Huang, Y., Fu, Y., Wang, Z. and Zhi, C., (2014). "Polymer composites of boron nitride nanotubes and nanosheets", Journal of Materials Chemistry C, 2(47):10049-10061.

[26] Zhang, X., Zhang, X., Yang, M., Yang, S., Wu, H., Guo, S. and Wang, Y., (2016). "Ordered multilayer film of (graphene oxide/polymer and boron nitride/polymer) nanocomposites: An ideal EMI shielding material with excellent electrical insulation and high thermal conductivity", Composites Science and Technology, 136:104-110.

[27] Rong, M.Z., Zhang, M.Q. and Ruan, W.H., (2006). "Surface modification of nanoscale fillers for improving properties of polymer nanocomposites: a review", Materials Science and Technology, 22(7):787-796.

[28] Kango, S., Kalia, S., Celli, A., Njuguna, J., Habibi, Y. and Kumar, R., (2013). "Surface modification of inorganic nanoparticles for development of organic–inorganic nanocomposites—A review", Progress in Polymer Science, 38(8):1232-1261.

[29] Soni, V., Abildskov, J., Jonsson, G. and Gani, R., (2009). "A general model for membrane-based separation processes", Computers & Chemical Engineering, 33(3):644-659.

[30] Mulder, J., (2012). Basic principles of membrane technology Place Springer Science & Business Media.

[31] Baker, R.W., Membrane Technology and Applications, John Willey & Sons, Ltd, West Sussex, England, 2004.

[32] Loeb, S. and Sourirajan, S., Sea water demineralization by means of an osmotic membrane, ACS Publications1962.

[33] Ng, L.Y., Mohammad, A.W., Leo, C.P. and Hilal, N., (2013). "Polymeric membranes incorporated with metal/metal oxide nanoparticles: A comprehensive review", Desalination, 308:15-33.

[34] Pendergast, M.M. and Hoek, E.M.V., (2011). "A review of water treatment membrane nanotechnologies", Energy & Environmental Science, 4(6):1946-1971.

[35] Nath, K., (2017). Membrane separation processes Place PHI Learning Pvt. Ltd.

[36] Lee, A., Elam, J.W. and Darling, S.B., (2016). "Membrane materials for water purification: design, development, and application", Environmental Science: Water Research & Technology, 2(1):17-42.

[37] Mar√?a Sastre, A. and Kumar Pabby, A., Hollow Fiber Membrane-Based Separation Technology, Solvent Extraction and Liquid Membranes, CRC Press2008, pp. 91-140.

[38] Munir, A., (2006). "Dead end membrane filtration", Laboratory Feasibility Studies in Environmental Engineering:1-33.

[39] Mohamed, K., Dope Solution, in: E. Drioli, L. Giorno (Eds.), Encyclopedia of Membranes, Springer Berlin Heidelberg, Berlin, Heidelberg, 2015, pp. 1-3.

[40] Drioli, E. and Giorno, L., (2010). Comprehensive membrane science and engineering Place Newnes.

[41] Yuan, Y. and Lee, T.R., Contact angle and wetting properties, Surface science techniques, Springer2013, pp. 3-34.

[42] Charcosset, C., (2012). Membrane processes in biotechnology and pharmaceutics Place Elsevier.

[43] Koros, W.J., Ma, Y.H. and Shimidzu, T., Terminology for membranes and membrane processes (IUPAC Recommendations 1996), Pure and Applied Chemistry, 1996, p. 1479.

[44] Wienk, I.M., (1993). Ultrafiltration membranes from a polymer blend: hollow fiber preparation and characterization Place University of Twente.

[45] Kools, W.F.C., (1998). Membrane formation by phase inversion in multicomponent polymer systems. Mechanisms and morphologies Place Universiteit Twente.

[46] Stropnik, Č., Musil, V. and Brumen, M., (2000). "Polymeric membrane formation by wet-phase separation; turbidity and shrinkage phenomena as evidence for the elementary processes", Polymer, 41(26):9227-9237.

[47] Mahon, H.I., Permeability separatory apparatus, permeability separatory membrane element, method of making the same and process utilizing the same, Google Patents, 1966.

[48] Chung, T.-S., Qin, J.-J. and Gu, J., (2000). "Effect of shear rate within the spinneret on morphology, separation performance and mechanical properties of ultrafiltration polyethersulfone hollow fiber membranes", Chemical Engineering Science, 55(6):1077-1091.

[49] Wang, K.Y., Matsuura, T., Chung, T.-S. and Guo, W.F., (2004). "The effects of flow angle and shear rate within the spinneret on the separation performance of poly(ethersulfone) (PES) ultrafiltration hollow fiber membranes", Journal of Membrane Science, 240(1):67-79.

[50] Peng, N., Widjojo, N., Sukitpaneenit, P., Teoh, M.M., Lipscomb, G.G., Chung, T.-S. and Lai, J.-Y., (2012). "Evolution of polymeric hollow fibers as sustainable technologies: Past, present, and future", Progress in Polymer Science, 37(10):1401-1424.

[51] Wienk, I.M., Olde Scholtenhuis, F.H.A., van den Boomgaard, T. and Smolders, C.A., (1995). "Spinning of hollow fiber ultrafiltration membranes from a polymer blend", Journal of Membrane Science, 106(3):233-243.

[52] Qin, J.-J., Gu, J. and Chung, T.-S., (2001). "Effect of wet and dry-jet wet spinning on the shear-induced orientation during the formation of ultrafiltration hollow fiber membranes", Journal of Membrane Science, 182(1):57-75.

[53] Yin, J., Zhu, G. and Deng, B., (2013). "Multi-walled carbon nanotubes (MWNTs)/polysulfone (PSU) mixed matrix hollow fiber membranes for enhanced water treatment", Journal of Membrane Science, 437(Supplement C):237-248.

[54] Feng, C.Y., Khulbe, K.C., Matsuura, T. and Ismail, A.F., (2013). "Recent progresses in polymeric hollow fiber membrane preparation, characterization and applications", Separation and Purification Technology, 111:43-71.

[55] Rana, D. and Matsuura, T., (2010). "Surface Modifications for Antifouling Membranes", Chemical Reviews, 110(4):2448-2471.

[56] Yuliwati, E. and Ismail, A.F., (2011). "Effect of additives concentration on the surface properties and performance of PVDF ultrafiltration membranes for refinery produced wastewater treatment", Desalination, 273(1):226-234.

[57] Bottino, A., Camera-Roda, G., Capannelli, G. and Munari, S., (1991). "The formation of microporous polyvinylidene difluoride membranes by phase separation", Journal of Membrane Science, 57(1):1-20.

[58] Yeow, M.L., Liu, Y.T. and Li, K., (2004). "Morphological study of poly(vinylidene fluoride) asymmetric membranes: Effects of the solvent, additive, and dope temperature", Journal of Applied Polymer Science, 92(3):1782-1789.

[59] Wu, L., Sun, J. and Wang, Q., (2006). "Poly(vinylidene fluoride)/polyethersulfone blend membranes: Effects of solvent sort, polyethersulfone and polyvinylpyrrolidone concentration on their properties and morphology", Journal of Membrane Science, 285(1–2):290-298.

[60] Cha, B.J. and Yang, J.M., (2006). "Effect of high-temperature spinning and PVP additive on the properties of PVDF hollow fiber membranes for microfiltration", Macromolecular Research, 14(6):596-602.

[61] Lang, W.-Z., Guo, Y.-J. and Chu, L.-F., (2011). "Evolution of the precipitation kinetics, morphologies, permeation performances, and crystallization behaviors of polyvinylidenefluoride (PVDF) hollow fiber membrane by adding different molecular weight polyvinylpyrrolidone (PVP)", Polymers for Advanced Technologies, 22(12):1720-1730.

[62] Khayet, M., Feng, C.Y., Khulbe, K.C. and Matsuura, T., (2002). "Study on the effect of a non-solvent additive on the morphology and performance of ultrafiltration hollow-fiber membranes", Desalination, 148(1):321-327.

[63] Zheng, L., Wu, Z., Zhang, Y., Wei, Y. and Wang, J., (2016). "Effect of non-solvent additives on the morphology, pore structure, and direct contact membrane distillation performance of PVDF-CTFE hydrophobic membranes", Journal of Environmental Sciences, 45(Supplement C):28-39.

[64] Wongchitphimon, S., Wang, R., Jiraratananon, R., Shi, L. and Loh, C.H., (2011). "Effect of polyethylene glycol (PEG) as an additive on the fabrication of polyvinylidene fluoride-co-hexafluropropylene (PVDF-HFP) asymmetric microporous hollow fiber membranes", Journal of Membrane Science, 369(1–2):329-338.

[65] Fontananova, E., Jansen, J.C., Cristiano, A., Curcio, E. and Drioli, E., (2006). "Effect of additives in the casting solution on the formation of PVDF membranes", Desalination, 192(1):190-197.

[66] Bottino, A., Capannelli, G., Munari, S. and Turturro, A., (1988). "High performance ultrafiltration membranes cast from LiCl doped solutions", Desalination, 68(2):167-177.

[67] Lin, D.-J., Chang, C.-L., Huang, F.-M. and Cheng, L.-P., (2003). "Effect of salt additive on the formation of microporous poly(vinylidene fluoride) membranes by phase inversion from LiClO4/Water/DMF/PVDF system", Polymer, 44(2):413-422.

[68] Shi, L., Wang, R., Cao, Y., Liang, D.T. and Tay, J.H., (2008). "Effect of additives on the fabrication of poly(vinylidene fluoride-co-hexafluropropylene) (PVDF-

HFP) asymmetric microporous hollow fiber membranes", Journal of Membrane Science, 315(1):195-204.

[69] Khayet, M., (2003). "The effects of air gap length on the internal and external morphology of hollow fiber membranes", Chemical Engineering Science, 58(14):3091-3104.

[70] Chung, T.S., Xu, Z.L. and Lin, W., (1999). "Fundamental understanding of the effect of air-gap distance on the fabrication of hollow fiber membranes", Journal of applied polymer science, 72(3):379-395.

[71] Wang, D., Li, K. and Teo, W.K., (1999). "Preparation and characterization of polyvinylidene fluoride (PVDF) hollow fiber membranes", Journal of Membrane Science, 163(2):211-220.

[72] Peng, N., Chung, T.-S. and Wang, K.Y., (2008). "Macrovoid evolution and critical factors to form macrovoid-free hollow fiber membranes", Journal of Membrane Science, 318(1):363-372.

[73] Chung, T.-S.N., Fabrication of Hollow-Fiber Membranes by Phase Inversion, Advanced Membrane Technology and Applications, John Wiley & Sons, Inc.2008, pp. 821-839.

[74] Kong, J. and Li, K., (2001). "Preparation of PVDF hollow-fiber membranes via immersion precipitation", Journal of Applied Polymer Science, 81(7):1643-1653.

[75] Wang, D., Li, K. and Teo, W.K., (2000). "Porous PVDF asymmetric hollow fiber membranes prepared with the use of small molecular additives", Journal of Membrane Science, 178(1):13-23.

[76] Khayet, M., Feng, C.Y., Khulbe, K.C. and Matsuura, T., (2002). "Preparation and characterization of polyvinylidene fluoride hollow fiber membranes for ultrafiltration", Polymer, 43(14):3879-3890.

[77] Bottino, A., Capannelli, G. and Munari, S., (1985). "Effect of coagulation medium on properties of sulfonated polyvinylidene fluoride membranes", Journal of Applied Polymer Science, 30(7):3009-3022.

[78] Deshmukh, S.P. and Li, K., (1998). "Effect of ethanol composition in water coagulation bath on morphology of PVDF hollow fibre membranes", Journal of Membrane Science, 150(1):75-85.

[79] Buonomenna, M.G., Macchi, P., Davoli, M. and Drioli, E., (2007). "Poly(vinylidene fluoride) membranes by phase inversion: the role the casting and coagulation conditions play in their morphology, crystalline structure and properties", European Polymer Journal, 43(4):1557-1572.

[80] Yeow, M.L., Liu, Y. and Li, K., (2005). "Preparation of porous PVDF hollow fibre membrane via a phase inversion method using lithium perchlorate (LiClO4) as an additive", Journal of Membrane Science, 258(1):16-22.

[81] Cheng, L.-P., (1999). "Effect of Temperature on the Formation of Microporous PVDF Membranes by Precipitation from 1-Octanol/DMF/PVDF and Water/DMF/PVDF Systems", Macromolecules, 32(20):6668-6674.

[82] Wang, X., Zhang, L., Sun, D., An, Q. and Chen, H., (2008). "Effect of coagulation bath temperature on formation mechanism of poly(vinylidene fluoride) membrane", Journal of Applied Polymer Science, 110(3):1656-1663.

[83] Wang, K.Y., Li, D.F., Chung, T.-S. and Chen, S.B., (2004). "The observation of elongation dependent macrovoid evolution in single-and dual-layer asymmetric hollow fiber membranes", Chemical engineering science, 59(21):4657-4660.

[84] Chou, W.L. and Yang, M.C., (2005). "Effect of take-up speed on physical properties and permeation performance of cellulose acetate hollow fibers", Journal of Membrane Science, 250(1):259-267.

[85] Qin, J.-J. and Wong, F.-S., (2002). "Hypochlorite treatment of hydrophilic hollow fiber ultrafiltration membranes for high fluxes", Desalination, 146(1):307-309.

[86] Yadav, K., Morison, K. and Staiger, M.P., (2009). "Effects of hypochlorite treatment on the surface morphology and mechanical properties of polyethersulfone ultrafiltration membranes", Polymer Degradation and Stability, 94(11):1955-1961.

[87] Rouaix, S., Causserand, C. and Aimar, P., (2006). "Experimental study of the effects of hypochlorite on polysulfone membrane properties", Journal of Membrane Science, 277(1):137-147.

[88] Qin, J.-J., Oo, M.H. and Li, Y., (2005). "Development of high flux polyethersulfone hollow fiber ultrafiltration membranes from a low critical solution temperature dope via hypochlorite treatment", Journal of Membrane Science, 247(1):137-142.

[89] Causserand, C., Rouaix, S., Lafaille, J.-P. and Aimar, P., (2008). "Ageing of polysulfone membranes in contact with bleach solution: Role of radical oxidation and of some dissolved metal ions", Chemical Engineering and Processing: Process Intensification, 47(1):48-56.

[90] Roesink, H.D.W., (1989). Microfiltration: membrane development and module design Place University of Twente.

[91] Wienk, I., Meuleman, E., Borneman, Z., Van Den Boomgaard, T. and Smolders, C., (1995). "Chemical treatment of membranes of a polymer blend: mechanism of the reaction of hypochlorite with poly (vinyl pyrrolidone)", Journal of Polymer Science Part A: Polymer Chemistry, 33(1):49-54.

[92] Gao, F., Wang, J., Zhang, H., Zhang, Y. and Hang, M.A., (2016). "Effects of sodium hypochlorite on structural/surface characteristics, filtration performance and fouling behaviors of PVDF membranes", Journal of Membrane Science, 519(Supplement C):22-31.

[93] Abdullah, S.Z. and Bérubé, P.R., (2013). "Assessing the effects of sodium hypochlorite exposure on the characteristics of PVDF based membranes", Water Research, 47(14):5392-5399.

[94] Yuliwati, E., Ismail, A.F., Matsuura, T., Kassim, M.A. and Abdullah, M.S., (2011). "Effect of modified PVDF hollow fiber submerged ultrafiltration membrane for refinery wastewater treatment", Desalination, 283(Supplement C):214-220.

[95] Peiris, R.H., Hallé, C., Budman, H., Moresoli, C., Peldszus, S., Huck, P.M. and Legge, R.L., (2010). "Identifying fouling events in a membrane-based drinking water treatment process using principal component analysis of fluorescence excitation-emission matrices", Water Research, 44(1):185-194.

[96] Stengaard, F.F., (1988). “Characteristics and performance of new types of ultrafiltration membranes with chemically modified surfaces”, Desalination, 70(1):207-224.

[97] Wei, J., Helm, G.S., Corner-Walker, N. and Hou, X., (2006). “Characterization of a non-fouling ultrafiltration membrane”, Desalination, 192(1):252-261.

[98] Du, J.R., Peldszus, S., Huck, P.M. and Feng, X., (2009). “Modification of poly(vinylidene fluoride) ultrafiltration membranes with poly(vinyl alcohol) for fouling control in drinking water treatment”, Water Research, 43(18):4559-4568.

[99] Barona, G.N.B., Cha, B.J. and Jung, B., (2007). “Negatively charged poly (vinylidene fluoride) microfiltration membranes by sulfonation”, Journal of Membrane Science, 290(1):46-54.

[100] Xu, Z., Li, L., Wu, F., Tan, S. and Zhang, Z., (2005). “The application of the modified PVDF ultrafiltration membranes in further purification of Ginkgo biloba extraction”, Journal of Membrane Science, 255(1–2):125-131.

[101] Boributh, S., Chanachai, A. and Jiraratananon, R., (2009). “Modification of PVDF membrane by chitosan solution for reducing protein fouling”, Journal of Membrane Science, 342(1):97-104.

[102] Düputell, D. and Staude, E., (1993). “Heterogeneous modification of ultrafiltration membranes made from poly (vinylidene fluoride) and their characterization”, Journal of membrane science, 78(1):45-51.

[103] Xi, Z.-Y., Xu, Y.-Y., Zhu, L.-P., Wang, Y. and Zhu, B.-K., (2009). “A facile method of surface modification for hydrophobic polymer membranes based on the adhesive behavior of poly (DOPA) and poly (dopamine)”, Journal of Membrane Science, 327(1):244-253.

[104] Rahimpour, A., Madaeni, S.S., Zereshki, S. and Mansourpanah, Y., (2009). “Preparation and characterization of modified nano-porous PVDF membrane with high antifouling property using UV photo-grafting”, Applied Surface Science, 255(16):7455-7461.

[105] Zhang, M., Nguyen, Q.T. and Ping, Z., (2009). “Hydrophilic modification of poly (vinylidene fluoride) microporous membrane”, Journal of Membrane Science, 327(1–2):78-86.

[106] Wang, P., Tan, K.L., Kang, E.T. and Neoh, K.G., (2002). “Plasma-induced immobilization of poly(ethylene glycol) onto poly(vinylidene fluoride) microporous membrane”, Journal of Membrane Science, 195(1):103-114.

[107] Singh, N., Husson, S.M., Zdyrko, B. and Luzinov, I., (2005). “Surface modification of microporous PVDF membranes by ATRP”, Journal of Membrane Science, 262(1–2):81-90.

[108] Chiang, Y.-C., Chang, Y., Higuchi, A., Chen, W.-Y. and Ruaan, R.-C., (2009). “Sulfobetaine-grafted poly (vinylidene fluoride) ultrafiltration membranes exhibit excellent antifouling property”, Journal of Membrane Science, 339(1):151-159.

[109] Zularisam, A.W., Ismail, A.F. and Salim, R., (2006). “Behaviours of natural organic matter in membrane filtration for surface water treatment — a review”, Desalination, 194(1):211-231.

[110] Guo, W., Ngo, H.-H. and Li, J., (2012). "A mini-review on membrane fouling", Bioresource Technology, 122:27-34.

[111] Amy, G., (2008). "Fundamental understanding of organic matter fouling of membranes", Desalination, 231(1):44-51.

[112] Zularisam, A.W., Ismail, A.F., Salim, M.R., Sakinah, M. and Ozaki, H., (2007). "The effects of natural organic matter (NOM) fractions on fouling characteristics and flux recovery of ultrafiltration membranes", Desalination, 212(1):191-208.

[113] Lee, N., Amy, G. and Croué, J.-P., (2006). "Low-pressure membrane (MF/UF) fouling associated with allochthonous versus autochthonous natural organic matter", Water Research, 40(12):2357-2368.

[114] Bowen, W.R., Calvo, J.I. and Hernández, A., (1995). "Steps of membrane blocking in flux decline during protein microfiltration", Journal of Membrane Science, 101(1):153-165.

[115] Lee, N., Amy, G., Croué, J.-P. and Buisson, H., (2004). "Identification and understanding of fouling in low-pressure membrane (MF/UF) filtration by natural organic matter (NOM)", Water Research, 38(20):4511-4523.

[116] Mansouri, J., Harrisson, S. and Chen, V., (2010). "Strategies for controlling biofouling in membrane filtration systems: challenges and opportunities", Journal of Materials Chemistry, 20(22):4567-4586.

[117] Liu, C.X., Zhang, D.R., He, Y., Zhao, X.S. and Bai, R., (2010). "Modification of membrane surface for anti-biofouling performance: Effect of anti-adhesion and anti-bacteria approaches", Journal of Membrane Science, 346(1):121-130.

[118] Kochkodan, V. and Hilal, N., (2015). "A comprehensive review on surface modified polymer membranes for biofouling mitigation", Desalination, 356:187-207.

[119] Pasmore, M., Todd, P., Smith, S., Baker, D., Silverstein, J., Coons, D. and Bowman, C.N., (2001). "Effects of ultrafiltration membrane surface properties on Pseudomonas aeruginosa biofilm initiation for the purpose of reducing biofouling", Journal of Membrane Science, 194(1):15-32.

[120] Saeki, D., Nagashima, Y., Sawada, I. and Matsuyama, H., (2016). "Effect of hydrophobicity of polymer materials used for water purification membranes on biofilm formation dynamics", Colloids and Surfaces A: Physicochemical and Engineering Aspects, 506:622-628.

[121] Shirazi, S., Lin, C.-J. and Chen, D., (2010). "Inorganic fouling of pressure-driven membrane processes — A critical review", Desalination, 250(1):236-248.

[122] Brant, J.A. and Childress, A.E., (2004). "Colloidal adhesion to hydrophilic membrane surfaces", Journal of Membrane Science, 241(2):235-248.

[123] Zhu, L.-P., Yu, J.-Z., Xu, Y.-Y., Xi, Z.-Y. and Zhu, B.-K., (2009). "Surface modification of PVDF porous membranes via poly(DOPA) coating and heparin immobilization", Colloids and Surfaces B: Biointerfaces, 69(1):152-155.

[124] Chang, Y., Shih, Y.-J., Ruaan, R.-C., Higuchi, A., Chen, W.-Y. and Lai, J.-Y., (2008). "Preparation of poly(vinylidene fluoride) microfiltration membrane with uniform surface-copolymerized poly(ethylene glycol) methacrylate and

improvement of blood compatibility", Journal of Membrane Science, 309(1–2):165-174.

[125] Chang, Y., Ko, C.-Y., Shih, Y.-J., Quémener, D., Deratani, A., Wei, T.-C., Wang, D.-M. and Lai, J.-Y., (2009). "Surface grafting control of PEGylated poly(vinylidene fluoride) antifouling membrane via surface-initiated radical graft copolymerization", Journal of Membrane Science, 345(1–2):160-169.

[126] Ma, X., Su, Y., Sun, Q., Wang, Y. and Jiang, Z., (2007). "Enhancing the antifouling property of polyethersulfone ultrafiltration membranes through surface adsorption-crosslinking of poly(vinyl alcohol)", Journal of Membrane Science, 300(1–2):71-78.

[127] Shi, H., Xue, L., Gao, A., Fu, Y., Zhou, Q. and Zhu, L., (2016). "Fouling-resistant and adhesion-resistant surface modification of dual layer PVDF hollow fiber membrane by dopamine and quaternary polyethyleneimine", Journal of Membrane Science, 498:39-47.

[128] Zhang, R., Liu, Y., He, M., Su, Y., Zhao, X., Elimelech, M. and Jiang, Z., (2016). "Antifouling membranes for sustainable water purification: strategies and mechanisms", Chemical Society Reviews, 45(21):5888-5924.

[129] Moghareh Abed, M.R., Kumbharkar, S.C., Groth, A.M. and Li, K., (2013). "Economical production of PVDF-g-POEM for use as a blend in preparation of PVDF based hydrophilic hollow fibre membranes", Separation and Purification Technology, 106:47-55.

[130] Kang, S., Asatekin, A., Mayes, A.M. and Elimelech, M., (2007). "Protein antifouling mechanisms of PAN UF membranes incorporating PAN-g-PEO additive", Journal of Membrane Science, 296(1–2):42-50.

[131] Hu, M.-X., Yang, Q. and Xu, Z.-K., (2006). "Enhancing the hydrophilicity of polypropylene microporous membranes by the grafting of 2-hydroxyethyl methacrylate via a synergistic effect of photoinitiators", Journal of Membrane Science, 285(1–2):196-205.

[132] Nakata, M. and Kumazawa, H., (2006). "Gas permeability and permselectivity of plasma-treated polyethylene membranes", Journal of Applied Polymer Science, 101(1):383-387.

[133] Zhu, L.-P., Zhu, B.-K., Xu, L., Feng, Y.-X., Liu, F. and Xu, Y.-Y., (2007). "Corona-induced graft polymerization for surface modification of porous polyethersulfone membranes", Applied Surface Science, 253(14):6052-6059.

[134] Liu, F., Zhu, B.-K. and Xu, Y.-Y., (2006). "Improving the hydrophilicity of poly(vinylidene fluoride) porous membranes by electron beam initiated surface grafting of AA/SSS binary monomers", Applied Surface Science, 253(4):2096-2101.

[135] Kochkodan, V.M. and Sharma, V.K., (2012). "Graft polymerization and plasma treatment of polymer membranes for fouling reduction: A review", Journal of Environmental Science and Health, Part A, 47(12):1713-1727.

[136] Zou, L., Vidalis, I., Steele, D., Michelmore, A., Low, S.P. and Verberk, J.Q.J.C., (2011). "Surface hydrophilic modification of RO membranes by plasma polymerization for low organic fouling", Journal of Membrane Science, 369(1–2):420-428.

[137] Liang, S., Kang, Y., Tiraferri, A., Giannelis, E.P., Huang, X. and Elimelech, M., (2013). "Highly hydrophilic polyvinylidene fluoride (PVDF) ultrafiltration membranes via postfabrication grafting of surface-tailored silica nanoparticles", ACS Applied Materials and Interfaces, 5(14):6694-6703.

[138] Braunecker, W.A. and Matyjaszewski, K., (2007). "Controlled/living radical polymerization: Features, developments, and perspectives", Progress in Polymer Science, 32(1):93-146.

[139] Hashim, N.A., Liu, F. and Li, K., (2009). "A simplified method for preparation of hydrophilic PVDF membranes from an amphiphilic graft copolymer", Journal of Membrane Science, 345(1–2):134-141.

[140] Hester, J.F., Banerjee, P., Won, Y.Y., Akthakul, A., Acar, M.H. and Mayes, A.M., (2002). "ATRP of Amphiphilic Graft Copolymers Based on PVDF and Their Use as Membrane Additives", Macromolecules, 35(20):7652-7661.

[141] Chen, Y., Sun, W., Deng, Q. and Chen, L., (2006). "Controlled grafting from poly(vinylidene fluoride) films by surface-initiated reversible addition–fragmentation chain transfer polymerization", Journal of Polymer Science Part A: Polymer Chemistry, 44(9):3071-3082.

[142] Mohmood, I., Lopes, C.B., Lopes, I., Ahmad, I., Duarte, A.C. and Pereira, E., (2013). "Nanoscale materials and their use in water contaminants removal—a review", Environmental Science and Pollution Research, 20(3):1239-1260.

[143] Theron, J., Walker, J.A. and Cloete, T.E., (2008). "Nanotechnology and Water Treatment: Applications and Emerging Opportunities", Critical Reviews in Microbiology, 34(1):43-69.

[144] Kim, J. and Van der Bruggen, B., (2010). "The use of nanoparticles in polymeric and ceramic membrane structures: Review of manufacturing procedures and performance improvement for water treatment", Environmental Pollution, 158(7):2335-2349.

[145] Hossain, F., Perales-Perez, O.J., Hwang, S. and Román, F., (2014). "Antimicrobial nanomaterials as water disinfectant: Applications, limitations and future perspectives", Science of The Total Environment, 466–467:1047-1059.

[146] Li, Q., Mahendra, S., Lyon, D.Y., Brunet, L., Liga, M.V., Li, D. and Alvarez, P.J.J., (2008). "Antimicrobial nanomaterials for water disinfection and microbial control: Potential applications and implications", Water Research, 42(18):4591-4602.

[147] Qu, X., Alvarez, P.J.J. and Li, Q., (2013). "Applications of nanotechnology in water and wastewater treatment", Water Research, 47(12):3931-3946.

[148] Jhaveri, J.H. and Murthy, Z.V.P., (2016). "A comprehensive review on anti-fouling nanocomposite membranes for pressure driven membrane separation processes", Desalination, 379:137-154.

[149] Daer, S., Kharraz, J., Giwa, A. and Hasan, S.W., (2015). "Recent applications of nanomaterials in water desalination: A critical review and future opportunities", Desalination, 367:37-48.

[150] Ong, C.S., Goh, P.S., Lau, W.J., Misdan, N. and Ismail, A.F., (2016). "Nanomaterials for biofouling and scaling mitigation of thin film composite membrane: A review", Desalination, 393:2-15.

[151] Qadir, D., Mukhtar, H. and Keong, L.K., (2017). "Mixed Matrix Membranes for Water Purification Applications", Separation & Purification Reviews, 46(1):62-80.

[152] Jhaveri, J.H. and Murthy, Z.V.P., (2016). "Nanocomposite membranes", Desalination and Water Treatment, 57(55):26803-26819.

[153] Baghbanzadeh, M., Rana, D., Lan, C.Q. and Matsuura, T., (2016). "Effects of Inorganic Nano-Additives on Properties and Performance of Polymeric Membranes in Water Treatment", Separation & Purification Reviews, 45(2):141-167.

[154] Al Aani, S., Wright, C.J., Atieh, M.A. and Hilal, N., (2017). "Engineering nanocomposite membranes: Addressing current challenges and future opportunities", Desalination, 401:1-15.

[155] Yin, J. and Deng, B., (2015). "Polymer-matrix nanocomposite membranes for water treatment", Journal of Membrane Science, 479:256-275.

[156] Yang, H.-C., Hou, J., Chen, V. and Xu, Z.-K., (2016). "Surface and interface engineering for organic-inorganic composite membranes", Journal of Materials Chemistry A, 4(25):9716-9729.

[157] Whan Cho, J. and Il Sul, K., (2001). "Characterization and properties of hybrid composites prepared from poly(vinylidene fluoride–tetrafluoroethylene) and SiO2", Polymer, 42(2):727-736.

[158] Zoppi, R.A. and Soares, C.G.A., (2002). "Hybrids of poly(ethylene oxide-b-amide-6) and ZrO2 sol–gel: Preparation, characterization, and application in processes of membranes separation", Advances in Polymer Technology, 21(1):2-16.

[159] Cuiming, W., Tongwen, X. and Weihua, Y., (2003). "Fundamental studies of a new hybrid (inorganic–organic) positively charged membrane: membrane preparation and characterizations", Journal of Membrane Science, 216(1–2):269-278.

[160] Nagarale, R.K., Shahi, V.K. and Rangarajan, R., (2005). "Preparation of polyvinyl alcohol–silica hybrid heterogeneous anion-exchange membranes by sol–gel method and their characterization", Journal of Membrane Science, 248(1–2):37-44.

[161] María Arsuaga, J., Sotto, A., del Rosario, G., Martínez, A., Molina, S., Teli, S.B. and de Abajo, J., (2013). "Influence of the type, size, and distribution of metal oxide particles on the properties of nanocomposite ultrafiltration membranes", Journal of Membrane Science, 428:131-141.

[162] Ma, P.-C., Siddiqui, N.A., Marom, G. and Kim, J.-K., (2010). "Dispersion and functionalization of carbon nanotubes for polymer-based nanocomposites: A review", Composites Part A: Applied Science and Manufacturing, 41(10):1345-1367.

[163] Razmjou, A., Mansouri, J. and Chen, V., (2011). "The effects of mechanical and chemical modification of TiO2 nanoparticles on the surface chemistry, structure and fouling performance of PES ultrafiltration membranes", Journal of Membrane Science, 378(1–2):73-84.

[164] Liu, F., Abed, M.R.M. and Li, K., (2011). "Preparation and characterization of poly(vinylidene fluoride) (PVDF) based ultrafiltration membranes using nano γ-Al2O3", Journal of Membrane Science, 366(1–2):97-103.

[165] Razmjou, A., Resosudarmo, A., Holmes, R.L., Li, H., Mansouri, J. and Chen, V., (2012). "The effect of modified TiO2 nanoparticles on the polyethersulfone ultrafiltration hollow fiber membranes", Desalination, 287:271-280.

[166] Yu, Z., Zeng, G., Pan, Y., Lv, L., Min, H., Zhang, L. and He, Y., (2015). "Effect of functionalized multi-walled carbon nanotubes on the microstructure and performances of PVDF membranes", RSC Advances, 5(93):75998-76006.

[167] Xu, Z., Zhang, J., Shan, M., Li, Y., Li, B., Niu, J., Zhou, B. and Qian, X., (2014). "Organosilane-functionalized graphene oxide for enhanced antifouling and mechanical properties of polyvinylidene fluoride ultrafiltration membranes", Journal of Membrane Science, 458:1-13.

[168] Teow, Y.H., Latif, A.A., Lim, J.K., Ngang, H.P., Susan, L.Y. and Ooi, B.S., (2015). "Hydroxyl functionalized PVDF–TiO2 ultrafiltration membrane and its antifouling properties", Journal of Applied Polymer Science, 132(21):n/a-n/a.

[169] Yu, L.-Y., Xu, Z.-L., Shen, H.-M. and Yang, H., (2009). "Preparation and characterization of PVDF–SiO2 composite hollow fiber UF membrane by sol–gel method", Journal of Membrane Science, 337(1–2):257-265.

[170] Hashim, N.A., Liu, Y. and Li, K., (2011). "Preparation of PVDF Hollow Fiber Membranes Using SiO2 Particles: The Effect of Acid and Alkali Treatment on the Membrane Performances", Industrial & Engineering Chemistry Research, 50(5):3035-3040.

[171] Zuo, X., Yu, S., Xu, X., Xu, J., Bao, R. and Yan, X., (2009). "New PVDF organic–inorganic membranes: The effect of SiO2 nanoparticles content on the transport performance of anion-exchange membranes", Journal of Membrane Science, 340(1–2):206-213.

[172] Yu, S., Zuo, X., Bao, R., Xu, X., Wang, J. and Xu, J., (2009). "Effect of SiO2 nanoparticle addition on the characteristics of a new organic–inorganic hybrid membrane", Polymer, 50(2):553-559.

[173] Wu, H., Mansouri, J. and Chen, V., (2013). "Silica nanoparticles as carriers of antifouling ligands for PVDF ultrafiltration membranes", Journal of Membrane Science, 433:135-151.

[174] Wang, H., Zhao, X. and He, C., (2016). "Enhanced antifouling performance of hybrid PVDF ultrafiltration membrane with the dual-mode SiO2-g-PDMS nanoparticles", Separation and Purification Technology, 166:1-8.

[175] Zeng, G., He, Y., Zhan, Y., Zhang, L., Shi, H. and Yu, Z., (2016). "Preparation of a Novel Poly(vinylidene fluoride) Ultrafiltration Membrane by Incorporation of 3-Aminopropyltriethoxysilane-Grafted Halloysite Nanotubes for Oil/Water Separation", Ind. Eng. Chem. Res., 55(6):1760-1767.

[176] Yan, L., Hong, S., Li, M.L. and Li, Y.S., (2009). "Application of the Al2O3–PVDF nanocomposite tubular ultrafiltration (UF) membrane for oily wastewater treatment and its antifouling research", Separation and Purification Technology, 66(2):347-352.

[177] Wang, X.-M., Li, X.-Y. and Shih, K., (2011). "In situ embedment and growth of anhydrous and hydrated aluminum oxide particles on polyvinylidene fluoride (PVDF) membranes", Journal of Membrane Science, 368(1–2):134-143.

[178] Yan, L., Li, Y.S., Xiang, C.B. and Xianda, S., (2006). "Effect of nano-sized Al2O3-particle addition on PVDF ultrafiltration membrane performance", Journal of Membrane Science, 276(1–2):162-167.

[179] Shi, H., He, Y., Pan, Y., Di, H., Zeng, G., Zhang, L. and Zhang, C., (2016). "A modified mussel-inspired method to fabricate TiO2 decorated superhydrophilic PVDF membrane for oil/water separation", Journal of Membrane Science, 506:60-70.

[180] Madaeni, S.S., Zinadini, S. and Vatanpour, V., (2011). "A new approach to improve antifouling property of PVDF membrane using in situ polymerization of PAA functionalized TiO2 nanoparticles", Journal of Membrane Science, 380(1–2):155-162.

[181] Wei, Y., Chu, H.-Q., Dong, B.-Z., Li, X., Xia, S.-J. and Qiang, Z.-M., (2011). "Effect of TiO2 nanowire addition on PVDF ultrafiltration membrane performance", Desalination, 272(1–3):90-97.

[182] Méricq, J.P., Mendret, J., Brosillon, S. and Faur, C., (2015). "High performance PVDF-TiO2 membranes for water treatment", Chemical Engineering Science, 123:283-291.

[183] Li, J.-H., Xu, Y.-Y., Zhu, L.-P., Wang, J.-H. and Du, C.-H., (2009). "Fabrication and characterization of a novel TiO2 nanoparticle self-assembly membrane with improved fouling resistance", Journal of Membrane Science, 326(2):659-666.

[184] Zhao, X., Su, Y., Liu, Y., Zhang, R. and Jiang, Z., (2015). "Multiple antifouling capacities of hybrid membranes derived from multifunctional titania nanoparticles", Journal of Membrane Science, 495:226-234.

[185] Song, H., Shao, J., He, Y., Liu, B. and Zhong, X., (2012). "Natural organic matter removal and flux decline with PEG–TiO2-doped PVDF membranes by integration of ultrafiltration with photocatalysis", Journal of Membrane Science, 405–406:48-56.

[186] Yu, L.-Y., Shen, H.-M. and Xu, Z.-L., (2009). "PVDF–TiO2 composite hollow fiber ultrafiltration membranes prepared by TiO2 sol–gel method and blending method", Journal of Applied Polymer Science, 113(3):1763-1772.

[187] Yuliwati, E., Ismail, A.F., Matsuura, T., Kassim, M.A. and Abdullah, M.S., (2011). "Characterization of surface-modified porous PVDF hollow fibers for refinery wastewater treatment using microscopic observation", Desalination, 283:206-213.

[188] Teow, Y.H., Ahmad, A.L., Lim, J.K. and Ooi, B.S., (2012). "Preparation and characterization of PVDF/TiO2 mixed matrix membrane via in situ colloidal precipitation method", Desalination, 295:61-69.

[189] Shi, F., Ma, Y., Ma, J., Wang, P. and Sun, W., (2012). "Preparation and characterization of PVDF/TiO2 hybrid membranes with different dosage of nano-TiO2", Journal of Membrane Science, 389:522-531.

[190] Yi, X.S., Yu, S.L., Shi, W.X., Sun, N., Jin, L.M., Wang, S., Zhang, B., Ma, C. and Sun, L.P., (2011). "The influence of important factors on ultrafiltration of

oil/water emulsion using PVDF membrane modified by nano-sized TiO2/Al2O3", Desalination, 281:179-184.

[191] Rahimpour, A., Jahanshahi, M., Rajaeian, B. and Rahimnejad, M., (2011). "TiO2 entrapped nano-composite PVDF/SPES membranes: Preparation, characterization, antifouling and antibacterial properties", Desalination, 278(1–3):343-353.

[192] Cao, X., Ma, J., Shi, X. and Ren, Z., (2006). "Effect of TiO2 nanoparticle size on the performance of PVDF membrane", Applied Surface Science, 253(4):2003-2010.

[193] Liang, S., Xiao, K., Mo, Y. and Huang, X., (2012). "A novel ZnO nanoparticle blended polyvinylidene fluoride membrane for anti-irreversible fouling", Journal of Membrane Science, 394–395:184-192.

[194] Balta, S., Sotto, A., Luis, P., Benea, L., Van der Bruggen, B. and Kim, J., (2012). "A new outlook on membrane enhancement with nanoparticles: The alternative of ZnO", Journal of Membrane Science, 389:155-161.

[195] Hong, J. and He, Y., (2014). "Polyvinylidene fluoride ultrafiltration membrane blended with nano-ZnO particle for photo-catalysis self-cleaning", Desalination, 332(1):67-75.

[196] Bottino, A., Capannelli, G. and Comite, A., (2002). "Preparation and characterization of novel porous PVDF-ZrO2 composite membranes", Desalination, 146(1):35-40.

[197] Zheng, Y.-M., Zou, S.-W., Nanayakkara, K.G.N., Matsuura, T. and Chen, J.P., (2011). "Adsorptive removal of arsenic from aqueous solution by a PVDF/zirconia blend flat sheet membrane", Journal of Membrane Science, 374(1–2):1-11.

[198] Ebert, K., Fritsch, D., Koll, J. and Tjahjawiguna, C., (2004). "Influence of inorganic fillers on the compaction behaviour of porous polymer based membranes", Journal of Membrane Science, 233(1–2):71-78.

[199] Pendergast, M.T.M., Nygaard, J.M., Ghosh, A.K. and Hoek, E.M.V., (2010). "Using nanocomposite materials technology to understand and control reverse osmosis membrane compaction", Desalination, 261(3):255-263.

[200] Bottino, A., Capannelli, G., D'Asti, V. and Piaggio, P., (2001). "Preparation and properties of novel organic–inorganic porous membranes", Separation and Purification Technology, 22–23:269-275.

[201] Arthanareeswaran, G., Sriyamuna Devi, T.K. and Raajenthiren, M., (2008). "Effect of silica particles on cellulose acetate blend ultrafiltration membranes: Part I", Separation and Purification Technology, 64(1):38-47.

[202] Oh, S.J., Kim, N. and Lee, Y.T., (2009). "Preparation and characterization of PVDF/TiO2 organic–inorganic composite membranes for fouling resistance improvement", Journal of Membrane Science, 345(1–2):13-20.

[203] Wang, Q., Wang, X., Wang, Z., Huang, J. and Wang, Y., (2013). "PVDF membranes with simultaneously enhanced permeability and selectivity by breaking the tradeoff effect via atomic layer deposition of TiO2", Journal of Membrane Science, 442:57-64.

[204] Madaeni, S.S. and Ghaemi, N., (2007). “Characterization of self-cleaning RO membranes coated with TiO2 particles under UV irradiation”, Journal of Membrane Science, 303(1–2):221-233.

[205] Cruz, N.K.O., Semblante, G.U., Senoro, D.B., You, S.-J. and Lu, S.-C., (2014). “Dye degradation and antifouling properties of polyvinylidene fluoride/titanium oxide membrane prepared by sol–gel method”, Journal of the Taiwan Institute of Chemical Engineers, 45(1):192-201.

[206] Han, L.-F., Xu, Z.-L., Yu, L.-Y., Wei, Y.-M. and Cao, Y., (2010). “Performance of PVDF/multi-nanoparticles composite hollow fibre ultrafiltration membranes”, Iran. Polym. J, 19(7):553-565.

[207] Qian, D., Wagner, G.J., Liu, W.K., Yu, M.-F. and Ruoff, R.S., (2002). “Mechanics of carbon nanotubes”, Applied Mechanics Reviews, 55(6):495-533.

[208] Coleman, J.N., Khan, U. and Gun'ko, Y.K., (2006). “Mechanical Reinforcement of Polymers Using Carbon Nanotubes”, Advanced Materials, 18(6):689-706.

[209] Coleman, J.N., Khan, U., Blau, W.J. and Gun’ko, Y.K., (2006). “Small but strong: A review of the mechanical properties of carbon nanotube–polymer composites”, Carbon, 44(9):1624-1652.

[210] Ganesh, E., (2013). “Single walled and multi walled carbon nanotube structure, synthesis and applications”, International Journal of Innovative Technology and Exploring Engineering (IJITEE) ISSN, 2278:3075.

[211] Das, R., Ali, M.E., Hamid, S.B.A., Ramakrishna, S. and Chowdhury, Z.Z., (2014). “Carbon nanotube membranes for water purification: A bright future in water desalination”, Desalination, 336:97-109.

[212] Huang, W., Edenzon, K., Fernandez, L., Razmpour, S., Woodburn, J. and Cebe, P., (2010). “Nanocomposites of poly(vinylidene fluoride) with multiwalled carbon nanotubes”, Journal of Applied Polymer Science, 115(6):3238-3248.

[213] Spitalsky, Z., Tasis, D., Papagelis, K. and Galiotis, C., (2010). “Carbon nanotube–polymer composites: Chemistry, processing, mechanical and electrical properties”, Progress in Polymer Science, 35(3):357-401.

[214] Upadhyayula, V.K.K., Deng, S., Mitchell, M.C. and Smith, G.B., (2009). “Application of carbon nanotube technology for removal of contaminants in drinking water: A review”, Science of The Total Environment, 408(1):1-13.

[215] Goh, P.S., Ismail, A.F. and Ng, B.C., (2013). “Carbon nanotubes for desalination: Performance evaluation and current hurdles”, Desalination, 308:2-14.

[216] Gupta, V.K., Moradi, O., Tyagi, I., Agarwal, S., Sadegh, H., Shahryari-Ghoshekandi, R., Makhlouf, A.S.H., Goodarzi, M. and Garshasbi, A., (2016). “Study on the removal of heavy metal ions from industry waste by carbon nanotubes: Effect of the surface modification: a review”, Critical Reviews in Environmental Science and Technology, 46(2):93-118.

[217] Lee, J., Jeong, S. and Liu, Z., (2016). “Progress and challenges of carbon nanotube membrane in water treatment”, Critical Reviews in Environmental Science and Technology, 46(11-12):999-1046.

[218] Ahn, C.H., Baek, Y., Lee, C., Kim, S.O., Kim, S., Lee, S., Kim, S.-H., Bae, S.S., Park, J. and Yoon, J., (2012). “Carbon nanotube-based membranes: Fabrication

and application to desalination", Journal of Industrial and Engineering Chemistry, 18(5):1551-1559.

[219] Vatanpour, V., Madaeni, S.S., Moradian, R., Zinadini, S. and Astinchap, B., (2011). "Fabrication and characterization of novel antifouling nanofiltration membrane prepared from oxidized multiwalled carbon nanotube/polyethersulfone nanocomposite", Journal of Membrane Science, 375(1–2):284-294.

[220] Celik, E., Park, H., Choi, H. and Choi, H., (2011). "Carbon nanotube blended polyethersulfone membranes for fouling control in water treatment", Water Research, 45(1):274-282.

[221] Ma, J., Zhao, Y., Xu, Z., Min, C., Zhou, B., Li, Y., Li, B. and Niu, J., (2013). "Role of oxygen-containing groups on MWCNTs in enhanced separation and permeability performance for PVDF hybrid ultrafiltration membranes", Desalination, 320:1-9.

[222] Yuen, S.-M., Ma, C.-C.M., Chiang, C.-L., Chang, J.-A., Huang, S.-W., Chen, S.-C., Chuang, C.-Y., Yang, C.-C. and Wei, M.-H., (2007). "Silane-modified MWCNT/PMMA composites – Preparation, electrical resistivity, thermal conductivity and thermal stability", Composites Part A: Applied Science and Manufacturing, 38(12):2527-2535.

[223] Kathi, J., Rhee, K.-Y. and Lee, J.H., (2009). "Effect of chemical functionalization of multi-walled carbon nanotubes with 3-aminopropyltriethoxysilane on mechanical and morphological properties of epoxy nanocomposites", Composites Part A: Applied Science and Manufacturing, 40(6–7):800-809.

[224] Lee, J.H., Rhee, K.Y. and Park, S.J., (2010). "The tensile and thermal properties of modified CNT-reinforced basalt/epoxy composites", Materials Science and Engineering: A, 527(26):6838-6843.

[225] Lavorgna, M., Romeo, V., Martone, A., Zarrelli, M., Giordano, M., Buonocore, G.G., Qu, M.Z., Fei, G.X. and Xia, H.S., (2013). "Silanization and silica enrichment of multiwalled carbon nanotubes: Synergistic effects on the thermal-mechanical properties of epoxy nanocomposites", European Polymer Journal, 49(2):428-438.

[226] Kim, M.T., Rhee, K.Y., Park, S.J. and Hui, D., (2012). "Effects of silane-modified carbon nanotubes on flexural and fracture behaviors of carbon nanotube-modified epoxy/basalt composites", Composites Part B: Engineering, 43(5):2298-2302.

[227] Sianipar, M., Kim, S.H., Min, C., Tijing, L.D. and Shon, H.K., (2016). "Potential and performance of a polydopamine-coated multiwalled carbon nanotube/polysulfone nanocomposite membrane for ultrafiltration application", Journal of Industrial and Engineering Chemistry, 34:364-373.

[228] Zhao, X., Ma, J., Wang, Z., Wen, G., Jiang, J., Shi, F. and Sheng, L., (2012). "Hyperbranched-polymer functionalized multi-walled carbon nanotubes for poly (vinylidene fluoride) membranes: From dispersion to blended fouling-control membrane", Desalination, 303:29-38.

[229] Esfahani, M.R., Tyler, J.L., Stretz, H.A. and Wells, M.J.M., (2015). "Effects of a dual nanofiller, nano-TiO2 and MWCNT, for polysulfone-based nanocomposite membranes for water purification", Desalination, 372:47-56.

[230] Zhao, Y., Xu, Z., Shan, M., Min, C., Zhou, B., Li, Y., Li, B., Liu, L. and Qian, X., (2013). "Effect of graphite oxide and multi-walled carbon nanotubes on the microstructure and performance of PVDF membranes", Separation and Purification Technology, 103:78-83.

[231] Zhang, J., Xu, Z., Shan, M., Zhou, B., Li, Y., Li, B., Niu, J. and Qian, X., (2013). "Synergetic effects of oxidized carbon nanotubes and graphene oxide on fouling control and anti-fouling mechanism of polyvinylidene fluoride ultrafiltration membranes", Journal of Membrane Science, 448:81-92.

[232] Mierzwa, J.C., Arieta, V., Verlage, M., Carvalho, J. and Vecitis, C.D., (2013). "Effect of clay nanoparticles on the structure and performance of polyethersulfone ultrafiltration membranes", Desalination, 314:147-158.

[233] Monticelli, O., Bottino, A., Scandale, I., Capannelli, G. and Russo, S., (2007). "Preparation and properties of polysulfone–clay composite membranes", Journal of Applied Polymer Science, 103(6):3637-3644.

[234] Anadão, P., Sato, L.F., Wiebeck, H. and Valenzuela-Díaz, F.R., (2010). "Montmorillonite as a component of polysulfone nanocomposite membranes", Applied Clay Science, 48(1–2):127-132.

[235] Ghaemi, N., Madaeni, S.S., Alizadeh, A., Rajabi, H. and Daraei, P., (2011). "Preparation, characterization and performance of polyethersulfone/organically modified montmorillonite nanocomposite membranes in removal of pesticides", Journal of Membrane Science, 382(1–2):135-147.

[236] Ma, Y., Shi, F., Wang, Z., Wu, M., Ma, J. and Gao, C., (2012). "Preparation and characterization of PSf/clay nanocomposite membranes with PEG 400 as a pore forming additive", Desalination, 286:131-137.

[237] Lai, C.Y., Groth, A., Gray, S. and Duke, M., (2014). "Preparation and characterization of poly(vinylidene fluoride)/nanoclay nanocomposite flat sheet membranes for abrasion resistance", Water Research, 57(Supplement C):56-66.

[238] Lai, C.Y., Groth, A., Gray, S. and Duke, M., (2014). "Enhanced abrasion resistant PVDF/nanoclay hollow fibre composite membranes for water treatment", Journal of Membrane Science, 449(Supplement C):146-157.

[239] Berthier, P., Analyse de l'halloysite, Annales de Chimie et de Physique, 1826, pp. 332-335.

[240] Joussein, E., Petit, S., Churchman, J., Theng, B., Righi, D. and Delvaux, B., (2005). "Halloysite clay minerals–a review", Clay minerals, 40(4):383-426.

[241] Liu, M., Jia, Z., Jia, D. and Zhou, C., (2014). "Recent advance in research on halloysite nanotubes-polymer nanocomposite", Progress in Polymer Science, 39(8):1498-1525.

[242] Vergaro, V., Abdullayev, E., Lvov, Y.M., Zeitoun, A., Cingolani, R., Rinaldi, R. and Leporatti, S., (2010). "Cytocompatibility and Uptake of Halloysite Clay Nanotubes", Biomacromolecules, 11(3):820-826.

[243] Luo, P., Zhao, Y., Zhang, B., Liu, J., Yang, Y. and Liu, J., (2010). "Study on the adsorption of Neutral Red from aqueous solution onto halloysite nanotubes", Water Research, 44(5):1489-1497.

[244] Yuan, P., Southon, P.D., Liu, Z., Green, M.E.R., Hook, J.M., Antill, S.J. and Kepert, C.J., (2008). "Functionalization of Halloysite Clay Nanotubes by Grafting with γ-Aminopropyltriethoxysilane", The Journal of Physical Chemistry C, 112(40):15742-15751.

[245] Zhi, C., Bando, Y., Tang, C. and Golberg, D., (2010). "Boron nitride nanotubes", Materials Science and Engineering: R: Reports, 70(3):92-111.

[246] Duan, L., Huang, W. and Zhang, Y., (2015). "High-flux, antibacterial ultrafiltration membranes by facile blending with N-halamine grafted halloysite nanotubes", RSC Advances, 5(9):6666-6674.

[247] Zhao, Q., Hou, J., Shen, J., Liu, J. and Zhang, Y., (2015). "Long-lasting antibacterial behavior of a novel mixed matrix water purification membrane", Journal of Materials Chemistry A, 3(36):18696-18705.

[248] Zhao, Q., Liu, C., Liu, J. and Zhang, Y., (2015). "Development of a novel polyethersulfone ultrafiltration membrane with antibacterial activity and high flux containing halloysite nanotubes loaded with lysozyme", RSC Advances, 5(48):38646-38653.

[249] Wang, Z., Wang, H., Liu, J. and Zhang, Y., (2014). "Preparation and antifouling property of polyethersulfone ultrafiltration hybrid membrane containing halloysite nanotubes grafted with MPC via RATRP method", Desalination, 344:313-320.

[250] Yu, H., Zhang, Y., Sun, X., Liu, J. and Zhang, H., (2014). "Improving the antifouling property of polyethersulfone ultrafiltration membrane by incorporation of dextran grafted halloysite nanotubes", Chemical Engineering Journal, 237:322-328.

[251] Chen, Y., Zhang, Y., Liu, J., Zhang, H. and Wang, K., (2012). "Preparation and antibacterial property of polyethersulfone ultrafiltration hybrid membrane containing halloysite nanotubes loaded with copper ions", Chemical Engineering Journal, 210:298-308.

[252] Ghanbari, M., Emadzadeh, D., Lau, W.J., Lai, S.O., Matsuura, T. and Ismail, A.F., (2015). "Synthesis and characterization of novel thin film nanocomposite (TFN) membranes embedded with halloysite nanotubes (HNTs) for water desalination", Desalination, 358:33-41.

[253] Chen, Y., Zhang, Y., Zhang, H., Liu, J. and Song, C., (2013). "Biofouling control of halloysite nanotubes-decorated polyethersulfone ultrafiltration membrane modified with chitosan-silver nanoparticles", Chemical Engineering Journal, 228:12-20.

[254] Zhang, J., Zhang, Y., Chen, Y., Du, L., Zhang, B., Zhang, H., Liu, J. and Wang, K., (2012). "Preparation and Characterization of Novel Polyethersulfone Hybrid Ultrafiltration Membranes Bending with Modified Halloysite Nanotubes Loaded with Silver Nanoparticles", Industrial & Engineering Chemistry Research, 51(7):3081-3090.

[255] Yu, L., Wang, H., Zhang, Y., Zhang, B. and Liu, J., (2016). "Recent advances in halloysite nanotube derived composites for water treatment", Environmental Science: Nano, 3(1):28-44.

[256] Zhang, Y., Tang, A., Yang, H. and Ouyang, J., (2016). "Applications and interfaces of halloysite nanocomposites", Applied Clay Science, 119, Part 1:8-17.

[257] Carli, L.N., Daitx, T.S., Soares, G.V., Crespo, J.S. and Mauler, R.S., (2014). "The effects of silane coupling agents on the properties of PHBV/halloysite nanocomposites", Applied Clay Science, 87:311-319.

[258] Liu, M., Guo, B., Du, M., Lei, Y. and Jia, D., (2008). "Natural inorganic nanotubes reinforced epoxy resin nanocomposites", Journal of Polymer Research, 15(3):205-212.

[259] Li, C., Liu, J., Qu, X. and Yang, Z., (2009). "A general synthesis approach toward halloysite-based composite nanotube", Journal of Applied Polymer Science, 112(5):2647-2655.

[260] Li, C., Liu, J., Qu, X., Guo, B. and Yang, Z., (2008). "Polymer-modified halloysite composite nanotubes", Journal of Applied Polymer Science, 110(6):3638-3646.

[261] Sun, P., Liu, G., Lv, D., Dong, X., Wu, J. and Wang, D., (2016). "Simultaneous improvement in strength, toughness, and thermal stability of epoxy/halloysite nanotubes composites by interfacial modification", Journal of Applied Polymer Science, 133(13):n/a-n/a.

[262] Guo, B., Zou, Q., Lei, Y. and Jia, D., (2009). "Structure and performance of polyamide 6/halloysite nanotubes nanocomposites", Polymer journal, 41(10):835-842.

[263] Albdiry, M.T. and Yousif, B.F., (2013). "Morphological structures and tribological performance of unsaturated polyester based untreated/silane-treated halloysite nanotubes", Materials & Design, 48:68-76.

[264] Zeng, G., He, Y., Zhan, Y., Zhang, L., Pan, Y., Zhang, C. and Yu, Z., (2016). "Novel polyvinylidene fluoride nanofiltration membrane blended with functionalized halloysite nanotubes for dye and heavy metal ions removal", Journal of Hazardous Materials, 317:60-72.

[265] Ghaee, A., Shariaty-Niassar, M., Barzin, J. and Matsuura, T., (2010). "Effects of chitosan membrane morphology on copper ion adsorption", Chemical Engineering Journal, 165(1):46-55.

[266] Moslehyani, A., Mobaraki, M., Ismail, A.F., Matsuura, T., Hashemifard, S.A., Othman, M.H.D., Mayahi, A., Rezaei DashtArzhandi, M., Soheilmoghaddam, M. and Shamsaei, E., (2015). "Effect of HNTs modification in nanocomposite membrane enhancement for bacterial removal by cross-flow ultrafiltration system", Reactive and Functional Polymers, 95:80-87.

[267] Wang, R., Jiang, G., Ding, Y., Wang, Y., Sun, X., Wang, X. and Chen, W., (2011). "Photocatalytic Activity of Heterostructures Based on TiO2 and Halloysite Nanotubes", ACS Applied Materials & Interfaces, 3(10):4154-4158.

[268] Zeng, G., He, Y., Yu, Z., Zhan, Y., Ma, L. and Zhang, L., (2016). "Preparation and characterization of a novel PVDF ultrafiltration membrane by blending with TiO2-HNTs nanocomposites", Applied Surface Science, 371:624-632.

[269] Safarpour, M., Khataee, A. and Vatanpour, V., (2014). "Preparation of a Novel Polyvinylidene Fluoride (PVDF) Ultrafiltration Membrane Modified with Reduced Graphene Oxide/Titanium Dioxide (TiO2) Nanocomposite with

Enhanced Hydrophilicity and Antifouling Properties", Industrial & Engineering Chemistry Research, 53(34):13370-13382.

[270] Pakdel, A., Bando, Y. and Golberg, D., (2014). "Nano boron nitride flatland", Chemical Society Reviews, 43(3):934-959.

[271] Weng, Q., Wang, X., Wang, X., Bando, Y. and Golberg, D., (2016). "Functionalized hexagonal boron nitride nanomaterials: emerging properties and applications", Chemical Society Reviews, 45(14):3989-4012.

[272] Duan, X., Yang, Z., Chen, L., Tian, Z., Cai, D., Wang, Y., Jia, D. and Zhou, Y., (2016). "Review on the properties of hexagonal boron nitride matrix composite ceramics", Journal of the European Ceramic Society, 36(15):3725-3737.

[273] Lei, W., Zhang, H., Wu, Y., Zhang, B., Liu, D., Qin, S., Liu, Z., Liu, L., Ma, Y. and Chen, Y., (2014). "Oxygen-doped boron nitride nanosheets with excellent performance in hydrogen storage", Nano Energy, 6:219-224.

[274] Chen, Z.-G. and Zou, J., (2011). "Field emitters: ultrathin BN nanosheets protruded from BN fibers", Journal of Materials Chemistry, 21(4):1191-1195.

[275] Uosaki, K., Elumalai, G., Noguchi, H., Masuda, T., Lyalin, A., Nakayama, A. and Taketsugu, T., (2014). "Boron Nitride Nanosheet on Gold as an Electrocatalyst for Oxygen Reduction Reaction: Theoretical Suggestion and Experimental Proof", Journal of the American Chemical Society, 136(18):6542-6545.

[276] Lei, W., Portehault, D., Liu, D., Qin, S. and Chen, Y., (2013). "Porous boron nitride nanosheets for effective water cleaning", Nature Communications, 4:1777.

[277] Yu, Y., Chen, H., Liu, Y., Craig, V.S.J., Wang, C., Li, L.H. and Chen, Y., (2015). "Superhydrophobic and Superoleophilic Porous Boron Nitride Nanosheet/Polyvinylidene Fluoride Composite Material for Oil-Polluted Water Cleanup", Advanced Materials Interfaces, 2(1):1400267-n/a.

[278] Guo, Z., Xu, X., Xiang, Y., Lu, S. and Jiang, S.P., (2015). "New anhydrous proton exchange membranes for high-temperature fuel cells based on PVDF–PVP blended polymers", Journal of Materials Chemistry A, 3(1):148-155.

[279] Peixoto, A.F., Fernandes, A.C., Pereira, C., Pires, J. and Freire, C., (2016). "Physicochemical characterization of organosilylated halloysite clay nanotubes", Microporous and Mesoporous Materials, 219:145-154.

[280] Sirisinha, K. and Sungmanee, B., (2014). "Silane Crosslinking of High Density Polyethylene as Catalyzed by Tin and Amine Catalyst", Journal of, 1(6):365-372.

[281] Zou, M., Du, M., Zhang, M., Yang, T., Zhu, H., Wang, P. and Bao, S., (2015). "Synthesis and deposition of ultrafine noble metallic nanoparticles on amino-functionalized halloysite nanotubes and their catalytic application", Materials Research Bulletin, 61:375-382.

[282] Kang, B., Li, Y.-D., Liang, J., Yan, X., Chen, J. and Lang, W.-Z., (2016). "Novel PVDF hollow fiber ultrafiltration membranes with antibacterial and antifouling properties by embedding N-halamine functionalized multi-walled carbon nanotubes (MWNTs)", RSC Advances, 6(3):1710-1721.

[283] Darvishmanesh, S., Tasselli, F., Jansen, J.C., Tocci, E., Bazzarelli, F., Bernardo, P., Luis, P., Degrève, J., Drioli, E. and Van der Bruggen, B., (2011). "Preparation

of solvent stable polyphenylsulfone hollow fiber nanofiltration membranes", Journal of Membrane Science, 384(1):89-96.

[284] Zou, M., Du, M., Zhu, H., Xu, C. and Fu, Y., (2012). "Green synthesis of halloysite nanotubes supported Ag nanoparticles for photocatalytic decomposition of methylene blue", Journal of Physics D: Applied Physics, 45(32):325302.

[285] Barrientos-Ramírez, S., Oca-Ramírez, G.M.d., Ramos-Fernández, E.V., Sepúlveda-Escribano, A., Pastor-Blas, M.M. and González-Montiel, A., (2011). "Surface modification of natural halloysite clay nanotubes with aminosilanes. Application as catalyst supports in the atom transfer radical polymerization of methyl methacrylate", Applied Catalysis A: General, 406(1):22-33.

[286] Gao, L. and Li, J., (2003). "Preparation of Nanostructured Hexagonal Boron Nitride Powder", Journal of the American Ceramic Society, 86(11):1982-1984.

[287] Hou, J., Li, G., Yang, N., Qin, L., Grami, M.E., Zhang, Q., Wang, N. and Qu, X., (2014). "Preparation and characterization of surface modified boron nitride epoxy composites with enhanced thermal conductivity", RSC Advances, 4(83):44282-44290.

[288] Moslehyani, A., Mobaraki, M., Ismail, A., Matsuura, T., Hashemifard, S., Othman, M., Mayahi, A., DashtArzhandi, M.R., Soheilmoghaddam, M. and Shamsaei, E., (2015). "Effect of HNTs modification in nanocomposite membrane enhancement for bacterial removal by cross-flow ultrafiltration system", Reactive and Functional Polymers, 95:80-87.

[289] Lun, H., Ouyang, J. and Yang, H., (2014). "Natural halloysite nanotubes modified an aspirin carrier", RSC Advances, 4(83):44197-44202.

[290] Ibrahim, G.P.S., Isloor, A.M., Moslehyani, A. and Ismail, A.F., (2017). "Bio-inspired, fouling resistant, tannic acid functionalized halloysite nanotube reinforced polysulfone loose nanofiltration hollow fiber membranes for efficient dye and salt separation", Journal of Water Process Engineering, 20:138-148.

[291] Lang, W.-Z., Ji, Q., Shen, J.-P., Guo, Y.-J. and Chu, L.-F., (2013). "Modified poly(vinylidene fluoride) hollow fiber composite membranes reinforced by hydroxyapatite nanocrystal whiskers", Journal of Applied Polymer Science, 127(6):4564-4572.

[292] Liu, T.-Y., Zhang, R.-X., Li, Q., Van der Bruggen, B. and Wang, X.-L., (2014). "Fabrication of a novel dual-layer (PES/PVDF) hollow fiber ultrafiltration membrane for wastewater treatment", Journal of Membrane Science, 472:119-132.

[293] Majeed, S., Fierro, D., Buhr, K., Wind, J., Du, B., Boschetti-de-Fierro, A. and Abetz, V., (2012). "Multi-walled carbon nanotubes (MWCNTs) mixed polyacrylonitrile (PAN) ultrafiltration membranes", Journal of Membrane Science, 403–404:101-109.

[294] Zhang, Q., Lu, X. and Zhao, L., (2014). "Preparation of Polyvinylidene Fluoride (PVDF) Hollow Fiber Hemodialysis Membranes", Membranes, 4(1):81.

[295] Widjojo, N. and Chung, T.-S., (2006). "Thickness and Air Gap Dependence of Macrovoid Evolution in Phase-Inversion Asymmetric Hollow Fiber Membranes", Industrial & Engineering Chemistry Research, 45(22):7618-7626.

[296] Boom, R.M., Wienk, I.M., van den Boomgaard, T. and Smolders, C.A., (1992). "Microstructures in phase inversion membranes. Part 2. The role of a polymeric additive", Journal of Membrane Science, 73(2):277-292.

[297] Vatanpour, V., Madaeni, S.S., Rajabi, L., Zinadini, S. and Derakhshan, A.A., (2012). "Boehmite nanoparticles as a new nanofiller for preparation of antifouling mixed matrix membranes", Journal of Membrane Science, 401-402:132-143.

[298] Sun, S.P., Wang, K.Y., Peng, N., Hatton, T.A. and Chung, T.-S., (2010). "Novel polyamide-imide/cellulose acetate dual-layer hollow fiber membranes for nanofiltration", Journal of Membrane Science, 363(1):232-242.

CURRICULUM VITAE

PERSONAL INFORMATION

Name Surname : Yaprak SUBAŞI

Date of birth and place : 15/05/1993, Kadıköy, İstanbul

Foreign Languages : English, French

E-mail : yapraksubasi@gmail.com

EDUCATION

Degree	**Department**	**University**	**Date of Graduation**
Undergraduate	Metallurgical and Materials Engineering	Yıldız Technical University	2016
High School	Sciences and Mathematics	Saint Benoit French High School	2012

WORK EXPERIENCE

Year	**Corporation/Institute**	**Enrollment**
2017 – Present	Koç University, Boron Based Materials & High Technology Chemicals Research & Application Center	Researcher

2017 – Present	Ak-Kim Kimya Sanayi ve Ticaret A.Ş., Directorate of Water Solutions	Assistant Specialist, Researcher
2016-2017	Ak-Kim Kimya Sanayi ve Ticaret A.Ş., Research & Development	Long Term Intern

PUBLISHMENTS

Papers

1. Subasi, Y. and Cicek, B., (2017) "Recent advances in hydrophilic modification of PVDF ultrafiltration membranes – a review: part II ", Membrane Technology, (2017) 5-11 https://doi.org/10.1016/S0958-2118(17)30233-1

2. Subasi, Y. and Cicek, B., (2017) "Recent advances in hydrophilic modification of PVDF ultrafiltration membranes – a review: part I", Membrane Technology, (2017) 7-12 https://doi.org/10.1016/S0958-2118(17)30191-X

Conference Papers

1. Subasi, Y., Cicek, B., Sarioglu, A., (2017) "Fabrication and Characterization of a Novel Polyvinylidene Fluoride Hollow Fiber Ultrafiltration Membranes Blended with 3-Aminopropyltriethoxysilane Grafted Halloysite Nanotubes: Preliminary Study", 2nd International Mediterranean Science and Engineering Congress (IMSEC 2017) Çukurova University, Congress Center, October 25-27, 2017, Adana / TURKEY, Pages: 1988-1988, Paper ID:869